Short-term control of the cardiovascular system: modelling and signal analysis

Alessandro Monti, Claire Médigue, Michel Sorine

INRIA

INSTITUT NATIONAL DE RECHERCHE EN INFORMATIQUE ET EN AUTOMATIQUE

Short-term control of the cardiovascular system: modelling and signal analysis

Alessandro Monti — Claire Médigue — Michel Sorine

N° 4427

April 12, 2002

THÈME 4

ISSN 0249-6399 ISRN INRIA/RT--0259--FR+ENG

INRIA
ROCQUENCOURT

Short-term control of the cardiovascular system: modelling and signal analysis

Alessandro Monti , Claire Médigue , Michel Sorine

Thème 4 — Simulation et optimisation
de systèmes complexes
Projets SOSSO

Rapport de recherche n° 4427 — April 12, 2002 — 104 pages

Abstract: Our aim is to relate classical cardiovascular signal analysis to models of the cardiovascular (CV) and control systems taking into account its multiple feedback loop organisation. We discuss knowledges on the short-term control of CV system, focusing on the analysis of CV time-series and control of arterial pressure and RR-interval. In the first and second sections, we introduce modelling concepts which lead us to the definition of a possible decentralised control of CV system, with several baroreflex control loops, and at a time-discrete approach for the estimation of their sensitivities. We consider two types of vascular compartment: a passive one composed of elastin and collagen fibers, and an active one characterised in addition by smooth muscle. Passive vascular compartment modelling leads us to introduce the classical Windkessel model, widely applied for blood pressure curve analyses. We demonstrate that Windkessel model can be derived from a distributed model of the vascular compartment by a three-point discretisation of the one-dimensional partial differential equations of blood flow. We relate the definition of the vascular resistance and compliance to physical peculiarities of the local vessel wall. Looking for a possible mechano-chemical command of the heart function, we conceive a hierarchical control of the heart, separating the mechanical from the chemical control of the cardiac pump. We model the aortic and carotid baroreceptors, considering the three different steps of transduction: baroreceptor sensitivity to the inside pressure, pressure-deformation transduction process and deformation neural firing rate transduction process. The model is based on accumulated physiological and histological evidences and incorporates a local sympathetic feedback mechanism. We demonstrate that the knowledge of the history of the time derivative of the vessel wall stress is rich enough to allow the estimation of the inner baroreceptor pressure without the need of a pressure set-point. Active vascular compartment modelling leads us to consider blood pressure in the compartment as an output of the model. Whereas state variables are blood volume of the vascular compartment, the strain and stress of smooth muscles which are controlled by the autonomic nervous system (ANS) and by a local control of blood oxygenation. Finally, we conceive the plan of a possible CV controller. In our point of view, the ANS regulates blood flow and pressure in different parts of the CV system with local feedback loops supposed to be fast and efficient. We demonstrate the necessary existence of negative and positive feedbacks: negative for blood pressure and/or flow, positive for blood flow. In the third section, we introduce actual knowledges and clinical relevance of (i) the origin of CV variability and (ii) of baroreflex mechanism, relating these concepts to CV modelling. In the last sections, we develop classical methods of CV spectral and time varying analysis, applying them in clinical conditions. A joint time-frequency distribution, the Smoothed Pseudo Wigner-Ville Distribution

Unité de recherche INRIA Rocquencourt
Domaine de Voluceau, Rocquencourt, BP 105, 78153 Le Chesnay Cedex (France)
Téléphone : +33 1 39 63 55 11 —Télécopie : +33 1 39 63 53 30

(SPWVD) and an harmonic analysis method, the Complex Demodulation (CDM), are evaluated on synthetic and real CV time-series. We show the ability of this SPWVD-CDM to estimate the instantaneous amplitude and frequency of CV oscillations and the instantaneous phase between respiratory and CV oscillations.

Key-words: Cardiovascular System, Respiratory System, Frequency and Time-Frequency Analysis, Biological Rhythms

Contrôle à court terme du système cardiovasculaire : modélisation et analyse des signaux

Résumé : Notre objectif est de faire le lien entre le traitement du signal cardiovasculaire (CV) classique et les modèles des sytèmes CV et de leur contrôle, en tenant compte de son organisation en multiples boucles rétroactives. Nous discutons de l'état des connaissances sur le contrôle court terme du système CV, en nous focalisant sur l'analyse des séries temporelles CV et le mécanisme de contrôle de la pression artérielle et de l'intervalle RR.
En première et seconde parties, nous introduisons les concepts de modélisation qui conduisent à la définition d'un possible contrôle décentralisé du système CV, avec plusieurs boucles baroréflexes, et à une approche de l'estimation de leur sensibilité en temps discret. Nous considérons deux types principaux de compartiments vasculaires : compartiments passifs, constitués d'éléments élastiques et de fibres de collagène et des compartiments actifs constitués en plus de muscles lisses. La modélisation des compartiments passifs nous conduit à introduire le modèle classique de Windkessel, largement appliqué en clinique à l'étude de la courbe de pression sanguine. Nous démontrons qu'il peut être dérivé d'un modèle à paramètres distribués du compartiment vasculaire, grâce à une discrétisation sur trois points des équations aux dérivées partielles décrivant l'écoulement mono-dimensionel du sang dans les vaisseaux. De plus, nous relions les définitions de résistance et de compliance vasculaire aux caractéristiques physiques locales de la paroi des vaisseaux. Nous introduisons une modélisation classique de la pompe cardiaque et nous proposons une commande hiérarchisée de la fonction cardiaque en séparant commande chimique et mécanique. Nous modélisons les barorécepteurs aortiques et carotidiens en considérant les trois principaux pas de transduction de l'information : sensibilité des barorécepteurs à la pression sanguine, processus de transduction pression-déformation et processus de transduction déformation-activité nerveuse. Le modèle a de très grandes connotations physiologiques et incorpore un mécanisme de régulation sympathique locale. Nous démontrons que la connaissance de l'histoire de la dérivée temporelle de la déformation de la paroi du barorécepteur est suffisamment riche d'information pour pouvoir reconstruire la pression à l'intérieur du vaisseau, sans avoir besoin de connaître une pression de référence. Nous proposons aussi une version possible de cet estimateur. La modélisation des compartiments vasculaires actifs, nous conduit à considérer la pression comme une sortie du modèle. Les variables d'états sont alors le volume sanguin vasculaire, les contraintes et déformations des muscles lisses. Ceux-ci sont contrôlés par le système nerveux autonome (SNA) mais aussi par la concentration locale en oxygène des tissus. Ensuite, nous abordons la conception d'un contrôleur du système CV. De notre point de vue, le SNA règle le débit et les pressions sanguines aux différents endroits du système CV avec des boucles de rétroaction locales supposées rapides et efficaces. Nous démontrons l'existence nécessaire de boucles de rétroaction positive et négative: négatives pour le débit sanguin et/ou la pression sanguine, positives pour le débit sanguin. En troisième partie, nous introduisons l'état actuel des connaissances et la pertinence clinique de (i) l'origine de la variabilité CV et (ii) du mécanisme baroréflexe, reliant ces concepts à ceux de la modélisation CV. En dernières parties, nous développons des méthodes classiques d'analyse spectrale et d'analyse *temps-variant*, que nous appliquons à des conditions physio-pathologiques. Une distribution temps-fréquence, la Pseudo Distribution de Wigner-Ville Lissée (SPWVD) jointe à une méthode d'analyse harmonique, la Démodulation Complexe (CDM), sont évaluées sur des séries CV synthétiques et réelles. Nous montrons la capacité de la SPWVD-CDM à estimer les amplitudes et fréquences instantanées des oscillations CV et la phase instantanée entre les oscillations CV et respiratoires.

Mots-clés : Système cardiovasculaire, Système respiratoire, Traitement de signal, Rythmes Biologiques

Contents

1 Physiological and Modelling Introduction

1.1 Introduction

The function of the circulation is to supply tissues with oxygen, nutrients and to remove carbon dioxide and other catabolits. The organs involved in this function are: the lungs which allow gas exchanges, the heart which pumps blood and the vascular system which carries molecules to the tissues, see fig. (1). The regulation of these exchanges is under *hemodynamic* mechanisms, which tend to keep physiological

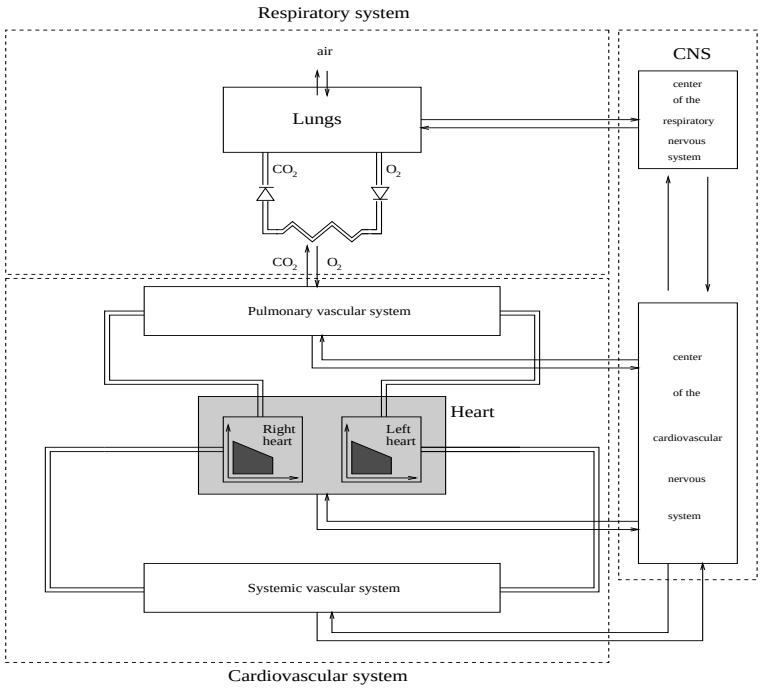

Figure 1: *Model of cardiorespiratory system. Different systems interact to supply tissues with oxygen: respiratory, vascular (systemic and pulmonary), central nervous system and heart.*

variables around a control level; these mechanisms have to adapt the cardiovascular system to changes (orthostatisme as well as exercise). A strict *homeostasis* point of view reduces the complexity of the living systems regulation. Variables involved in cardiovascular regulation, such as blood flow, blood pressure level, oxygen blood concentration, are kept around their reference point by feedback control mechanisms, as illustrated in fig. (18).

These control mechanisms have different dynamics and we are interested only in the short term control, about a few minutes, of the cardiovascular system, which is assumed by the nervous system, more precisely by its autonomic part (ANS). This short term control involves fast mechanisms of blood flow and pressure regulation, the baroreceptor control loop, neglecting slower ones, such as hormonal regulation. A good autonomic function is of crucial importance for life and is of great prognostic value in many diseases.

1.2 Purposes of our studies: RR-interval, blood pressure variability and baroreflex effector

The aim of this report is to discuss knowledges on the short-term control of cardiovascular system, focusing on the analysis of cardiovascular time-series and on the arterial pressure RR-interval control mechanism. Classical cardiovascular signal processing will be related to a cardiovascular model and to a reasonable control law. The respiratory activity will be "applied" here as an external input to investigate the ANS control of CV system. In addition, we developed a signal processing tool box (LARY_CR, *logiciel d'analyse des rythmes - cardiovasculaires et respiratoire*) in a scientific environment (SCILAB/SCICOS). LARY_CR is the object of the INRIA Technical Report $n^o 259$ ([95]). Classical signal processing methods, such as spectral decomposition or time-frequency representations, are adapted to estimate respiratory and cardiovascular interactions in various situations. Indeed, cardiovascular and respiratory rhythms and their adaptation are studied under physiological (orthostatisme, sleep), pathological (chronic heart failure, vasovagal syncope) and pharmacological conditions (activator/inhibitor of the ANS). Respiratory, electrocardiographic (EKG) and arterial blood pressure (ABP) signals are easily and non invasively recorded. But only cardiac beat to beat variables extracted from raw signals are used for the estimation of baroreflex sensitivity and cardiovascular variability, as explained in section (3).

1.2.1 Cardiovascular and respiratory time series

A typical pattern of blood pressure, respiratory and electrocardiographic signals is shown in fig. (2). From these signals, four time series are extrapolated: RR interval, systolic blood pressure (SBP), diastolic blood pressure (DBP) and respiratory time series.

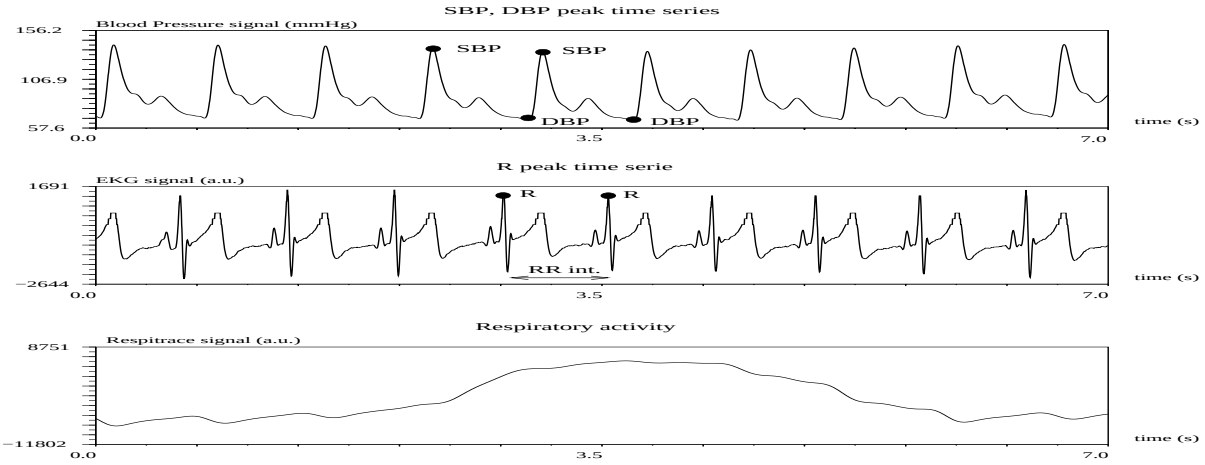

Figure 2: *Blood pressure, electrocardiographic and respiratory raw signals obtained respectively by Finapres, thoracic electrodes and Respitrace.*

SBP and DBP rhythms are the successive amplitudes of blood pressure corresponding to mechanical cardiac events: SBP is the maximum value of the pressure, corresponding to the ejection of the blood into the aorta, DBP is the minimal value of the pressure, occurring during the cardiac diastole.

The respiratory rhythm is slower than the cardiac rhythm and a respiratory cycle can contain approximately from three to ten heart beats.

Signal analysis in the time domain, frequency domain or in a joint time-frequency domain is therefore applied to these time series as illustrated in the following chapters.

1.2.2 RR interval and blood pressure variability

It is well known that mean cardiovascular values can vary according to different physical conditions, such as rest and exercise, but also cardiovascular values fluctuate under relative stable conditions. This dynamic behaviour implies that cardiovascular mean values and variability have to be studied together to reflect the autonomic nervous system (ANS) short-term control of the cardiovascular system. Cardiovascular fluctuations can be studied through beat-to-beat arterial blood pressure and RR means and variances and, as has more recently been done, through frequency domain analysis. RR power spectrum is considered to be an effective non invasive measure for studying neural modulations of RR in many clinical and research studies. The major interest in measuring cardiac nerve traffic is not surprising, considering

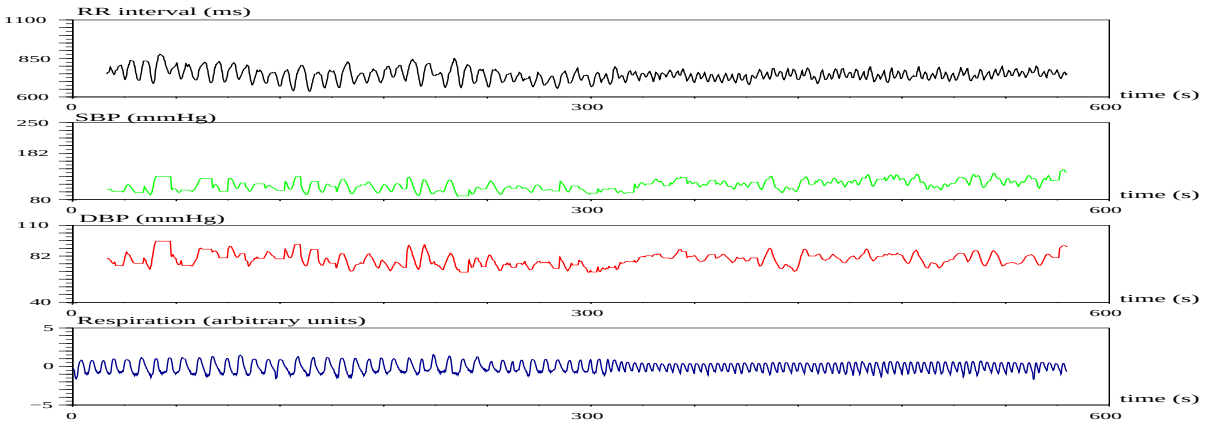

Figure 3: *RR interval, SBP, DBP and respiratory time series with a 2 Hz resampling.*

the great prognostic value of autonomic nervous system behaviour in normal and unhealthy subjects. But more precise characterisations of RR control have been performed by relating RR variability (RRV) to respiration and arterial blood pressure variability (BPV). Three major oscillatory components are usually detectable in both RRV and BPV with more or less pronounced spectral peaks [2, 132, 115, 114]:

1. the highest, synchronous with respiration (the so called respiratory sinus arrhythmia, RSA, in RR signal, and respiratory oscillations in blood pressure signal), is described as "*high frequency*" (HF, about 0.25Hz and varying with respiratory frequency);

2. the spectral peak in the middle, which corresponds to slow waves [71] (or Mayer waves) is described as "*low frequency*" (LF, about 0.1Hz). However, the central frequency of the LF component can also vary considerably (from 0.04 to 0.13Hz) [46, 47].

3. the slowest, corresponding to the very slow waves is described as "*very low frequency*" (VLF, from 0 to 0.04Hz).

We are interested only in LF and HF spectral peaks, which reflect short term control of the cardiovascular system.

2 Cardiovascular system: models and signals

2.1 Cardiovascular system Modelling

The cardiovascular system consists of a complex double chamber pump (the heart), pumping a complex fluid (the blood) into complex pipes (the blood vessels) organised into vascular compartments, as shown in fig. (4).

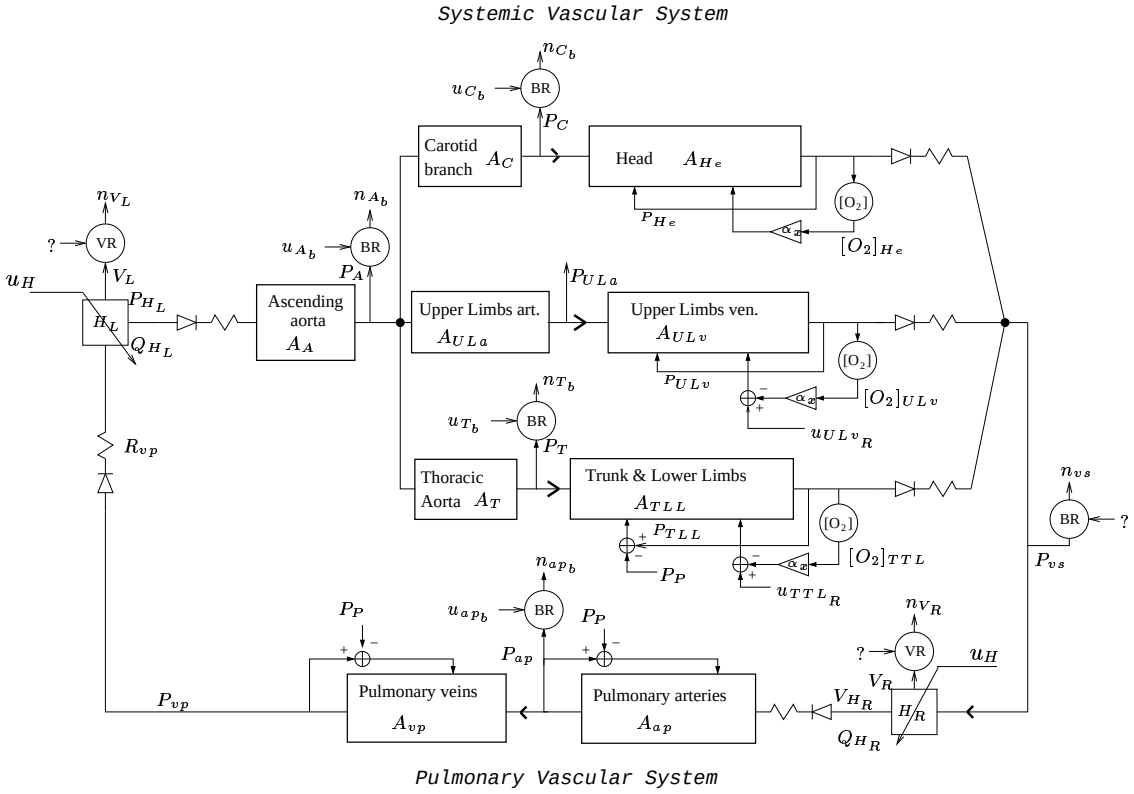

Figure 4: *Diagram of the cardiovascular system. H_R and H_L stand for the right and left part of the heart, respectively. V_R and V_L are the volumes of the right and left ventricles, respectively, measured by voloreceptors (VR). We do not know if voloreceptors are controlled by the ANS. Each vascular compartment is characterised by its local cross-sectional area-pressure relationship A_x and its pressure P_x (x=A, C, He, ULa, ULv, T, TLL, ap, vp). The arterial pressure P_{ULa} measured at the upper limbs by external devices, i.e. at the finger level by FINAPRES. P_x (x=A, C, T, ap, vs) are the measured blood pressure at differentm points in the cardiovascular system by ANS-controlled baroreceptors (BR). We do not know if baroreceptor in the vs compartment is controlled by the ANS. This system is under control of the ANS (inputs u_H, u_{ULv_R}, u_{TLL_o}, u_{A_b}, u_{C_b}, u_{T_b}, u_{ap_b}), under respiratory mechanical influence (input P_P, pulmonary pressure) and under local control of blood oxygen concentration (input $[O_2]_{He}$, $[O_2]_{Ulv}$, $[O_2]_{TLL}$). The diodes and the resistances stand for a $Q = |\Delta P|_+ / R$ characteristic where ΔP is the blood pressure drop across the diode.*

In fig. (4), the systemic vascular system is split in three main parts evidencing the measures available by ANS to control the cardiovascular system. These measures are provided by aortic and carotid baroreceptors, by low-pressure arterial pulmonary stretchreceptors, by stretchreceptors localised in the thoracic aorta and in the ventricle walls. In addition, in classical clinical studies, a non invasive measure of arterial blood pressure is taken on the upper limb arteries by FINAPRES device or other instruments. Remark that:

1. head compartment is submitted to a local control of blood flow;
2. skeletal muscles are provided with local blood flow control mechanism.

Therefore, the control system is structured in various feedback loops which must efficiently cooperate.

2.1.1 Passive vascular compartment modelling

Several kinds of models have been proposed: some simulate the response of a distributed vascular system model to a beat-to-beat blood pumping [152], see fig. (5). Other models simulate vascular system using

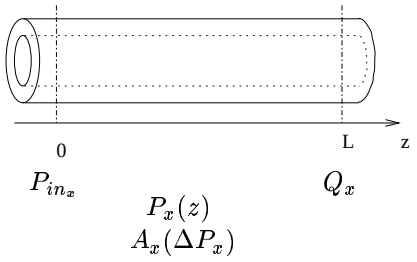

Figure 5: *Distributed model of the x vascular compartment.* P_{in_x} *is the input pressure,* Q_x *is the output blood flow and* $A_x(P_x, z)$ *is the cross-sectional area-pressure relationship of the x vascular compartment.*

lumped parameters. The most popular is the 2-element Windkessel model [159]. In this model the whole arterial tree is modelled as an elastic chamber with a constant compliance (C=dV/dP, V being systemic blood volume and P pressure) and a resistance (R) representing the total resistance of the arterial tree, see fig. (6). Although the classic 2-WK model still finds application, both the magnitude

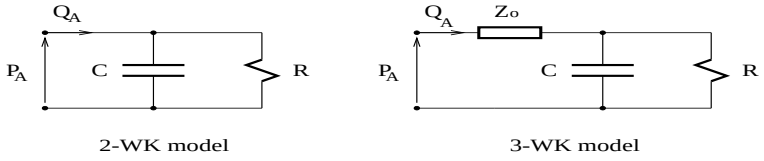

Figure 6: *Lumped model of vascular compartment.*

and phase of its input impedance display significant discrepancies when compared to measured values at high frequencies [159, 150]. To overcome to this limitation a 3-WK has been proposed including the characteristic impedance of the ascending aorta (Z_o) placed proximally to the 2-WK model. This impedance can be a real number (merely a resistance effect) [159, 150] or a complex number (a parallel of a resistance and a inductance) providing, in simulations, better results [151]. Finally, based on measured

pressure-volume relationship on blood vessels [76] a 3 non-linear WK model ($Z_o = Z_o(P)$ and $C = C(P)$) has been proposed [170]. All these models have been applied to compute aortic flow from pressure curve or to characterise the vascular system using very simple parameters.

To be more precise, we give the relationship between the 2-WK, 3-WK and distributed models. A distributed model of vascular compartment can be defined as follows:

$$\left\{ \begin{array}{l} \dfrac{\partial A_x}{\partial t} + \dfrac{\partial Q_x}{\partial z} = 0 \\ \\ c_u \dfrac{\partial Q_x}{\partial t} + \dfrac{\partial}{\partial z}\left(\dfrac{Q_x^2}{A_x}\right) = -\dfrac{A_x}{\rho}\dfrac{\partial P_x}{\partial z} - \dfrac{8\, c_v\, \pi\, \mu}{\rho}\dfrac{Q_x}{A_x} \end{array} \right. \tag{1}$$

This model is based on the one-dimensional flow equations resulting from the integration of the continuity and momentum equations over the cross section of the vessel [152]. Where $A_x(P,z)$ is the cross-sectional area of the vessel, $Q_x(P,z)$ the distributed blood flow in the vessel, c_u coefficient of the inertia term in shear stress model, c_v coefficient of the viscous term in shear stress model, $P_x(z,t)$ is the distributed pressure in the vessel, ρ is the blood density, μ is the blood viscosity. The system of equations is completed by a model of the local compliance of the vessels $A_x = \Gamma_x(\Delta P_x)$, a "state equation". An example of the increasing monotonic function Γ_x is:

$$A_x(\Delta P_x) \stackrel{\text{def}}{=} \Gamma_x(\Delta P_x) = A_{x_o}\left[1 + C_{x_o}\,\Delta P_x + C_{x_1}\,\Delta P_x^2\right] \tag{2}$$

where $\Delta P_x = P_x - P_{x_o}$ being P_{x_o} the external pressure and A_{x_o} is the reference cross-sectional area in the x vascular compartment [152]. Other kind of state equations have been proposed: a logarithmic [135] or a tangent [76] pressure-area relationship, accounting for the nonlinear elastic behaviour of the arterial wall. The distributed model could have, for example, the following (pressure-flow P-Q) boundary conditions, as shown in fig. (5):

$$\left\{ \begin{array}{l} P|_{z=0} = P_{in} \\ \\ Q|_{z=L} = -\dfrac{1}{\lambda\rho}\, A_x^2(\Delta P_x)\, \dfrac{\partial P}{\partial z}\Big|_{z=L} = Q_x \end{array} \right. \tag{3}$$

It is also possible to consider other boundary conditions (P-P, Q-P, Q-Q, ...). Neglecting the inertial terms $c_u \frac{\partial Q_x}{\partial t}$ and $\frac{\partial}{\partial z}\left(\frac{Q_x^2}{A_x}\right)$ we can write:

$$\left\{ \begin{array}{l} \dfrac{\partial A_x}{\partial t} - \dfrac{1}{\lambda}\dfrac{\partial}{\partial z}\left(A_x^2\, \dfrac{\partial P_x}{\partial z}\right) = 0 \\ \\ Q_x = -\frac{1}{\lambda}\, A_x^2\, \frac{\partial P_x}{\partial z} \end{array} \right.$$

where $\lambda = 8\, c_v\, \pi\, \mu$. Taking into account the state equation (2), we have a simple partial differential equation

$$\left\{ \begin{array}{l} \dfrac{\partial A_x(P_x - P_{x_o})}{\partial P_x}\, \dfrac{\partial P_x}{\partial t} - \dfrac{1}{\lambda}\dfrac{\partial}{\partial z}\left(A_x^2(P_x - P_{x_o})\, \dfrac{\partial P_x}{\partial z}\right) = 0 \\ \\ Q_x = -\frac{1}{\lambda}\, A_x^2(P_x - P_{x_o})\, \frac{\partial P_x}{\partial z} \end{array} \right. \tag{4}$$

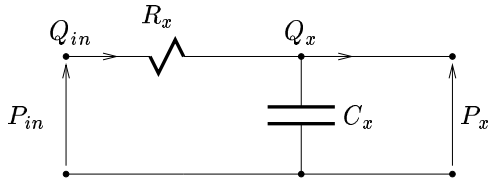

Figure 7: *Two-element vascular compartment model deduced by the distributed model, neglecting inertial terms.*

Taking into account only three points, see fig (5), the enter- with pressure P_{in}, the middle- P_x and at the exit-point with a blood flow Q_x, discretisation of (4) leads to:

$$\begin{cases} \dfrac{d\,A_x}{d\,P_x}\,\dfrac{d\,P_x}{dt} + \dfrac{1}{\Delta z}\left[Q_x + \dfrac{A_x^2(P_x - P_{x_o})}{\lambda\,\Delta z}\,(P_x - P_{in})\right] = 0 \\ \\ Q_{in} = -\dfrac{A_x^2(P_x - P_{x_o})}{\lambda\,\Delta z}\,(P_x - P_{in}) \end{cases} \tag{5}$$

The vessel compliance defines the changes in the blood volume due to a given changes in the distending pressure and in a distributed model can be expressed as $C_x(\Delta P_x) = \frac{\partial A_x}{\partial \Delta P_x}(\Delta P_x)$. In a three-points model, eq (5), the lumped compliance can be expressed as

$$C_x(\Delta P_x) = \Delta z\,\frac{dA_x}{d\Delta P_x}(\Delta P_x) \tag{6}$$

The vessel resistance defines the drop in blood pressure across the vessel. In a three-points models it can be expressed as

$$R_x(\Delta P_x) = \frac{8\,\pi\;c_v\,\mu\,\Delta z}{A_x^2(\Delta P_x)} \tag{7}$$

Therefore, principal vessel characteristics can be deduced from the cross-sectional area-pressure relationship and a two-element vascular compartment model (RC-cell model) can be easily obtained by distributed model neglecting the inertial terms. Taken into account eq. (6) and (7), eq. (5) becomes

$$\begin{cases} C_x(P_x - P_{x_o})\,\dfrac{d\,P_x}{dt} + \left[Q_x + \dfrac{P_x - P_{in}}{R_x(P_x - P_{x_o})}\right] = 0 \\ \\ Q_{in} = -\dfrac{1}{R_x(P_x - P_{x_o})}\,(P_x - P_{in}) \end{cases} \tag{8}$$

Remark that

$$Q_{in} = Q_x + C_x\,\dot{P}_x$$

The usual description of the circulation leads to a clear separation between the resistance and compliance functions of the different vessels. We recover this property noting that in large arteries and veins, the resistive effects are smaller due to (7): only small pressure differences are needed to drive the cardiac output through these vessels, while their changes in volume are highly significant. The main site of

resistance is in the tissues themselves (primarily at the level of smallest arteries, the arterioles), where the volume changes are less important but where large pressure drop are observed. In large vessels, the resistance can be neglected, so $P_x \approx P_{in}$. In arterioles, the blood volume changes can be neglected being the input pressure filtered by upstream vascular compartiments, so $Q_x \approx Q_{in}$.

Concerning the vascular compartiments, the ANS controls primary the external pressures (P_{ULV_o}, P_{TLL_o}) and in particular the volume of the systemic veins (systemic veins take into account the 70% of total blood volume), and resistance of arterioles, as shown in fig. (4).

Finally, remark that classical 2-WK lumped model of the entire vascular compartiment, see fig. (6), can be obtained by two RC-cell models in series when one neglects the aorta resistance, the peripheral compliance and consider the output pressure of the second RC-cell equal to zero. The 3-WK model can be deduced by RC-model taking into account the aorta resistance and neglecting the peripheral compliance. In addition, taking into account the inertial term $c_u \frac{\partial Q_x}{\partial t}$ in eq. (1) the corresponding model would include the inertance term recently added to the 3-WK model [151].

2.1.2 Heart Modelling

The heart can be considered as a double chamber pump that accepst fluid at low pressure (P_1) and transfers it into a region where the pressure is high ($P_2 > P_1$). Thus, the heart performs works on the fluid and the power of the pump can be estimate by the product $Q\ (P_2 - P_1)$, where Q is the fluid flow. Consider, for example, the left ventricle. The left ventricle is equipped with an inflow (mitral) valve and an outflow (aortic) valve. When the ventricle is relaxed (diastole) the inflow valve is open and the outflow valve is closed. During this period of time, the left ventricle receives blood from the left atrium at a pressure that is essentially that of the pulmonary veins, thus, for the left ventricle $P_1 = P_{PV} = 5\ mmHg$, see fig. (4). When the ventricle contracts (systole), the inflow valve closes and the outflow valve remains closed (isovolumetric contraction) and opens (ejection) only when the pressure in the left ventricle is greater than the pressure in the ascending aorta. Therefore, the left ventricle actively pumps blood into the systemic arterial tree. Thus, for the left ventricle, $P_2 = P_A \approx 100\ mmHg$. What determines the output of the left ventricle under these conditions?

To answer to this question, recently, an heart model has been proposed [10]. This model is very peculiar has it is derived from a micro (myofibres) to macro (muscular fibres) mathematical passage. It intrinsically includes a lot of muscular characteristics and it is quite simple. For the left ventricle in cylindrical geometry, it can be simplified to:

$$\begin{cases} \dot{k}_{c_L} & = -\ (|u_H| + |\dot{\varepsilon}_{c_L}|)\ k_{c_L} \ + \ k_{c_{L_o}}\ |u_H|_+ \\ \dot{\sigma}_{c_L} & = -\ (|u_H| + |\dot{\varepsilon}_{c_L}|)\ \sigma_{c_L} \ + \ k_{c_L}\ \dot{\varepsilon}_{c_L} \ + \ \sigma_{c_{L_o}}\ |u_H|_+ \\ \ddot{\varepsilon}_{c_L} & = -(2\zeta\omega + \eta\ \alpha)\ \dot{\varepsilon}_{c_L} - \omega^2\ \varepsilon_{c_L} - \alpha\ d_o(\varepsilon_{c_L})\ (k_{c_L}\ \xi_0 + \sigma_{c_L}) + \beta\ \dfrac{\sqrt{V_{H_L}} - \sqrt{V_{0_{H_L}}}}{\sqrt{V_{0_{H_L}}}} \\ \dot{V}_{H_L} & = \dfrac{1}{R_{pv}} |P_{pv} - P_{H_L}(V_{H_L}, \sigma_{c_L}, \varepsilon_{c_L})|_+ - \dfrac{1}{R_A} |P_{H_L}(V_{H_L}, \sigma_{c_L}, \varepsilon_{c_L}) - P_A|_+ \\ \text{where} \quad & P_{H_L}(V_{H_L}, \sigma_{c_L}, \varepsilon_{c_L}) = k_L \dfrac{d_o(\varepsilon_{c_L})}{V_{H_L}}\ \sigma_{c_L} \end{cases} \tag{9}$$

where

- k_{c_L} is the total left ventricle muscular controlled stiffness;

- σ_{c_L} is the total left ventricle muscular controlled stress;
- ε_{c_L} is the total left ventricle wall strain;
- $\dot{\varepsilon}_{c_L}$ is the left ventricle wall speed;
- $d_o(\varepsilon_{c_L})$ is the lenght-tension relationship of the muscle fibers;
- P_{H_L} is the left ventricle pressure;
- V_{H_L} is the left ventricle volume;
- P_{pv} and R_{pv} are shown in fig. (4);
- $u_H(t)$ is the chemical command controlling the left ventricle contraction and $d_o(\varepsilon)$ appears as a mechanical gain adaptation which takes into account the Starling effect, see fig (8). In fact the

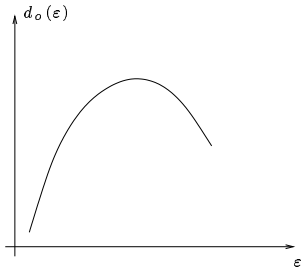

Figure 8: *Mechanical command $d_o(\varepsilon)$ of the heart to take into account the Starling effect.*

Starling's law of the heart is an expression of the length-tension relationship in the muscles. In the ascending limb of the Starling curve, the more is filled the heart the more amount of blood the pump will push out (a stable condition), on the other hand in the descending limb the more is filled the heart the smaller amount of blood the pump will push out (an instable condition). Assuming a separation of the mechanical and chemical command, we are lead to conceive a hierarchical control of the heart. At the upper level $u_H(t)$ is the command which is applied to guarantee a well oxygenation of the body tissue assuming a steady filling of the heart, i.e. the controller acts as the heart pumps in a open loop system. At the lowest level, given a central command $u_H(t)$ and the actual filling condition of the heart, $d_o(\varepsilon_{c_L})$ regulates the command $u_H(t)$ to finally have the correct heart command. Remark that, in the ventricular and atrium walls are located stretchreceptors that can be used to estimate this $d_o(\varepsilon_{c_L})$ regulation.

Other models based on a time variant elastance [60] have been proposed, but they are reductionistic and behavioural models. Moreover, model parameters have no direct physiological meaning but they are chosen *ad doc*. An application of such models in a cardiovascular system can be found in [60, 160].

2.1.3 Baroreceptor Modelling

Physiology

When a change in carotid sinus (or in the aorta) arterial pressure occurs, the cross-sectional area of the sinuses changes, whereby the viscoelastic walls is deformed (pressure-mechanical deformation). The

receptors at the nerve endings are located in the lateral wall of the carotid sinus. The mechano-electrical transduction takes place in these receptors themselves by a poorly understood coupling mechanism. Hence, a change in pressure causes deformation in the spatial structure, which results in a change of activity of the baroreceptor nerves. This activity is denoted the firing rate. Principal peculiarities of carotid sinus baroreceptor response are the followings:

- firing rate increases with carotid pressure;
- response curves exhibit threshold (the positive and stable equilibrium value which the firing rate approaches when no change in pressure appears) and saturation (maximum value of the firing rate) in a sigmoidal shape and show asymmetric behaviour depending on the direction of pressure changes;
- sufficiently fast decreases in pressure cause firing to drop even below the threshold value;
- a step change in pressure causes a step change in firing rate followed by resetting phenomenon, i.e. a decay in firing rate towards the threshold value. Resetting is called adaptation;
- finally, observations indicate that the response curves for hypotensive sinus and hypertensive sinus simply are translations to the left and right along the pressure axis, respectively, of the response curve for normotensive sinus.

A more detailed summary of these peculiarities can be found in [73, 103, 112, 155, 164]. There has been a large effort to model these nonlinear characteristics of the baroreceptors [112, 155], but all are descriptive models. In fact, they do not separate the pressure-mechanical deformation of the carotid sinus wall model from the mechano-electrical transduction in the receptors themselves. Moreover, any model take into account the efferent sympathetic influence on baroreceptor activity, as discussed below. In [73], a first step in this direction has been made without a clear formalisation of the model. We will overcome this limitation developing a pressure-mechanical deformation model and analysing the possible usefulness of the sympathetic feedback for baroreceptor activity control.

Modelling of the baroreceptor compartment

The carotid and aortic baroreceptors can be modelled as shown in fig. (9), the measured pressure does not coincide to the pressure inside the blood vessels, as also well known in physiology [155]. In fact, baroreceptors are sensibles to local vessel stretch (and they are usually called also mechanoreceptors), therefore their characteristics are based on the local relationship between inside pressure and vessel cross section strain. Applying eq. (8) to the vascular compartment upstream (x_{b-}) the baroreceptor, to the baroreceptors (x_b) and finally to the vascular compartment downstream the baroreceptors (x_{b+}), we have

$$\begin{cases} Q_{in_{x_{b-}}} = C_{x_{b-}} \dot{P}_{x_{b-}} + Q_{x_{b-}} & , \quad Q_{in_{x_{b-}}} R_{x_{b-}} = P_{in_{x_{b-}}} - P_{x_{b-}} \\ Q_{x_{b-}} = C_{x_b} \dot{P}_{x_b} + Q_{x_b} & , \quad Q_{x_{b-}} R_{x_b} = P_{x_{b-}} - P_{x_b} \\ Q_{x_b} = C_{x_{b+}} \dot{P}_{x_{b+}} + Q_{x_{b+}} & , \quad Q_{x_b} R_{x_{b+}} = P_{x_b} - P_{x_{b+}} \end{cases} \tag{10}$$

where $C_{x_b} = \Delta z \, \frac{dA_{x_b}}{dP_{x_b}}$, $R_{x_b} = \Delta z \, \frac{\lambda}{A^2_{x_b}(\Delta P_{x_b})}$ and so on.

Assuming that the baroreceptor lies in a very narrow zone, such as $L_{x_b} \to 0$ in the fig. (9) then both $R_{x_b} \to 0$ and $C_{x_b} \to 0$ since $\Delta z \to 0$. In this case

$$P_{x_b} - P_{x_{b-}} = \mathcal{O}(\Delta z) \tag{11}$$

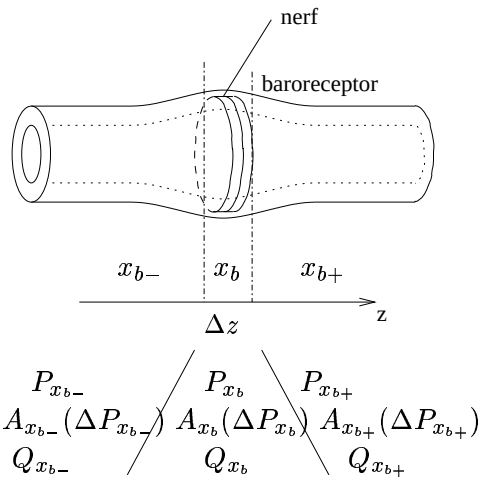

Figure 9: *Baroreceptor compartment modelling.*

we will refer to this case as the zero order approximation of baroreceptor model. It is interesting to underline that considering a pure compliant model for the baroreceptor, one obtain the same approximation.

A first order approximation can be obtained assuming $\Delta z \to 0$ that implies $C_{x_b}\, R_{x_b} \to 0$, in this case we have

$$P_{x_b} - \left(P_{x_{b-}} - R_{x_b}\, Q_{x_b}\right) = \mathcal{O}(\Delta z^2) \tag{12}$$

taking into account eq. (10), we have a simple first order approximation of inside baroreceptor pressure:

$$P_{x_b} = P_{x_{b-}} \left(1 + \frac{R_{x_b}}{R_{x_{b-}}}\right) + R_{x_b}\, C_{x_{b-}}\, \dot{P}_{x_{b-}} - \frac{R_{x_b}}{R_{x_{b-}}}\, P_{in_{x_{b-}}} + \mathcal{O}(\Delta z^2) \tag{13}$$

This model relates the inside baroreceptor pressure P_{x_b} to the pressure in the upward vascular compartment.

We consider now the mechanical deformation of the carotid sinus wall induced by intrasinus pressure changes. The conception of a realistic model needs a deep knowledge of the carotid wall tissue structure and characteristic.

Modelling of the pressure-deformation transduction process.

Assuming the following spatial arrangement of the receptors, as shown in fig. (10):

- the stretch-receptors are in the middle of the vessel wall, in fact the baroreceptor nerve terminals are located along the media-adventitial border and in the deep layers of the adventitia of the sinus wall [73].
- the vessel wall is constituted by both smooth muscles, collagens and elastic membrane constituting three coats: intima, media and adventitia. The carotid sinus wall contains only small amounts of smooth muscle but a high elastic content. The thin intima layer comprises endothelial cells, and an internal elastic membrane. Tunic media comprises alternating layers of concentric elastic membranes and longitudinal and circular smooth muscle cells. Thick adventitia layer comprises

elastic and collagen fibers with external elastic membrane establishing the border between the media and adventitia. The latter consists of a network of collagenous fibers within which smooth muscle cells are interspersed in a parallel organisation and which encases the external elastic lamina. The special arrangement of collagen and smooth muscle within the arterial wall forms a "jacket" which controls the distensibility of the artery [73].

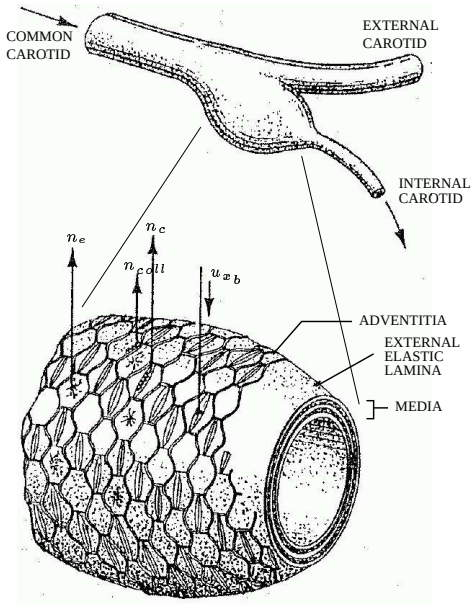

Figure 10: *Spatial arrangement of baroreceptor (bottom) within the carotid sinus wall and their innervations, from [72, 73]. In [73], it was assumed that baroreceptor activity originates from receptors mechanically linked to the three specific wall structures : elastin , collagen fibers and smooth muscles (receptors outputs are respectively* n_e, n_{coll}, n_c*). The ANS control smooth muscle contraction by local sympathetic efferent activity (baroreceptor smooth muscle input* u_{x_b} *with* $x = A, C, T, ap$*). We will demonstrate that information provided by collagen and elastin receptors is sufficient for blood pressure tranduction process.*

- the gross baroreceptor nerve is envisioned as consisting of a mixture of three fiber types A, B, and C. Discharge patterns, threshold characteristic, adaptation dynamics and conduction velocity have been studied. C-fibers have a slow conduction velocity (0.5 and 1.8 m/s^{-1}), a lower discharge rate, an high adaptation time-constant and a higher threshold pressure. In contrast, A-fibers have a much higher conduction velocity, a higher discharge rate, a small adaptation time-constant and a lower threshold pressure, [73, 112]. The relationship between discharge rate and nerve conduction is outside the aim of this report, but by applying nerve modelling concepts, based on partial differential equations and on Hodgkin-Heuxley formalism, it is possible to demonstrate that the higher is the discharge rate the higher is the conduction velocity, i.e. the higher is the pressure error the faster will be the response. Similarly to [73], we can assume that baroreceptor activity originates from: (i) collagen receptors located within the adventitial collagenous fibers, n_{coll} in fig. (10) (ii) elastin receptors located within the external elastic membrane, n_e in fig. (10). We will demonstrate that information provided by these receptors is sufficient for blood pressure transduction process. Smooth

muscle receptors are not strictly necessary, therefore, they can provide complementary information or they does not exist. Clear information about this topic is not available. Interestingly, there are smooth muscles located within the adventitial smooth muscles which are innervated by sympathetic efferents u. Stimulation of these efferents causes an increase in the baroreceptor nerve activity, a decrease in the carotid sinus diameter and its elastic modulus. This effect is evident for intrasinus pressure below 130 mmHg, above 130 mmHg this effect is largely reduced and it disappears at very high intrasinus pressures.

Assuming the following functioning of the receptors:

- these receptors are sensible to the time derivative of the stress. Some researchers assumed that they are sensible to the strain and/or to the time derivative of the strain, [73]. In fact, assuming that (i) locally, ionic channels are sensible to time derivative of the strain and (ii) local strain and fiber stress are linearly related, we can related firing rate to the time derivative of the fiber stress. Therefore, the two assumptions are not different. Regardless of receptor spatial location, stretch-receptors lie in parallel with the wall structures whose deformation is being monitored.
- at normal blood pressure the collagen fibers are not strained, i.e. they are buckled, and the elastic modulus of the elastin tissue dominates in determining the shape of the carotid sinus pressure-deformation curve.
- as the intrasinus pressure increases above the normal blood pressure, "recrutement" of collagen fibers causes an increase in the elastic modulus with a corresponding decrease in distensibility. This means that the collagen fibers, which are buckled at low pressure, become taut as the sinus expands, thereby taking up an increasing portion of the stress.
- at considerably higher intrasinus pressure (hypertensive levels), the excessive stretching of the wall also stretches the smooth muscles anchored to the collagen fibers as well as stretching the collagen fibers.
- the observed sigmoidal pressure-firing rate relationship seems to be more related to the deformation-firing rate transduction process than to the pressure-deformation transduction process, [73];
- the baroreceptor impulse has an inhibitory effect on the vasomotor center and on the sympathetic outflow.

Elastin element modelling

We can write a linear stress-strain relationship for elastin fibers strain ε_e and stress σ_e [45]

$$\sigma_e = \mathcal{H}_e(\varepsilon_e) = k_e \varepsilon_e \tag{14}$$

Collagen fiber modelling

Strain-stress relation in collagen fibers can be modelled by a visco-elastic rate-independent differential equation. In fact, the visco-elastic rate-independent salient feature of collagen fibers has been already observed [45] and is taken into account from the beginning of the modelling procedure. For simulation purposes, a model which is able to reproduce these observations can be constructed as follows. Defining $\beta = \Sigma(\sigma)$ where $\Sigma : \mathcal{R} \to \mathcal{R}$ is a monotonic function such as $\Sigma(0) = 0$, for collagen fiber modelling, we propose

$$\left[1 + sgn(\dot{\beta}\,\beta)\right]\ (\tau_+\ \dot{\varepsilon}\ +\ |\dot{\beta}|\ \varepsilon)\ =\ 2\ \varepsilon_o\ \dot{\beta}\ +\ \tau_-\ \dot{\varepsilon}\ \beta\ \frac{\varepsilon_o}{\varepsilon}\ \left[1 - sgn(\dot{\beta}\ \beta)\right] \tag{15}$$

where $\varepsilon_o > 0$ correspond to the maximal deformation, i.e. $|\varepsilon(t)| < \varepsilon_o$. By eq. (15) we explicitly separate the stretching/contracting ($|\beta| \nearrow$) characteristic of collagen fibers from the relaxation ($|\beta| \searrow$) characteristic. In fact:

$$\begin{cases} \tau_+ \dfrac{d\varepsilon}{|d\beta|} = -\varepsilon + \varepsilon_o \dfrac{d\beta}{|d\beta|} & |\beta| \nearrow \\ \tau_- \dfrac{d\varepsilon}{|d\beta|} = \dfrac{\varepsilon}{|\beta|} & |\beta| \searrow \end{cases} \tag{16}$$

Eq. (16) demonstrates the rate-independent property of eq. (15). By Fung's terminology, eq. (16) is an incremental constitutive law of viscoelasticity, [45].

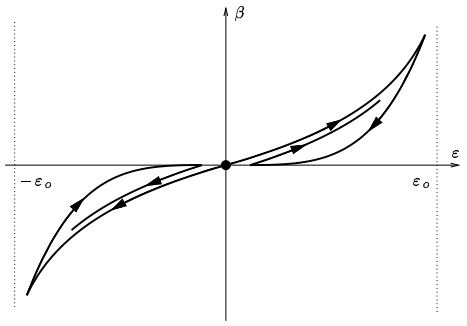

Figure 11: *Rate-independent $\beta - \varepsilon$ characteristic of collagen fibers as defined by eq. (16).*

Fig. (11) shows two trajectories starting from the origin. Eq. (16) underlines the role of the τ_+ and τ_- parameters: τ_+ is a stress space-constant and regulates the exponential $\beta - \varepsilon$ relationship, whereas τ_- is without unit and the greater it is the faster β tends to zero during relaxation. Both of them act for large stress and strain values, whereas the monotonic function $\Sigma(\sigma)$ can be chosen to reproduce collagen fiber σ-ε relationship for little stress and strain values. In fact, for little strain values, collagen fibers are

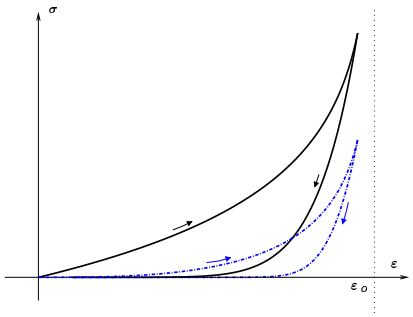

Figure 12: *Rate-independent $\sigma - \varepsilon$ characteristic of collagen fibers as defined by eq. (16). Continuous lines stand for $\sigma = \beta$ choice, whereas dotted line stands for $\sigma = \beta^{(b+1)}/(\beta^b + a^b)$ (with $a > 0$ and $b > 1$) choice to have an exponential σ-ε relationship for large σ, ε values and a backlash for small σ, ε values.*

characterised by a backlash corresponding to negligible strain values as they are buckled. Taking $\beta = \sigma$ in eq. (15) this characteristic is not reproduced. Hence, thanks to the $\Sigma(\sigma)$ monotonic function, we can adapt eq. (15) to the stress-strain relationship for little σ and ε values maintaining an exponential σ-ε relationship when ε approaching the maximal strain value ε_o, as already described for the parallel element of the contractile element [96]. Fig. (12) shows two different trajectories in the $\sigma - \varepsilon$ plane when we chose either $\beta = \sigma$ or $\sigma = \beta^{(b+1)}/(\beta^b + a^b)$, with $a > 0$ and $b > 1$. The second choice reproduces better the backlash zone of the collagen fiber $\sigma - \varepsilon$ characteristic than the first choice.

Smooth muscle modelling

A simplified version (without active relaxation) of the model of the contractive element, developped in [10], is considered. It provides the $\sigma_{x_b} = \mathcal{H}_{x_b}(\varepsilon_x, u_{x_b})$ with $x = A, C, T, ap, vs$. We consider now one contractile element in a general baroreceptor and, to simplify notations, we used a c index for contractile element variables. So the $\sigma_c = \mathcal{H}_c(\varepsilon_c, u_{x_b})$ relationship is:

$$\begin{cases} \dot{k}_c &= -\left(u_{x_b} + |\dot{\varepsilon}_c|\right)\, k_c + k_{c_0}\, u_{x_b} \\ \dot{\tilde{\sigma}}_c &= -\left(u_{x_b} + |\dot{\varepsilon}_c|\right)\, \tilde{\sigma}_c + k_c\, \dot{\varepsilon}_c + \sigma_{c_0}\, u_{x_b} \\ \sigma_c &= d_o(\varepsilon_c)\, \left(k_c\, \xi_0 + \tilde{\sigma}_c\right) + \eta\, \dot{\varepsilon}_c \end{cases} \tag{17}$$

as already introduced for heart modelling, see paragraph (2.1.2).

Vessel wall modelling

The organisation of the elastin, collagen and contractive elements (fig. (13)) implies, for small deformations and small membrane thickness, the following relationships

$$\begin{cases} \bar{l}_{coll_1}\, (1 + \varepsilon_{coll_1}) + \bar{l}_{coll_2}\, (1 + \varepsilon_{coll_2}) = \bar{l}_e\, (1 + \varepsilon_e) & (18a) \\ \bar{l}_{coll_2}\, (1 + \varepsilon_{coll_2}) = \bar{l}_c\, (1 + \varepsilon_c) & (18b) \\ \sigma_{coll_1}\, (\bar{h}_c + \bar{h}_{coll_2}) = \sigma_c\, \bar{h}_c + \sigma_{coll_2}\, \bar{h}_{coll_2} & (18c) \end{cases} \tag{18}$$

where $\bar{l}_e$, $\bar{l}_c$, $\bar{l}_{coll_i}$ (i=1, 2) are unstrained lengths of the elastin, contractive and collagen element, respectively, and $\bar{h}_e$, $\bar{h}_c$, $\bar{h}_{coll_2}$ ($\bar{h}_{coll_1} = \bar{h}_c + \bar{h}_{coll_2}$) are the "constant" width of the elastin, contractive and collagen layers, respectively. We assumed constant widths to simplify the model.

From the ANS point of view, the knowledge of collagen strains, i.e. ε_{coll_1}, ε_{coll_2}, and stress, i.e. σ_{coll_1}, σ_{coll_2}; of elastin strain, i.e. ε_e, and of the command values u_x allows the estimation of the other system parameters, in particular the inner baroreceptor pressure P_{x_b}:

$$P_{x_b} = \frac{2\,\pi\,\left[\sigma_{coll_1}\, \left(\bar{h}_c + \bar{h}_{coll_2}\right) + \sigma_e\, \bar{h}_e\right]}{\bar{l}_e\, (1 + \sigma_e/k_e)} + P_{ext} \tag{19}$$

where P_{ext} is an external pressure that can be considered as an external constant pertubation.

The strategic location of smooth muscles cells within the adventitial collagenous net, with their sympathetic innervation, provides for a mechanism by which neural stimuli could alter the mechanical properties of the sinus wall and the stress-strain relationship of the receptors involved. This mechanism can be used by ANS to estimate the intrasinus blood pressure, as we will discuss in the following paragraphs.

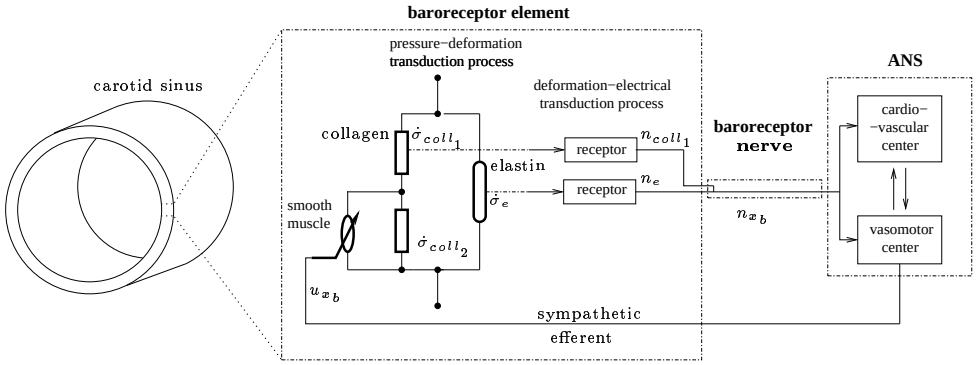

Figure 13: *Simplified model of spatial arrangement of elastin, collagen and smooth muscle elements within the carotid sinus wall, illustrated in fig. (10).* u_{x_b} *(*$x = A, C, T, ap$*) is the local sympathetic control of the slow and weak smooth muscles.* n_{x_b} *(*$x = A, C, T, ap$*) is the firing rate recorded on the baroreceptor nerve.*

Modelling of the deformation-firing rate transduction process

To model the deformation-firing rate transduction process, we used a simplified version of the model proposed by Ottesen in [112] which related intrasinus pressure to neural activity (only two firing rate ranges are considered here to code $\dot{\sigma}_{coll_1}$ and $\dot{\sigma}_e$). Assuming that stretchreceptors are sensibles to the time derivative of the stress:

$$\begin{cases} \dot{n}_{coll_1} = k_{coll_1}\ \dot{\sigma}_{coll_1}\ \frac{n_{coll_1}\ (M_{coll_1} - n_{coll_1})}{(M_{coll_1}/2)^2}\ -\ \frac{1}{\tau_{coll_1}}(n_{coll_1} - N_{coll_1}) \\ \dot{n}_e = k_e\ \dot{\sigma}_e\ \frac{n_e\ (M_e - n_e)}{(M_e/2)^2}\ -\ \frac{1}{\tau_e}(n_e - N_e) \qquad\qquad x = A, C, T, ap \\ n_{x_b} = k_1\ n_{coll_1}\ +\ k_2\ n_e \end{cases} \tag{20}$$

where $\dot{n}$ denotes the time derivative of the firing rate n, $\dot{\sigma}$ the time derivative of the stress, k is a proportional constant, M the maximal firing rate, τ a characteristic time constant describing the resetting and N the threshold, i.e. the positive and stable equilibrium value which the firing rate approaches when no change in pressure appears. Remarks that eq. (20) has, implicitly, all the well known characteristics of the baroreceptor response to blood pressure stimulation: asymmetric sigmoidal shape depending on the direction of strain changes, resetting mechanisms and, finally, it does not depend of strain value, therefore, it can be easily applied to normo-, hyper- or hypo-tensive subjects after a transient due to the baroreceptor adaptation. Ottesen, using eq. (20), was able to reproduce classical experimental findings concerning the blood pressure-baroreceptor nerve activity relationship. A question arises: if eq. (20) really describe deformation-firing rate transduction process, how is it possible for the ANS to estimate the inner pressure in the baroreceptor P_{x_b}?

Pressure estimation by a tonic control of weak, slow smooth muscle elements

The estimation is not a trivial task because, as indicated by (19), σ_{coll_1} and σ_e are required, but as it appears in (20), the output of the baroreceptor are $\dot{\sigma}_{coll_1}$ and $\dot{\sigma}_e$: there is not reference stress. In fact, we will show that the presence of the stress deadzone in the $\sigma - \varepsilon$ collagen characteristic, makes possible the estimation of the stresses for some particular time instants.

Looking at the scheme in fig. (13), we will demonstrate that ANS can estimate $P_{x_b} - P_{ext}$ by the knowledge of the history of $\dot{\sigma}_{coll_1}$, $\dot{\sigma}_{coll_2}$ and $\dot{\sigma}_e$ and by a tonic control of weak, slow smooth muscle elements. The tonic control made by the chemical control u_c of smooth muscle consists of the $u_x = 0$, for high pressure values, and $u = u_x^{max} > 0$ for slow pressures values.

Estimation problem

- estimate collagen and elastin stresses $\sigma_{coll_1}(t)$, $\sigma_e(t)$ (and hence $P_{x_b} - P_{ext}$) from their time derivatives $\dot{\sigma}_{coll_1}(t)$, $\dot{\sigma}_e(t)$.

Assumptions

- an alternance of diastolic ($\dot{P}_{x_b} \leq 0$) and systolic ($\dot{P}_{x_b} > 0$) phases takes place. We note $T_n = [t_n, t_{n+1}]$ so that T_{2n} will represent diastolic phases and T_{2n+1} systolic phases, $n = 0, 1 \ldots$
- collagen characteristic is idealized, as shown in fig. (14), and we assume that ANS has an *a priori* estimation of k_e and of $\bar{\varepsilon}_i$ ($i = 1, 2$), the upper limits of the deadzone;
- σ_c is nearly constant, in the following we suppose $\sigma_c = \bar{\sigma}_c \geq 0$. Then, by eq. (18c), $\dot{\sigma}_{coll_1} = \frac{\bar{h}_{coll_2}}{\bar{h}_c + \bar{h}_{coll_2}} \dot{\sigma}_{coll_2}$;
- we assume that there is always an instant in the recent past where collagen enters into the deadzone. More precisely, noting

$$z(n) = \max\{n_o | n_o \leq n,\ \dot{\sigma}_{coll_1}(t_{2n_o}) < 0 \text{ and } \exists t \in T_{2n_o},\ \dot{\sigma}_{coll_1}(t) = 0\} \tag{21}$$

we assume that $\sup_n(n - z(n)) < +\infty$. In the following, we will note:

$$\bar{t}_{2z(n)} = \min\left\{t | t \in T_{2z(n)},\ \dot{\sigma}_{coll_1}(t) = 0\right\} \tag{22}$$

Properties:

$$\forall t\ \dot{\sigma}_e(t) \neq 0 \text{ and } \dot{\sigma}_{coll_i}(t) = 0\ (i = 1, 2) \Rightarrow \sigma_{coll_1}(t)\ \sigma_{coll_2}(t) = 0 \tag{23}$$

Proof: $\dot{\sigma}_e \neq 0 \Rightarrow \dot{\varepsilon}_e \neq 0 \Rightarrow |\dot{\varepsilon}_{coll_1}| + |\dot{\varepsilon}_{coll_2}| > 0$, with (18c). Then $\dot{\varepsilon}_{coll_i} \neq 0$ (i=1 or 2) and $\dot{\sigma}_{coll_i} = \mathcal{H}'_{coll}(\varepsilon_{coll_i})\ \dot{\varepsilon}_{coll_i} = 0 \Rightarrow \mathcal{H}'_{coll}(\varepsilon_{coll_i}) = 0 \Rightarrow \sigma_{coll_i} = 0$ (i=1 or 2).

$$\forall n,\ \forall t \in T_{2n}\ \dot{P}_{x_b}(t) \leq 0 \Rightarrow\ \dot{\sigma}_e(t) \leq 0 \text{ and } \dot{\sigma}_{coll}(t) \leq 0 \tag{24}$$

Proof: $A_{x_b}(\Delta P_{x_b})$ and $\mathcal{H}_x(\varepsilon_x)$ ($x = e$, *coll*) are monotonic functions.

$$\forall n,\ \forall t \in T_{2n+1}\ \dot{P}_{x_b}(t) > 0 \Rightarrow\ \dot{\sigma}_e(t) > 0 \text{ and } \dot{\sigma}_{coll}(t) \geq 0 \tag{25}$$

Proof: $A_{x_b}(\Delta P_{x_b})$ and $\mathcal{H}_x(\varepsilon_x)$ ($x = e$, *coll*) are monotonic functions.

Estimation of $P_{x_b}(t) - P_{ext}$

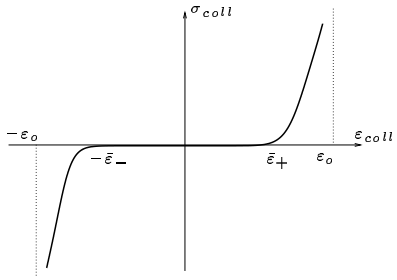

Figure 14: *Idealized* $\sigma_{coll} = \mathcal{H}_{coll}(\varepsilon_{coll})$ *relationship of collagen fibers.*

$P_{x_b}(t) - P_{ext}$ can be estimated by:

$$\begin{cases} \hat{\sigma}_{coll_1}(t) = \hat{\sigma}_{coll_1}(\bar{t}_{2z(n)}) + \displaystyle\int_{\bar{t}_{2z(n)}}^{t} \dot{\sigma}_{coll_1}(t)\, dt \\ \\ \hat{\sigma}_e(t) = \hat{\sigma}_e(\bar{t}_{2z(n)}) + \displaystyle\int_{\bar{t}_{2z(n)}}^{t} \dot{\sigma}_e(t)\, dt \\ \\ \hat{P}_{x_b}(t) - \hat{P}_{ext} = \dfrac{2\,\pi\,\left[\hat{\sigma}_{coll_1}(t)\,\left(\bar{h}_c + \bar{h}_{coll_2}\right) + \hat{\sigma}_e(t)\,\bar{h}_e\right]}{\bar{l}_e\,(1 + \hat{\sigma}_e(t)/k_e)} \end{cases} \tag{26}$$

where

$$\begin{cases} \hat{\sigma}_e(\bar{t}_{2z(n)}) = k_e\,\left(\dfrac{\bar{l}_{coll_1}\,(1 + \max\left(\varepsilon_{1+}, \mathcal{H}^{-1}_{coll_1}(\bar{\sigma}_c)\right) + \bar{l}_{coll_2}\,(1 + \varepsilon_{2+})}{\bar{l}_e} - 1\right) \\ \\ \hat{\sigma}_{coll_1}(\bar{t}_{2z(n)}) = \bar{\sigma}_c\,\dfrac{\bar{h}_c}{\bar{h}_c + \bar{h}_{coll_2}} \end{cases} \tag{27}$$

$\bar{t}_{2z(n)}$ being given by (21) and (22).

Proof:

The ANS can estimate the time instant $t_{2z(n)}$ by eqs. (21) and (22), and then, by properties (23)-(25), the stress and strain in all vascular elements are given by:

$$\begin{cases} \varepsilon_{coll_1}(t_{2z(n)}) \approx \max\left(\bar{\varepsilon}_{1+}, \mathcal{H}^{-1}_{coll_1}(\bar{\sigma}_c)\right) \\ \\ \varepsilon_{coll_2}(t_{2z(n)}) \approx \bar{\varepsilon}_{2+} \\ \\ \sigma_{coll_1}(t_{2z(n)}) \approx \bar{\sigma}_c\,\frac{\bar{h}_c}{\bar{h}_c + \bar{h}_{coll_2}} \\ \\ \sigma_{coll_2}(t_{2z(n)}) \approx 0 \end{cases}$$

Hence, by the integration of the measurements and by eq. (19), (26) follows.

Comments:

1. The estimation of $P_{x_b}(t) - P_{ext}$ is based on the detection of "buckled collagen fiber" condition during a local diastolic phase;

2. The oscillating behaviour of the inside blood pressure allows intrasinus blood pressure estimation, in steady condition blood pressure estimation will be not possible.

3. The presence of elastin elements is not sufficient for blood pressure estimation, collagen fibers are needed.

4. Blood pressure estimation is finally very simple and needs the knowledge of k_e, $\bar{\varepsilon}_{i+}$ $(i = 1, 2)$, $\bar{\sigma}_c$ and an accurate observation of the sign of $\dot{\sigma}_{coll}$ and the history of $\dot{\sigma}_{coll}$ and $\dot{\sigma}_e$.

5. Blood pressure estimation can be made by a very simple smooth muscle control law: $\bar{\sigma}_c = 0$ or $\bar{\sigma}_c = \sigma_c^{max} > 0$. By eq. (26) we can conclude that active blood pressure estimation ($\bar{\sigma}_c = \sigma_c^{max}$) is useful only for high blood pressure values, whereas passive blood pressure estimation without smooth muscle contraction ($\bar{\sigma}_c = 0$) can be used for low blood pressure values, using eq. (27).

In the following, we assume that the ANS knows the arterial blood pressure P_{x_b} at the baroreceptor level.

2.1.4 Active vascular compartment modelling

We are now interested to model an active vascular compartment, as the one shown in fig (15). The aim of this paragraph is to find a dynamical relationship between local cross-sectional area A_x, local pressure difference $P_x - P_{x_o}$ and local chemical command of smooth muscles u_x, with $x = ULv, TTL$.

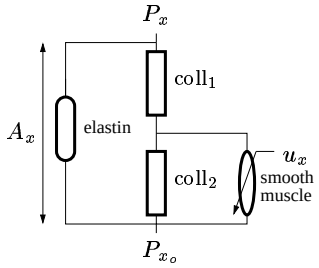

Figure 15: *Simplified rheological model of a vascular compartment x. u_x is the chemical command of smooth muscles. P_{x_o} is an external pressure that can be considered as an external constant perturbation. P_x is the blood pressure in the vascular compartment. A_x is the cross-sectional area of the vascular compartment. Assuming a constant length of the vascular compartment $\bar{l}_x$, the volume of the x vascular compartment is given by $V_x = \bar{l}_x\, A_x$.*

We assume that vascular wall structure is similar to baroreceptor wall structure, so the rheological diagram shown in fig. (15) is the same of the one shown in fig. (13). To describe collagen, elastin and smooth muscle elements, we considered the same stress-strain relationships introduced at paragraph (2.1.3).

Considering eqs. (17), (18), (19) and an idealized stress-strain model for collagen element, see fig. (14), for example

$$\sigma_{coll_i} = \mathcal{H}_{coll_i}(\varepsilon_{coll_i}) = k_{coll_i} \; |e^{\frac{\varepsilon_{coll_i} - \varepsilon_{i+}}{\tau_{i+}}} - 1|_+ \quad i = 1, 2 \qquad \text{with } \varepsilon_{coll_i} \ll \varepsilon_o$$

Noting V_x and $\bar{l}_x$ the volume and length, respectively, of x vascular compartment, we can write:

$$\begin{cases} \varepsilon_e(V_x) = \sqrt{\dfrac{4\,\pi\,V_x}{\bar{l}_e^2\,\bar{l}_x}} \; - 1 \\ \varepsilon_{coll_2}(\varepsilon_{c_x}) = \dfrac{\bar{l}_c}{\bar{l}_{coll_2}}\,(1 + \varepsilon_{c_x}) \; - 1 \\ \varepsilon_{coll_1}(V_x, \varepsilon_{c_x}) = \dfrac{\bar{l}_e}{\bar{l}_{coll_1}}\,(1 + \varepsilon_e(V_x)) \; - \dfrac{\bar{l}_c}{\bar{l}_{coll_1}}\,(1 + \varepsilon_{c_x}) \; - 1 \\ \sigma_{c_x}(V_x, \varepsilon_{c_x}) = \frac{\bar{h}_{coll_2} + \bar{h}_c}{\bar{h}_c}\,\mathcal{H}_{coll_1}(\varepsilon_{coll_1}(V_x, \varepsilon_{c_x})) \; - \frac{\bar{h}_{coll_2}}{\bar{h}_c}\,\mathcal{H}_{coll_2}(\varepsilon_{coll_2}(\varepsilon_{c_x})) \end{cases}$$

Finally, a dynamic model of the active Windkessel compartment has four state variables: k_{c_x}, $\tilde{\sigma}_{c_x}$, ε_{c_x}, V_x. Considering P_{in} and Q_x as inputs, the model is:

$$\begin{cases} \dot{k}_{c_x} & = -(u_x \; + \; |\dot{\varepsilon}_{c_x}|)\; k_{c_x} \; + \; k_{c_{x_o}}\, u_x \\ \dot{\tilde{\sigma}}_{c_x} & = -\;(u_x \; + \; |\dot{\varepsilon}_{c_x}|)\; \tilde{\sigma}_{c_x} \; + \; k_{c_x}\, \dot{\varepsilon}_{c_x} \; + \; \sigma_{c_{x_o}}\, u_x \\ \dot{\varepsilon}_{c_x} & = \dfrac{1}{\eta_x}\{d_o(\varepsilon_{c_x})\;\,[k_{c_x}\;\xi_0 + \tilde{\sigma}_{c_x}] \; - \; \sigma_{c_x}(V_x, \varepsilon_{c_x})\} \\ \dot{V}_x & = -Q_x \; - \; [\Delta P_x(V_x, \varepsilon_{c_x}) - P_{in} + P_{x_o}]\; \dfrac{V_x^2}{8\,\pi\,c_v\,\mu\,\bar{l}_x^3} \\ \text{where} \quad \Delta P_x(V_x, \varepsilon_{c_x}) & = \dfrac{2\,\pi\,\{[\bar{h}_c \; + \; \bar{h}_{coll_2}]\;\,\mathcal{H}_{coll_1}(\varepsilon_{coll_1}(V_x, \varepsilon_{c_x})) \; + \; k_e\,\bar{h}_e\,\varepsilon_e(V_x)\;\}}{\bar{l}_e\;[1 + \varepsilon_e(V_x)]} \end{cases} \tag{28}$$

if Q_{in} is given instead of P_{in}, we can use

$$Q_{in} = [\Delta P_x(V_x, \varepsilon_{c_x}) - P_{in} + P_{x_o}]\; \frac{V_x^2}{8\,\pi\,c_v\,\mu\,\bar{l}_x^3}$$

Interestingly, blood pressure in the x active vascular compartment is an output variable and not a state variable as in passive case. Remark the similitude between the heart model eq. (9) and this active vascular compartment model eq. (28).

2.2 Cardiovascular short-term control

2.2.1 Local control of vascular smooth muscles

There is a local control of cross-sectional area-pressure relationship as well known in physiology [53]. We expressed it as a feedback law:

$$u_x = u_{x_R} - \alpha\ [O_2]_x \qquad x = ULv,\ TLL \tag{29}$$

where u_{x_R} is the reference values for smooth muscle chemical command in the x vascular compartment

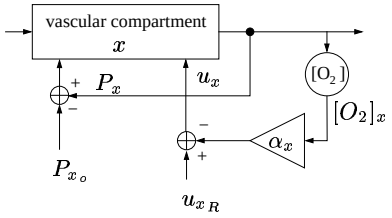

Figure 16: *Simplified functional diagram of the interaction between local and central control of vascular smooth muscle in a x vascular compartment.* u_{x_R} *is the reference values for smooth muscle chemical command coming from the ANS.* $[O_2]_x$ *is a local information on oxygen concentration which affects smooth muscle contraction.* P_{x_o} *is an external pressure that can be considered as an external constant perturbation.* P_x *is the blood pressure in the vascular compartment.*

provided by the α sympathetic efferent nerves of the ANS. But locally, to assure a good supply of oxygen to working muscles $[O_2]_x$, these set-points can be corrected or not. We represent this last mechanism with a dependence upon $[O_2]_x$ as shown in fig. (16) and in eq. (29).

2.2.2 Beat-to-beat estimation of aortic blood flow

We relate the time-average aortic blood flow to time-discrete cardiovascular variables.
Considering the model of the heart introduced at paragraph (2.1.2), eq. (9), and the model of the ascending aorta compartment introduced at paragraph (2.1.1), eq. (8):

$$\begin{cases} \dot{V}_L = \dfrac{|P_{vp} - P_{H_L}|_+}{R_{vp}} - \dfrac{|P_{H_L} - P_A|_+}{R_A(P_A - P_{A_o})} \\ \\ Q_A = -C_A(P_A - P_{A_o})\,\dot{P}_A + |\dot{V}_L|_- \end{cases} \tag{30}$$

We assume $C_A(\Delta P) = \frac{d\Gamma_A}{d\Delta P}(\Delta P)$ (for example $\Gamma_A(\Delta P) = C_{A_0}\ \Delta P + C_{A_1}\ (\Delta P)^2$, considering eqs. (2) and (6).
Assumption

- an alternance of blood ejecting ($\dot{V}_L < 0$) and heart relaxing, filling, contracting ($\dot{V}_L \geq 0$) phases takes place. We note $I_m = [t_m, t_{m+1}]$ ($m = 0,\ 1,\ \ldots$) so that I_{2m} represent the m-th heart ejecting phase, I_{2m+1} represent the m-th heart relaxing, filling and iso-volumic contracting phase;
- we assume, and physiologicaly have, that $\forall t$, $P_{vp}(t) < P_A(t)$, i.e. blood pressure in the pulmonary venous compartment $P_{vp}(t)$ is always smaller than the pressure in the ascending aorta compartment P_A;

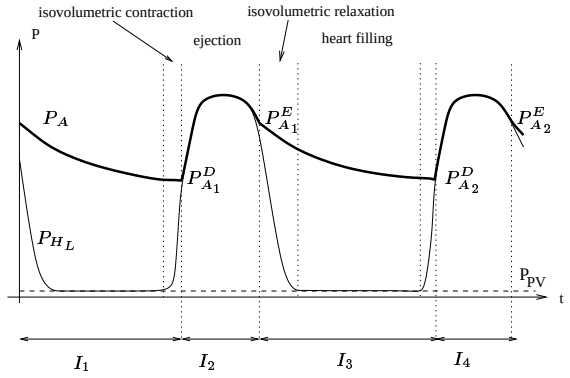

Figure 17: *Idealised pressure curves in the left ventricle P_{H_L} and in the ascending aorta P_A. The cardiac cycle is split in systolic and diastolic phases.*

Noting

- $HR_m = t_{2m} - t_{2m-2}$ is the m-th heart rate;
- $P^D_{A_m} = P_A(t_{2m})$ is the m-th aortic diastolic pressure;
- $P^E_{A_m} = P_A(t_{2m+1})$ is the aortic pressure at the end of the m-th heart ejection;
- $V^D_{A_m} = V_A(t_{2m})$ is the blood volume in the ascending aorta compartment at the end of the m-th isovolumetric phase;
- $V^E_{A_m} = V_A(t_{2m+1})$ is the blood volume in the ascending aorta compartment at the end of the m-th ejection;
- $V^D_{L_m} = V_L(t_{2m})$ is the left ventricular volume at the end of the m-th isovolumetric phase;
- $V^E_{L_m} = V_L(t_{2m+1})$ is the left ventricular volume at the end of the m-th ejection;

$\bar{Q}_{A_m} \stackrel{\text{def}}{=} HR_m \int_{t_{2m-2}}^{t_{2m}} Q_A(t)\,dt$ is given by

$$\bar{Q}_{A_m} = HR_m \left\{ \left[C_A(P^D_{A_{m-1}} - P_{A_o})\, P^D_{A_{m-1}} - C_A(P^D_{A_m} - P_{A_o})\, P^D_{A_m} \right] + V^D_{L_{m-1}} - V^E_{L_{m-1}} \right\} \tag{31}$$

Proof

By definition, $\bar{Q}_{A_m}$ can be calculated as

$$\bar{Q}_{A_m} = HR_m \left[\int_{t_{2m-2}}^{t_{2m-1}} Q_A(t)\,dt + \int_{t_{2m-1}}^{t_{2m}} Q_A(t)\,dt \right]$$

but $\forall t \in I_{2m}, \dot{V}_L(t) > 0$ and $\forall t \in I_{2m+1}, \dot{V}_L(t) \leq 0$, and $C_A(P_A - P_{A_o})\dot{P}_A = \dot{V}_A$, hence

$$\bar{Q}_{A_m} = -HR_m \left[\int_{t_{2m-2}}^{t_{2m-1}} \left(\dot{V}_A(t) + \dot{V}_L(t) \right) dt + \int_{t_{2m-1}}^{t_{2m}} \dot{V}_A(t)\,dt \right]$$

and, solving,

$$\bar{Q}_{A_m} = HR_m \left[V^D_{A_{m-1}} - V^D_{A_m} + V^D_{L_{m-1}} - V^E_{L_{m-1}} \right]$$

and expressing $V^D_{A_{m-1}}$ and $V^D_{A_m}$ by $\Gamma_A(\Delta P)$, we have eq. (31).

2.2.3 Feedbacks in cardiovascular short-term control

The autonomic nervous system regulates blood flow and arterial blood pressure through sympathetic and parasympathetic neural innervation, u_s and u_v on fig. (18). Sympathetic and parasympathetic (vagal) have an antagonistic effect on heart rate: the sympathetic is a slow accelerator and the parasympathetic a fast inhibitor. Therefore, heart rate is the result of the autonomic balance on the cardiac pacemaker

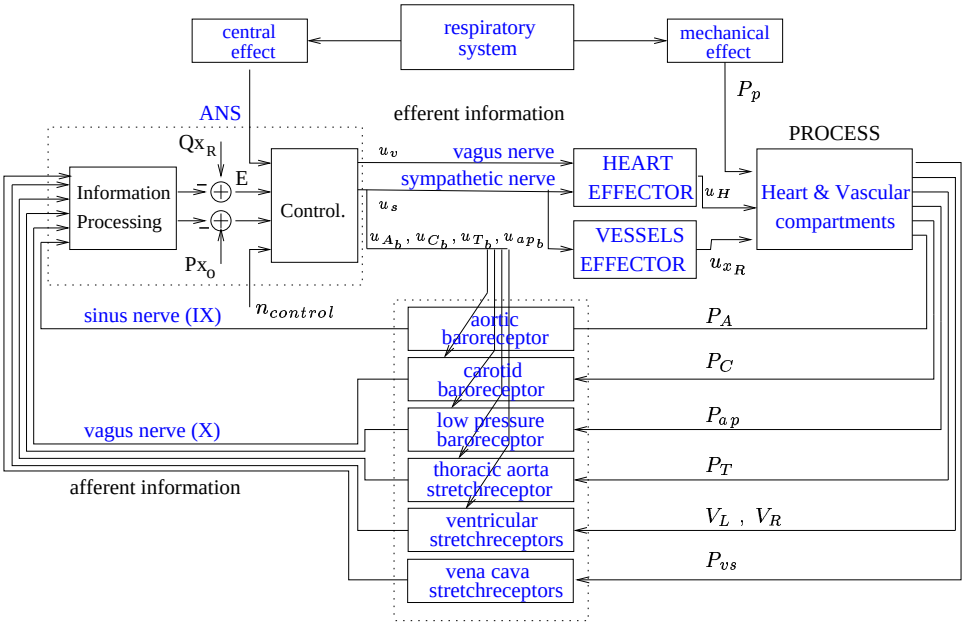

Figure 18: *Diagram of the feedback control loop in the cardiovascular system. Through the sympathetic and parasympathetic neural innervation, u_s and u_v, the ANS control the cardiovascular system regulating the heart function (rate HR_r and stroke volume SV_R) and the blood vessel resistance and compliance R_{x_R} and C_{x_R}, respectively, through vessel constriction. Respiratory system has both a central and mechanical effect on cardiovascular control. Mechanical effect is function of the pulmonary volume V_p and pulmonary pressure P_p. In our point of view, blood flow is the controlled variable, Q_R the reference input for blood flow regulation, E the error or actuating signal and P_A, P_C, P_{ap} and P_T are the aortic, the carotidian, the pulmonary and the thoracic aortic blood pressure. Blood flow could be estimated by afferent information coming from baroreceptors.*

firing rate. In addition, the sympathetic component u_s has a slow cardiac contractive force effect and a

slow vasoconstrictor effect on the vessels. Respiratory system has both a central and mechanical effect on cardiovascular control. In fact in the nervous system the respiratory and cardiovascular centers may interact each other (central effect) and the respiratory activity has a mechanical effect by stretching and/or collapsing pulmonary and thoracic vessels, this is function of the pulmonary pressure P_p.

We can describe the control of the cardiovascular system in the standard form of a physical feedback system, as illustrated in fig. (18). The aortic blood pressure (P_A) and the carotidian blood pressure (P_C) are the measured variables in the high pressure circulatory system. P_T represents the blood pressure in the thoracic aorta and P_P is the blood pressure (or the venous volume) measured by the low pressure receptors. The aortic and carotid sinus baroreceptors, the thoracic aorta stretch-receptors and the low pressure baroreceptors are the pressure sensors which generate the afferent neural information. The cardiovascular system is the controlled process and the autonomic nervous system (ANS) is the controller. In our point of view, the ANS may regulate blood flow in the different parts of the cardiovascular system, in the head as well as in the general systemic part, maintaining a particular sensible blood pressure, i.e. in the head, the lungs and the ascending aorta, within normal limits ($P_{x_{min}} \leq P_x \leq P_{x_{max}}$, x=A, C, P) to avoid tissue damages and vessel collapses. In fact, blood flow (Q_x) could be estimated by afferent information and the ANS could control effectors in order to maintain small the difference (E) between the estimated blood flow ($\hat{Q}_x$) and the reference value (Q_{x_R}), see fig. (18).

A proportional control law, as example, could model the mechano-chemical heart control in a distributed structure:

$$\begin{cases} u_{H,n+1} = -\alpha_A\, e_{Q_{a_n}} - \displaystyle\sum_{x=A,P} \beta_x \left|P_x^S - P_{x_{max}}\right|_+ - \sum_{x=A,P} \gamma_x \left|P_{x_{min}} - P_x^S\right|_+ \\ u_{ULV_{R,n+1}} = -\dfrac{\alpha_C}{R_C}\left(\Delta P_C - \Delta P_{C_R}\right) + \beta_C \left|P_C^S - P_{C_{max}}\right|_+ - \gamma_C \left|P_{C_{min}} - P_C^S\right|_+ \\ u_{TLL_{R,n+1}} = -\dfrac{\alpha_T}{R_T}\left(\Delta P_T - \Delta P_{T_R}\right) + \beta_T \left|P_T^S - P_{T_{max}}\right|_+ - \gamma_T \left|P_{T_{min}} - P_T^S\right|_+ \end{cases} \tag{32}$$

where $\Delta P_x = P_A - P_x$. The command u_{n+1} regulates the cardiac function to regulate the aortic blood flow and to maintain pressure in the aorta and in the lungs within normal limits. Remark that the ANS by the knowledge of $P_A(t)$ and $V_L(t)$ can estimate the error of blood flow regulation e_{Q_A} in a beat-to-beat basis, cf. eq. (31). Blood flow in the different blood compartment will be regulate by $A_{ULV_{n+1}}$ and $A_{TLL_{n+1}}$, which in fact control the pressure difference in the vascular system and, obviously, this coincide to regulate blood flow in the low frequency as $Q = \Delta P/R$. The proposed control law is a distributed control law, there is no single structure in the controller that can estimate the $A_{ULV_{n+1}}$ and $A_{TLL_{n+1}}$ command, as R_x (x=C,T) is only known by local controller,whereas α_x (x=C,T) is known only by the central controller, but it it the result of the whole control structure. Intrinsically this control law make a cooperation between the central and the local controllers: by increasing α_x the central controller may reduce the $\Delta P_x - \Delta P_{x_R}$ increasing or decreasing the vasoconstriction which corresponds to a greater or smaller blood flow into that blood compartment. On the other hand, by increasing R_x, whenever local blood compartment needs a smaller quantity of oxygen, the peripheral controller reduce the control of the $\Delta P_x - \Delta P_{x_R}$ term reducing therefore the control action of blood flow regulation of the central controller.

We can find classical "positive" and "negative" feedback results :

Negative feedback and pressure control in the cardiovascular control system

The stimulation of the aortic (P_A) and the carotid baroreceptors (P_C) induces a vagal activation, see eq. (32), sympathetic inhibition, bradycardia, diminished cardiac contrac-

tive force, vasodilatation on the vessels and a fall in mean blood pressure revealing a multi-input multi-output blood pressure control feedback in the cardiovascular system.

Positive feedback and flow control in the cardiovascular control system

Malliani and co-workers, stretching the thoracic aorta (P_T), produced a significant increase in both heart rate and blood pressure, revealing a positive reflex [84, 118]. In fact, in a multi input-output control system the term positive or negative feedback is meaningless: the input is not a single input; the reaction is not a single output therefore we can not establish an a priori sign in a vectorial input-output relationship. In our point of view, the function of the heart is to pump the blood into the vascular system and the blood flow depends on the pressure difference between ventricular and aortic pressure (usually called the after-load). It is likely that the function of the stretch receptors in the thoracic aorta is to measure the pressure against which the heart has to pump the blood. Then the role of the positive feedback is to control the heart function in order to maintain the blood flow into the vascular system. Therefore, it is obvious that stretching the thoracic aorta can induce reflex changes opposite to those which would be obtained by stretching a carotid sinus [87]. By eq. (32), an increase in P_T yields to a vagal inhibition and therefore an increase in heart rate and blood pressure.

In conclusion, assuming that ANS controls the blood flow in the cardiovascular system we are able to explain the apparently contradictory results of these two experiences.

2.3 Measured Cardiovascular signals

The principal non invasive available signals of the cardiovascular system are:

- EKG (electrocardiographic signal).
  The EKG represents the electrical events of depolarisation and repolarisation of the cardiac atrium and ventricles, preceding the mechanical events of contraction and ejection of blood in arterial vessels. To analyse the effects of the ANS on the sinus node, located in the atrium, the best way should be to detect the P wave, corresponding to the atrium depolarisation. But the R peak, corresponding to the maximum of the ventricular depolarisation, is the easiest event to detect and usually accepted to represent the global effect of the ANS on the heart. So, the RR intervals series, expressed in ms, represents the time interval length between two consecutive heart beats; its inverse, the heart rate (HR) is expressed in beats/min.

- Photo-plethysmography.
  A lamp and a photocell are put at the internal side of a cuff, to measure local cardiovascular parameters.

  - volume assessment. If the pressure of the cuff is gradually increased or decreased, the vascular volume changes in a characteristic way: at lower pressure only the low pressure compartment collapses and at higher pressure (greater than 36 mmHg) arterial compartment collapses linearly with the cuff pressure [128].
  - pressure assessment - principle of FINAPRES measure (FINger Arterial PRESsure). The basic parts of the instruments are a photoelectric plethysmograph equipped with a transparent inflatable cuff and the pressure within which is controlled by an electro-pneumatic system and a PID (Proportional, Integral and Derivator) controller. In this case the cuff pressure

is controlled by the plethysmographic signal so that the vascular volume is clamped to a pre-set value. Any deviation of vascular volume due to changes of intravascular pressures are instantaneously compensated by automatic adjustment of the cuff pressure which thus continuously and quantitatively follows the intravascular pressure [128].

- Impedance-plethysmography.
  Tissue impedance is measured by passing a small constant alternating current (I) through the body and measuring the voltage drop (V) produced as a product of R X I, since I is constant V is directly proportional to R. A shift in the phase angle between the current and voltage defines reactance or a complex impedance measurement including the dielectric non conducting space attributed to cell membrane capacitance. The impedance of a geometrical system, in this case the human body, is related to conductor length and geometrical size, its cross-sectional area and signal frequency. Using a constant signal frequency and fairly constant configuration, the body's impedance to current flow can be related to its volume, since conductor volume equals the cross-sectional area x length or height. When the resistivity of the conductive material is known then the electrical volume equals the physical volume. Therefore, electrical bioimpedance measurements permit quantification of blood flow as a result of changes in electrical conductivity of a body segment. The electrical impedance technique for measuring cardiac output is based upon changes in thoracic electrical impedance caused by cardiovascular activity [149, 167].

- Echocardiography and Color Doppler Echocardiography
  Two-dimensional echocardiography provides noninvasively dimensional and area measurements that can be integrated into a variety of geometric models to calculate the volume of the organ, i.e. the cardiac output. However, routine application of echocardiography has unfortunately been limited by the need for off-line calibration, hand-drawn borders and computation. Accordingly, considerable effort has been devoted to semiautomatic border detection [23, 105]. Moreover, color Doppler method enables reliable determination of flow volumes across the atrioventricular valves [38, 37].

- Respiratory activity
  Oronasal thermistor, thoracic and abdominal movement sensors and finger oxymetry are the principal measurements made to estimate the respiratory flow and volume.

2.4 Principal cardiovascular indexes for clinical decision making

Several cardiovascular indexes are nowadays estimated to evaluate clinical conditions of a patient, the most important are the following:

- stroke volume

  Cardiac output is an important hemodynamic variable continuously regulated by ANS. The study of stroke volume reflex may provide useful tools to explore and evaluate the ANS reflex mechanisms. It is studied in physiological experiments and it is monitored in surgical and critical care patients. Several methods have been developed noninvasively monitoring the cardiac output: echocardiography [23, 38, 37, 105]; impedance-plethysmography [149, 167] or blood pressure curve (Modelflow or pulse analysis) [51, 55, 153, 154, 169, 171] methods. The major problem of the blood pressure method is the necessity of a calibration, once for each patient, to obtain absolute values, and the reliability under varying hemodynamic and pharmacological circumstances. All these methods have been compared to invasive one such as thermodilution [29, 66] or estimation of the cardiac output by Fick principle [42].

- total peripheral resistance

  The peripheral resistance effector is another of the mechanisms by which the ANS control cardiovascular system. In general, peripheral resistance is estimated by the flow to pressure ratio in the aorta or by fitting a 3-WK model to the measured aortic pressure and blood flow curves [158, 150].

- total arterial compliance

  Total arterial compliance (C_T) of the systemic arterial tree is an important determinant of the cardiac load. Alterations in the arterial compliance are linked to various physiological or pathological conditions, and thus its estimation has long interested clinicians and researchers of cardiovascular physiology. By definition, C_T defines the change in the arterial blood volume due to a given change in the distending pressure. Its estimation is very difficult as C_T depends strongly on pressure, so that there exists no single number that can characterise arterial compliance over the whole physiological range. Nevertheless, several methods have been proposed to estimate C_T. These methods are based either on linear 2-WK model or linear and non-linear 3-WK model [21, 152, 150, 151, 158]. The estimated values have been compared to real value by a simulated distributed vascular system [150].

- Baroreflex sensitivity

  The arterial blood pressure - RR interval neural reflex is the most studied ANS control effector as both signals are easily non-invasively available. In addition, quantification of the heart rate baroreflex has been useful in the study of pathological states such as myocardial infarction, hypertension, congestive heart failure and dysautonomias.

- RR-interval and blood pressure variability

  A reduced RR-interval and blood pressure variability is used as a prognostic markers for heart diseases. In recent years, event quite simple analysis of the variability phenomena, such as those offered by the use of standard deviation, frequency histograms, or scattograms of discrete series events, have provided important information on pathophysiological processes like myocardial infarction and diabetic neuropathy.

Throughout this report we will introduce and discuss only the cardiovascular variability and the baroreflex sensitivity concepts concentrating ourselves to only one of the baroreflex mechanisms used by the ANS to control the cardiovascular system.

3 Cardiovascular variability

3.1 Introduction

This section is meant to be a review of the major non-invasive spectral markers widely used in the literature and in clinical studies to estimate the autonomic nervous system activity. We will introduce the physiological basis and the experimental findings that corroborate the usefulness of these markers in several physiological and pathological conditions.

In the literature, the cardiovascular system is usually studied from one of the two points of view:

- *cardiac neural traffic.* The heart period signal is studied and interpreted alone (adopting a neural output point of view) using RR-interval oscillations as a non-invasive estimate of human cardiac nerve outflow:

  > Katona and Jih [69] showed that in anesthetized dogs with constant breathing rates, respiration-related peak-valley RR fluctuations (respiratory sinus arrhythmia) are linearly related to vagal firing rates. On the basis of this empirical observation, RR interval fluctuations have been promoted as an accurate non invasive quantitative estimate of human vagal-cardiac nerve outflow traffic. In recent years, the time-domain method used by Katona and Jih has been supplanted by frequency-domain methods. Power spectral density (PSD) of HR variability (HRV) revealed spectral peaks which carry information about sympatho/vagal interactions [2, 132, 115, 114]. Nowadays, several spectral parameters are used to estimate the cardiac autonomic nervous system activity leading researchers to contradicting results. Throughout this section, we will introduce these spectral parameters discussing their assumptions and limitations.

- *cardiac neural control.* Since RR-interval is one of the control effector mechanisms by which autonomic nervous system regulates blood flow and arterial blood pressure (ABP), heart period and ABP signals are studied and interpreted together to make inferences on the controlling system mechanisms (adopting a neural input/output point of view).

  > Smyth at al. [147] showed a linear correlationship between RR-interval and the SBP of the preceding beat when pressure was elevated with bolus administration of phenylephrine. The regression coefficient of the correlationship between RR and SBP was identified as the *baroreflex sensitivity* (BRS) in ms of interval prolongation per mmHg of pressure rise. This technique is currently the gold standard in baroreflex studies. Measurement of BRS has gained considerable interest as a new clinical tool, since alterations in the baroreflex control of heart period have been associated with an increased propensity for cardiac mortality or sudden cardiac death. Nowadays, two different methods estimate baroreflex sensitivity in time and in frequency domain. Throughout this section, we will introduce these two methods discussing their assumptions and limitations.

Throughout this chapter both of these approaches will be used to develop these general concepts.

3.2 Origin of the cardiovascular oscillations

3.2.1 The Respiratory activity and the High Frequency Variability

Respiratory sinus arrhythmia (RSA) can be defined simply as the variations in the heart rate that occur simultaneously with respiratory activity. Although a vast number of investigators have tried to unravel

the precise mechanisms of RSA, so far its origins are still open to debate. It is likely that each of the following mechanisms plays at least some part in generating RSA [142]:

- **autonomic** mechanisms
  - *mechanical* mechanism. RSA could be mediated through the *baroreflex* as a secondary effect of mechanically induced respiratory ABP fluctuations:

    > As phrenic nerve signals are transformed into mechanical ventilation, respiration directly and indirectly influences arterial and central venous pressure and flows through mechanical thoracic coupling changes in the right ventricular preload. These respiratory-induced changes in arterial and central venous pressure must, in turn, influence the afferent signals from the arterial and cardiopulmonary baroreceptors, respectively.

  - *central* mechanism. RSA could be the result of a direct neural coupling of the respiratory center and the vasomotor center:

    > Several studies demonstrated that a RSA synchronised to phrenic nerve activity, but not necessarily with mechanical respiratory activity, exists in various animal preparations. Therefore the effects of afferent neural stimuli that result from the mechanical influence of respiration on the lungs, the chest wall, the heart and the thoracic vasculature are unable to account entirely for the presence of RSA. Two possible mechanisms have been proposed to explain the central link between respiration and heart rate:
    >
    > 1. a direct central link between respiratory centers and the cardiovascular autonomic center in the brain stem, such that cardiac neural efferent activity decreases, both in the vagal and in the sympathetic branches, just prior to the onset of respiration.
    > 2. a direct neural link between respiratory centers and the central sensitivity of the arterial baroreflex, such that a pre-inspiratory decrease in sensitivity to baroreceptor afferent stimuli leads to a decrease in vagal efferent activity.

  - *stretch receptors* mechanism. RSA origin may be due to a reflex involving the stimulation of stretch receptors in the lungs and chest wall.

    > The stimulation of the stretch receptors in the lungs and the chest provokes an inhibitory effect on vagal outflow, and this inhibitory effect leads to a decrease in RR-interval with inspiration.

- **non autonomic** mechanism: *intracardiac* mechanism

  > A part of RSA originates from an intracardiac mechanism, either an intracardiac reflex or mechanical stretch of the sinus-atria node:
  >
  > > Though markedly reduced, RSA is still present even after combined pharmacological cardiac sympathetic and vagal blockade and its value is similar to that reported in the transplanted denervated human heart.

RSA reflects the complex effects of central respiratory drive on the integration of autonomic afferent signals and the production of autonomic efferent signals in the brain stem, and of respiratory mechanics on the cardiovascular structures within the thorax. In addition this phenomenon is dependent on the frequency and on the amplitude of respiration, as well as on the underlying autonomic state of the organism.

3.2.2 Low Frequency Variability

More or less periodical fluctuations in arterial blood pressure slower than respiratory rhythm were described by Mayer in 1876. Despite a vast body of literature examining LF oscillations, their origins remain poorly understood. In addition, the 0.1 Hz phenomenon is certainly not a stable oscillation, changing both in amplitude (waxing and waning) and in frequency, see for example fig. (19).

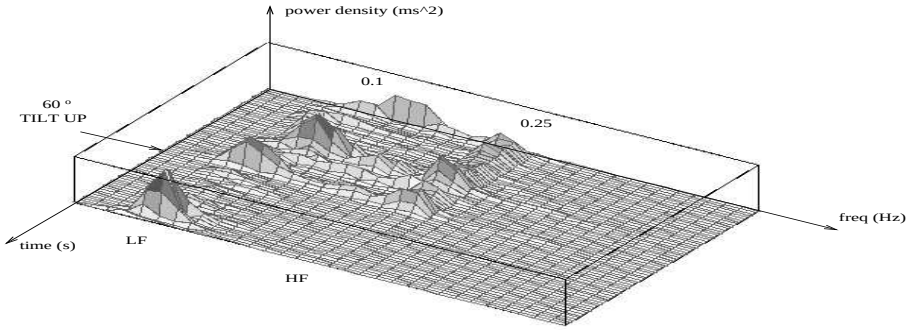

Figure 19: *Frequency and amplitude instability in time of LF oscillation in RR-interval signal during a* 60^0 *tilt-up test and paced breathing at 0.25 Hz. Unpublished data.*

Two possible mechanisms have been proposed to explain LF oscillations in RR interval:

- *resonance mechanism.* LF variability in cardiovascular signals may be due to a resonance characteristic of the baroreflex mediated sympathetic vasoconstriction control loop.

  α_1-adrenergic blockade, inhibiting the baroreflex mediated sympathetic peripheral vasoconstriction control loop, reduces LF variability in arterial blood pressure signal [116], revealing thus the importance of this control mechanism on LF presence in cardiovascular oscillations. Moreover, atrial pacing and combined pharmacological cardiac sympathetic and vagal blockade confirm that the presence of LF variability in ABP is not dependent on a similar variability in the RR signal [156].

  In addition, several physiological non linear models suggest that LF oscillation in the RR interval could be produced by a resonance phenomenon (at a frequency of $\approx$ 0.1Hz) due to the slow peripheral sympathetic control loop of vascular resistance in response to beat-to-beat changes in ABP [15, 140, 157, 164]. In fact, considering a control loop, such as the

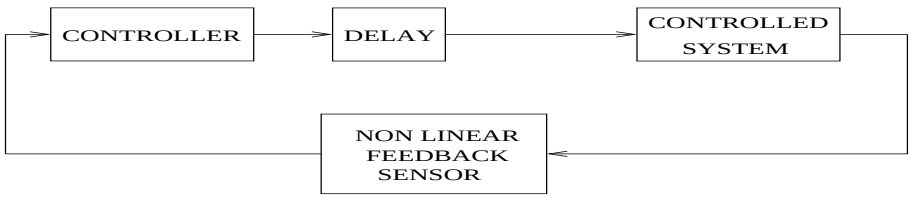

Figure 20: *Diagram of a feedback control loop characterised by a delayed regulatory action and a non linear feedback sensor. When the controller functions, the system oscillates. The baroreflex mediated sympathetic vasoconstriction control loop could be described in this form.*

one depicted in fig. (20), characterized by a delayed regulatory action on the controlled system and by a non linear feedback sensor, the presence of an oscillation within the loop is not an undesired noise, but the result of a working regulatory mechanism. The baroreflex mediated sympathetic vasoconstriction control loop presents the same elements: a non linear feedback sensor (the baroreceptors); a controller (the ANS) acting on the controlled system (the cardiovascular system), only after a delayed reaction (the sluggish baroreflex mediated sympathetic response).

- *central mechanism.* LF variability in cardiovascular signals could be due to a central rhythmic modulation of neural activity.

  Vagotomized, sinoaortic denervated and decerebrated cats present vasomotor and respiratory rhythms in the discharge of medullary neurons involved in the regulation of the cardiovascular system [99]. In addition, human patients with an LVAD (Left Ventricular Assist Device) present a dominant LF oscillation in the RR interval despite the absence of any LF and HF oscillations in blood pressure spectra [31].

In our view, LF oscillation in cardiovascular variability represents, in part, a central oscillation in autonomic outflow and, in part, depends on the baroreflex vasomotion control loop.

3.3 RR-variability and sympathovagal balance

3.3.1 Neural Pattern and spectral normalisation

For arterial baroreflex areas and the heart, the activation of either sympathetic or vagal outflow is accompanied, in most physiological conditions, by the inhibition of the other. A stimulation of cardiac sympathetic afferents induces a reflex sympathetic excitation and a vagal inhibition [88, 89, 87], whereas the opposite effect is elicited by stimulating cardiac vagal afferents [144]. Sympathetic excitation and simultaneous vagal inhibition, or vice versa, both modify cardiac performance and RR spectral pattern. In cats a sympathetic excitation (obtained with a reduction in arterial pressure during inferior vena cava occlusion) modified the relationship between the LF and HF components present in the sympathetic discharge, increasing LF predominance over the HF component [100]. Conversely, during sympathetic inhibition (obtained with a baroreceptor stimulation during aortic occlusion) the relationship clearly shifted towards HF predominance [100]. Therefore, a "pattern" point of view was suggested: a reciprocal relation between these two rhythms similar to that characterizing the sympathovagal neural interactions. The core of the sympathovagal balance concept, seen as a reciprocal relation between these rhythms, is that the two rhythms, the one a marker of excitation and intrinsic in sympathetic excitation (LF) and the other a marker of inhibition and linked to vagal predominance (HF), would, in physiological conditions, be organized in a reciprocal manner [85, 89, 98]. A balanced system may be a reasonable simplified model of the complex controlling mechanisms of cardiovascular system which can be described using spectral normalized index [114] computed as follows:

$$LFnu_{RR} = \frac{LF_{RR}}{{\sigma_{RR}}^2 - VLF_{RR}} * 100 \qquad HFnu_{RR} = \frac{HF_{RR}}{{\sigma_{RR}}^2 - VLF_{RR}} * 100 \tag{33}$$

where HF_{RR} and LF_{RR} represent the power in LF and HF band of RR variability respectively, in normalised units [nu] or in absolute units $[ms^2]$, ${\sigma_{RR}}^2$ in $[ms^2]$ represents the total power (or variance) and VLF_{RR} in $[ms^2]$ indicates the power of the VLF component. The normalization procedure is only a tool to explore the reciprocal relation between the two neural rhythms and the different spectral profiles or "patterns" accompanying different states of sympathovagal interactions [86]. The simple "push-pull" model

	Rest	90^o tilt
var_{RR} $[ms^2]$	1250	417
VLF_{RR} $[ms^2]$	600	110
LF_{RR} $[ms^2]$	420	279
HF_{RR} $[ms^2]$	255	21
$LFnu_{RR}$ [nu]	56	91
$HFnu_{RR}$ [nu]	36	7

Table 1: *Spectral analysis of HRV in a young subject at rest and during* 90^o *tilt. After the tilt, the total power (i.e. variance,* var_{RR}*) is markedly reduced and consequently LF and HF powers are both decreased when expressed in absolute units. Normalized units (nu) show a difference in the spectral pattern, i.e in the relation between LF and HF. From [86].*

can be usefully employed to explain various phenomena: $LFnu_{RR}$ and $HFnu_{RR}$ components (together with the ratio LF_{RR}/HF_{RR}). In all study conditions (infusion of nitroglycerine, tilt-up test, coronary occlusion and so on), any increase in sympathetic neural activity is associated with a meaningful increase in the $LFnu_{RR}$ component [22, 46, 82, 113, 137] and, moreover the $LFnu_{RR}$ value does not decrease with parasympathetic blocker [114, 137].

3.3.2 Absolute and normalised spectral values relationship

A clear difference between absolute and normalised units is shown in passive tilt tests, enhancing sympathetic activity, as shown in table (1). The tilt-up is the first physiological test to shift sympathovagal balance towards sympathetic excitation. The drastic changes in RR-spectral profile are, however, accompanied by a marked decrease in total power (corresponding to variance, RR_{var}). When a sympathetic excitation is accompanied by a reduction in variance, the absolute values of LF_{RR} undergo contrasting influences - as they tend to be decreased by the reduction in the variance, but also tend to be increased by the greater concentration of power in the LF_{RR} component, as reflected by its constant rise in n.u. ($LFnu_{RR}$). Conversely, the HF_{RR} component is decreased during tilt in both absolute and normalised units [86].

Nowadays, non invasive estimation of cardiac nerves activity is mainly based upon results obtained from RR relative spectral power - $HFnu_{RR}$, $LFnu_{RR}$, using equations (33). We list here the principal findings in the literature that corroborate this choice:

- HF_{RR} and LF_{RR} are correlated to the subject's age; $HFnu_{RR}$ and $LFnu_{RR}$ values are not [114, 80].
- LF_{RR} is not greatly increased by tilt-up test; neural sympathetic activity and $LFnu_{RR}$ value are [30, 67].
- LF_{RR} is greatly decreased by atropine, a vagal antagonist, [132]; $LFnu_{RR}$ value is not [114, 137].
- HF_{RR} and LF_{RR} are not correlated to tilt-up angle; neural sympathetic activity, $HFnu_{RR}$ and $LFnu_{RR}$ values are [101].
- HF_{RR} and LF_{RR} are correlated to ${\sigma_{RR}}^2$; $HFnu_{RR}$ and $LFnu_{RR}$ values are not [114].
- HF_{RR} and LF_{RR} are constant between sleep stages; $HFnu_{RR}$ value increases and sympathetic neural activity and $LFnu_{RR}$ value decreases passing from REM to non-REM sleep stages [104].

Concluding, normalised units correctly represent the physiological sympathovagal reciprocal relationship, whereas the meaning of spectral absolute values is until now not really understood and therefore very often neglected in the literature.

3.3.3 $mean_{RR}$ and RR-variability relationship

$mean_{RR}$ and RR-variability (RRV) depend both on the autonomic nervous system (ANS) and therefore they are not independent, but provide different information on the ANS functioning. The following experiments suggest that the spectral indexes alone do not completely describe the cardiac nervous outflow:

- *assessment of changes in sympathovagal interactions between sleep stages.* During the night, sleep follows several cycles, each comprising nocturnal awakening, light sleep, slow wave sleep and rapid eye movement (REM) sleep stages. Our group showed no $mean_{RR}$ difference between sleep stages, whereas RRV (if expressed in normalised units) underwent large changes passing from non-REM to REM sleep [104]. In our view, this is evidence of the presence of two different regulatory mechanisms.

- *assessment of parasympathetic tone in pharmacological studies.* Cardiac parasympathetic tone is defined as the difference between $mean_{RR}$, after eliminating cardiac sympathetic influences (with propanolol) and $mean_{RR}$ after a complete cardiac autonomic blockade, vagal and sympathetic (with atropine and propanolol). Phenylephrine studies clearly show that the relationship between cardiac parasympathetic tone and RRV may not be monotonic [50], therefore evaluating cardiac parasympathetic tone using only RRV techniques should be undertaken cautiously. In addition, our group, using atropine, found a different dynamic between the regulation of cardiac parasympathetic tone and the regulation of the cardiac parasympathetic modulation of the RR-interval (expressed as HF_{RR}) [94]. Therefore, blocking the cardiac sympathetic branch, it is possible to dissociate the regulation of $mean_{RR}$ from that of RRV.

- *assessment of sympathovagal interaction during paced respiration.* Breathing rhythm, within a physiological range, does not affect $mean_{RR}$, therefore it does not alter net level of cardiac autonomic traffic [19, 52, 57, 93, 114, 127], but it has a strong effect on RRV. Therefore, it clearly appears that RRV can vary without changes in $mean_{RR}$: the neural modulation of the RR interval can change, whereas its overall tonic level remains constant.

- *information provided by $mean_{RR}$ in complementary to the information provided by spectral markers $HFnu_{RR}$, $LFnu_{RR}$.* Malliani recently found that - $HFnu_{RR}$, $LFnu_{RR}$ and $mean_{RR}$ - are the three variables with the highest information content in the two autonomic nervous profiles related to posture [86]. When one of these three variables is not taken into account a part of information is lost. Therefore, RRV neural control (measure of the sympathovagal modulation to the sinus node activity) could be described using normalised units, whereas tonic neural control (global measure of sympathovagal tone) could be described using $mean_{RR}$.

Previous examples support the idea that RR-variability and $mean_{RR}$ are controlled by two different mechanisms: normalised units represent the concept of a balance beam pivoted around its center, that corresponds to $mean_{RR}$ value.

3.4 Neural control of the Sino-atrial node: arterial blood pressure - heart period reflex

3.4.1 Arterial blood pressure - heart period reflex: a primary reflex mechanism?

As previously introduced, see paragraph (1.2), the aim of this report is the study of only one of the principal reflex mechanisms for the short-term control of the cardiovascular system. We will discuss on the baroreflex sensitivity concept, its meaning, its quantification and its limitations, but now we have to spend some words on the implications of this choice. Is it reasonable to discard the other reflex mechanisms showed in fig. (18)? In our point of view, the ANS may regulate blood flow in the different parts of the cardiovascular system, in the head as well as in the general systemic part, maintaining some particular sensible blood pressures, i.e. in the head, the lungs and the ascending aorta, within normal limits ($P_{x_{min}} \leq P_x \leq P_{x_{max}}$, x=A, C, P) to avoid tissue damages and vessel collapses. In fact, blood flow (Q_x, x=A, C, T) could be estimated by afferent information and the ANS could control effectors in order to maintain small the difference (E) between the estimated blood flow ($\hat{Q}_x$) and the reference value (Q_{x_R}), see fig. (18). The effector mechanism available by ANS to control in the short-term the cardiovascular system are principally two: the heart function (stroke volume and heart rate) and peripherally vasoconstriction (resistance and compliance). In fact, the control of the peripheral resistance and compliance by vascular smooth muscles, see paragraph (2.2), is very slow when compared to the control of the cardiac function. Therefore, exploiting this dynamical separation of the different reflexes, we can consider the vascular control constant over the period of BRS estimation. Obviously this is true only for a brief lapse of time. On the other hand, the control of the cardiac function concerns two important quantities: the heart period (RR) and the stroke volume (SV), the two fastest reflex mechanisms. We had already remarked that the mechano-chemical command u, in fig. (18) and eq. (9), which controls the heart contraction can be explicitly split into the mechanical and chemical part, see paragraph (2.1.2). The chemical command is responsible for RR control, whereas the mechanical command is responsible for SV control. Assuming a fast and efficient local control of the Starling effect, the stroke volume is supposed to be determined by pre-load filling conditions of the heart, i.e. diastolic volume V_{D_L}, and measured by ventricular stretch receptors. In this case, the control input is the mechano-chemical command $u(t)$ and RR-interval is its period, fixed to V_{D_L}/Q_{A_R}. . Since, the diastolic volume of the heart is function of the arterial blood pressure, this leads to the arterial blood pressure RR baroreflex sensitivity which is classicaly studied by signal processing techniques.

3.4.2 Definition of spectral baroreflex sensitivity

The instantaneous RR may be seen as the output variable of a very complex multi-feedback network, continuously monitored and carefully regulated by the ANS. However, only limited inferences on the controlling system mechanisms can be made regarding the spontaneous fluctuations in an output variable alone. Determining a more accurate and detailed characterization of the system's behavior requires knowledge about the input perturbations that drive the system as well. With appropriate choices for input and output signals we are able to investigate more extensively the ANS characteristics in regulating cardiovascular system.

Considering the arterial blood pressure (ABP) as one of the inputs and RR-interval as one of the outputs of baroreflex system, it is possible to define the partial controller gain or as commonly defined, *baroreflex sensitivity*, between them. The term "baroreflex sensitivity" is based on the assumption that in the high and low frequency bands only fast mechanisms of regulation are effective (such as baroreceptors), whereas slower control mechanisms could be completely neglected (such as hormonal control).

To account for reciprocal influences between ABP and RR, a closed-loop conceptual scheme of the RR-ABP relationship, see figure (21), appears more appropriate than an open-loop scheme.

The two transfer functions H_{hemo} and H_{contr} describe the simultaneous effects of RR on ABP and of ABP on RR: H_{hemo} stands for the hemodynamic transfer function from RR to ABP, whereas H_{contr} represents the overall neural feedback from ABP to RR. Respiration may enter the cardiovascular system at two points:

- centrally (R_{centr}), causing RSA directly and consequently through the hemodynamic transfer H_{hemo} results in ABP fluctuations linked to respiratory activity.

- mechanically (R_{mech}), causing respiratory ABP variations, which, through the feedback transfer H_{contr}, leads to RSA.

Two sources of noise, n_{RR} and n_{ABP}, are also indicated to describe the external inputs to the system (such as small adjustments by the central command, mechanical disturbances or other input of the reflex mechanism), to take into account all the possible sources that cause variability in the ABP and RR signals independently of ABP, RR or respiratory activity.

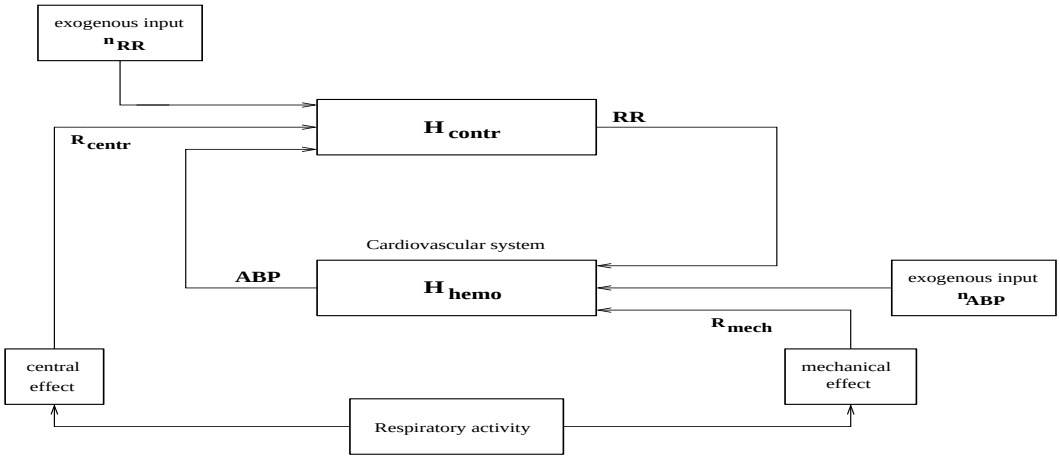

Figure 21: *Simplified diagram of closed-loop neural reflex with only the control of the ABP made by RR-interval. H_{hemo} is the hemodynamic transfer from (RR,n_{RR},R_{centr}) and ABP and H_{contr} is the neural feedback transfer from (ABP,n_{ABP},R_{mech}) and RR. Depending on the entrance point of respiration (central R_{centr} or mechanical R_{mech}) and on the "amplitude" of the exogenous input n_{RR} one can obtain relatively unbiased estimates of either H_{hemo} or H_{contr} in closed-loop operation.*

In general conditions, RR and ABP are the results of complex nonlinear dynamic systems, therefore we can write:

$$\begin{cases} RR = f(ABP, n_{RR}, R_{centr}) \\ \\ ABP = g(RR, n_{ABP}, R_{mech}) \end{cases}$$

We are interested here on the neural feedback functions from (ABP,n_{RR},R_{centr}) to RR. Applying the harmonic balance method [166] (associating a describing function to each linearity present in the system),

it is possible to find out the relationship between the principals components of the signals :

$$\begin{cases} LF_{RR} = LF_f(mean_{ABP}, LF_{ABP}, HF_{ABP}, mean_{n_{RR}}, LF_{n_{RR}}, HF_{n_{RR}}, mean_{R_{centr}}, LF_{R_{centr}}, HF_{R_{centr}}) \\ HF_{RR} = HF_f(mean_{ABP}, LF_{ABP}, HF_{ABP}, mean_{n_{RR}}, LF_{n_{RR}}, HF_{n_{RR}}, mean_{R_{centr}}, LF_{R_{centr}}, HF_{R_{centr}}) \end{cases}$$

In [164, 102, 103] this method has been applied in simplified model of the cardiovascular and autonomic nervous systems defining a based model nonlinear baroreflex sensitivity.
On the other hand, assuming a linear input-output relationship in the baroreflex mechanism, an hypothesis verified by coherence analysis in RR and SBP real time-series, the gain of the neural feedback from ABP to RR can be expressed as:

$$H_{contr} = -\frac{RR}{ABP} + \frac{n_{RR} + R_{centr}}{ABP} \tag{34}$$

Now, respiratory activity does not contribute to the LF component, therefore equation (34) could be written, for the LF component, as:

$$LF_{H_{contr}} = -\frac{LF_{RR}}{LF_{ABP}} + \frac{LF_{n_{RR}}}{LF_{ABP}} \tag{35}$$

where $LF_{n_{RR}}$ takes into account the possible central origin of LF oscillations. Since external noises do not contribute to the HF component, equation (34) could be written:

$$HF_{H_{contr}} = -\frac{HF_{RR}}{HF_{ABP}} + \frac{HF_{R_{centr}}}{HF_{ABP}} \tag{36}$$

for the HF equation. When $LF_{n_{RR}}/LF_{ABP}$ and $HF_{R_{centr}}/HF_{ABP}$ tend to zero, it is possible to estimate the gain H_{contr} of the neural regulation in both the HF and LF band:

- Estimating $LF_{H_{contr}}$ from ABP and RR-interval signals is only possible when the influence of a central LF oscillation on RR is small: $LF_{n_{RR}} \ll LF_{RR}$, by equation (35). Therefore, it is possible to estimate LF baroreflex gain value only if LF activity enters, for the most part, at the mechanical hemodynamic side by the sympathetic vasomotor control loop.
- Estimating $HF_{H_{contr}}$ from ABP and RR-interval signals is only possible when the central direct influence of respiration on RR is small: $HF_{R_{centr}} \ll HF_{RR}$, by equation (36). Therefore, it is possible to estimate HF gain value only if respiratory activity enters, for the most part, at the mechanical hemodynamic side.

These hypotheses are very relevant for estimating the neural ABP-RR gain in closed loop circumstances: if they are not satisfied, the estimate gain values will be biased.

Central versus Mechanical Respiratory Variability

The following relation must be satisfied in order to have an unbiased HF estimate baroreflex gain:

$$\frac{HF_{H_{contr}}\ HF_{ABP}}{HF_{R_{centr}}} \gg 1 \tag{37}$$

Akselrod et al. [1], using a combination of atrial pacing and autonomic blockade in dogs, found that respiratory-related fluctuations of arterial pressure result from changes in heart rate (RSA). But differences between species in mean vagal tone and differences in central nervous modulation of vagal activity

by respiration are marked. Taylor and Eckberg using fixed-rate atrial pacing in humans have demonstrated that the HF component in the RR-interval can actually contribute to HF oscillations in arterial pressure [156]. Along the same line, Saul found that combined pharmacological cardiac sympathetic and vagal blockade abolish most of the RR-variability and decrease HF_{ABP} [140]. From these results, they concluded that ABP variability is at least partly caused by RSA and not vice-versa and consequently that a centrally mediated RSA must exist. In fact, the disappearance of resonance in the baroreflex control system, by a pharmacologically blockage of RR-interval neural control, may sufficiently explain a decrease in ABP modulation [157]. Therefore no conclusion about the validity or not of equation (37) could be made by these experiments.

By modelling results, DeBoer concluded that, in humans, RSA resulted from mechanically-induced fluctuations of arterial pressure [15]. In addition, Baselli and Faes conclude, from the identification process of autoregressive models, that the amount of RSA centrally induced is less important than the baroreflex induced [7, 41]. This validates, at least in part, equation (37) allowing the estimation of $HF_{H_{contr}}$ from ABP and RR-interval signals.

So far, because of the closed-loop nature of the interaction between RR and ABP, quantitative conclusions on the relative weight of the mechanical vs. the autonomic effects (RSA) of the respiration on RR remain difficult to draw. Therefore, there is not an *a priori* answer to the question: the estimation of $HF_{H_{contr}}$ by equation (36) is significantly biased or not?

Central versus reflex LF variability

The following relation must be satisfied in order to have an unbiased LF estimate baroreflex gain:

$$\frac{LF_{H_{contr}}\ LF_{ABP}}{LF_{R_{centr}}} \gg 1 \tag{38}$$

Akselrod and Baselli made the simplifying hypothesis that all disturbances, in the LF band, enter the system only at the ABP level through n_{ABP} [1, 6] allowing, therefore, the estimation of $LF_{H_{contr}}$ from ABP and RR-interval signals. Also in this case, there is no *a priori* answer to the question whether the estimation of $LF_{H_{contr}}$ by eq. (35) is significantly biased.

3.4.3 Baroreflex interpretation

The neural control of circulation has to be envisaged as a *closed loop system* in which multiple reflexes contribute to what is called the baroreflex [86]. In our view, the so called *baroreflex sensitivity* (BRS) must be seen as a partial gain of the complex neural regulatory network and it gives insights into the relationship between heart period and arterial pressure variabilities.

3.4.4 Controlled variable: arterial blood pressure

It is widely recognized that the baroreceptors play a key role in the reflex regulation of the arterial blood pressure (ABP) under normal and pathological conditions. Even if the baroreceptors are well suited to following fast ABP changes within a single heart beat, in baroreceptor-RR studies, the detailed arterial pressure wave is never assumed as input. Moreover, it appears from the literature that there is little consensus about which beat-to-beat pressure parameters should be considered as the most appropriate baroreceptor input pressure. Some researchers use a linear combination of systolic, diastolic and a threshold pressure, others just take one parameter such as beat-to-beat mean arterial pressure or systolic pressure [7, 15, 157, 140]. The picture becomes even more complicated when we take into account that

there are several pressure sensitive receptors in human circulation and the interactions between them are not clearly understood.

Nowadays, *baroreflex sensitivity* is calculated using the systolic blood pressure measured at the finger level by Ohmeda Finapres (usually referred to as finger arterial pressure FAP) based on Penaz principle [128] for the simply reason that it is the only blood pressure signal easily, continuously and non-invasively measurable. The interpretation of baroreflex sensitivity based on the diastolic pressure is very difficult as it is affected also by peripheral resistance and compliance regulation. In fact, the accuracy of non-invasive FAP measure was tested by comparing it with intra-arterial pressure (IAP) measured in radial artery [109, 111] and several critical reviews have discussed the reliability of this estimate [65]. Spectral analysis demonstrated good reproducibility and coherence between the diastolic-, systolic-IAP and the diastolic-, systolic-FAP fluctuations in both the LF and HF bands. But, for the assessment of beat-to-beat changes in blood presure and assessment of blood pressure variability Finapres proved a reliable alternative for invasive measurements when mean and diastolic pressure are concerned. Differences in systolic pressure are larger and reach statistical significance but are not of clinical relevance [65]. Therefore, Finapres can adequately assess both mean IAP values and IAP variability and it can be recommended as a reliable substitute for intra-arterial recording when cardiovascular control mechanisms are studied by the most frequently used methods, such as Fourier Transform. Nevertheless, there is a great difference between finger, radial and aortic blood pressure [20]. In fact, propagation of the pressure wave towards the periphery influences the pressure waves and thus the FAP-IAP differences, causing pulse wave distortion and pressure gradient. Nevertheless, finapres waveform can be filtered to obtain brachial artery [17, 168] or even ascending aortic pressure [68]. In this report, we will use systolic-FAP to assess the baroreflex sensitivity.

3.4.5 Effector mechanism: Heart-Rate or RR-interval?

If the neural reflex, controlling cardiac pacemaker firing, linearly modulates interval lengths, the use of the RR-interval as the output variable of the complex controlling mechanism would be the logical one. However, if cardiac pacemaker behaves as a linear frequency modulator, the output signal should be the heart rate (HR). Thus the fundamental question now is whether to use the RR-interval or HR. On the one hand, it has been argued that the RR-interval representation is the most natural choice, because it represents the 'basic' data recorded for EKG measurement. On the other hand, it has been argued that HR is more natural and easier to interpret in the general medical community. However, the choice between interval and rate representation is not as arbitrary as it might seem and some points have to be considered: inverting the RR intervals to get the instantaneous HR is obviously non-linear and the exact nature of the neural modulation of the cardiac pacemaker activity still remains unclear.

Heart-Rate: Human cardiac pacemaker modelling

Very simplified models of the control of cardiovascular system by ANS will lead to the conclusion that the real effector mechanism is the heart rate rather than heart period. They are based only on the SA node control and ignore the heart physiology, contrary to the modelling of RR-interval.

The actual HR is determined by the cardiac pacemaker cells in the sinoatrial node. The SA-node triggers every new heart beat by starting the depolarisation wave over the right atria. These pacemakers cells are characterized by a spontaneous depolarisation. When the transmembrane potential has reached a threshold level, a new action potential is initiated. Eliminating all autonomic influences by pharmacological agents results, in humans, in an estimate for the intrinsic pacemaker rate of 100 bpm (beats per minute). Acetylcholine and noradrenaline are realised in the vicinity of the cardiac pacemaker cells by

increased parasympathetic and sympathetic activity respectively. The neurotransmitters may influence

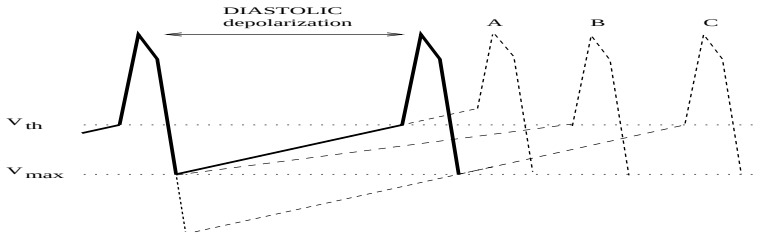

Figure 22: *Schematic depolarisation pattern of SA-node cells. Different ways to alter pacemaker frequency: A) increasing threshold potential V_{thr}. B) decreasing the slope of depolarisation. C) increasing the negative maximum diastolic potential V_{max}. From [58].*

threshold potential, diastolic depolarisation rate, maximal diastolic potential, or all three, thereby changing the pulse frequency of the pacemaker cell [58], see fig. (22). Hyndman and Mohn presented a simple

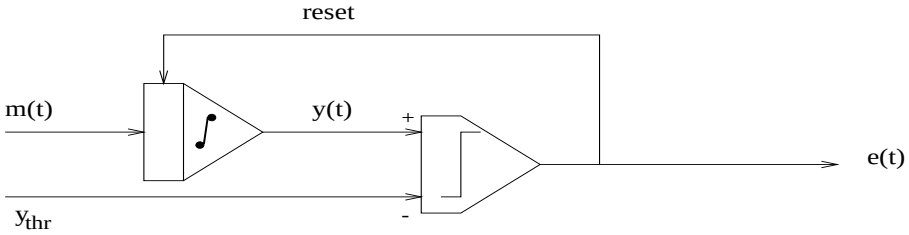

Figure 23: *Integral pulse frequency modulator (IPFM). The cardiac event e(t) is generated by integration of the neural modulating signal m(t), yielding y(t). When y(t) reaches a threshold value y_{thr} a spike is generated and the integrator is reset to the maximal diastolic potential y_{max}.*

model for the cardiac pacemaker, the Integral Pulse Frequency Modulator (IPFM), shown in fig. 23, in order to determine the autonomic modulating signal from the cardiac event sequence [63]. Although the pacemaker region is a cluster of cells, they modelled it as single effective cell, because the individual cells are electrically synchronized. In addition, diastolic depolarisation was simulated by integrating a time varying modulating function m(t) which includes all autonomic influence on the diastolic as well as a constant input that assure the intrinsic pacemaker frequency. When the integrated signal y(t) exceeds a threshold y_{thr} an impulse is generated and the integrator is reset to the maximal diastolic potential y_{max}. Therefore, assuming that at t=0 an impulse is generated, we can write:

$$y(t) = y_{max} + \int_0^t m(\tau)d\tau$$

Then, an impulse is generated when $y(t) = y_{thr}$:

$$y_{thr} = y_{max} + \int_0^{RR} m(\tau)d\tau$$

where RR is the time interval between two cardiac events or the actual pulse interval. Assuming a nearly constant autonomic modulation of the diastolic slope within a heart beat, we can rewrite the previous

equation as:

$$y_{thr} - y_{max} = \bar{m}\ RR$$

In a linear control hypothesis of ABP, the autonomic neural modulation of the pacemaker activity will be proportional to the ABP value:

$$HR = \frac{k}{y_{thr} - y_{max}} + \frac{\alpha}{y_{thr} - y_{max}} ABP$$

where k takes into account the intrinsic pacemaker rate and α the baroreceptor sensitivity to arterial pressure. Therefore estimating the ABP-HR gain in bpm/mmHg would be the obvious choice.

This model does not take into account the heart physiology and the effector mechanism is not only limited to RR interval, there are all: the pulsatile behaviour of the cardiac pump with its physiological cycles.

Evidences reported in the literature for HR as a suitable effector mechanism

Ten Voorde reported two examples in favour of the hypothesis of linear frequency modulation [157] :

1. One example is taken from BRS measurements with the phenylephrine ramp method published by Karemaker and Borst [16]: their pressure-interval relations were rather non-linear, but the transfer from interval to rate, surprisingly leads to an almost perfectly linear fit between pressure and HR.

2. A second example is taken from BRS measurements in a baroreflex study of the α_1-adrenoreceptor blocker ketanserin. The author evoked a significant pressure rise (by phenylephrine) and fall (by nitroprusside) reporting a BRS of 15.4 ms/mmHg and 5.7 ms/mmHg, respectively. Therefore taking the RR-interval as output, the BRS estimate by a vasoconstrictor and a vasodilator differs by 170%. However, expressing BRS in HR changes per mmHg, these BRS value became 0.83 bpm/mmHg and 0.52 bpm/mmHg, respectively. A difference of 60%. Still asymmetric, but almost three time less asymmetric that when BRS is expressed in intervals.

One other example is taken from invasive cardiac neural stimulation:

Levy and Zieske reported an hyperbolic relation between HR and cardiac vagus stimulation frequency [79]. Then, other researchers suggested using the RR-interval to quantify efferent autonomic effects [54, 123]. But, Rosemblueth in 1932 changed the frequency of stimulation of the sympathetic (vagal) cardiac nerves and noted the increases (decreases) in HR. The response were quite linear, in both cases, over a wide range of stimulation frequencies and over changes in HR of 50 bpm (100 bpm). These above nonlinear effects appear to be often due to the interaction of sympathetic and vagal effects on heart rate [78, 143].

RR-interval: Human cardiac phase modelling

Physiological models which describe the cardiac function and the different cardiac phases lead to the conclusion that the real effector mechanism is the heart period rather than heart rate. In fact, the recently developed model of the overall cardiovascular system lead us in this direction [10].

It is widely accepted that each cardiac phase is in fact controlled by ANS:

- preload period:

The heart is filled by blood until a satisfying filling condition is reached (by using informations coming from atria and ventricular stretch-receptors), the ANS control the time-length of this phase.

- isovolumic contraction:

  Assuming that ANS is able to control the dP/dt (the time derivative of the ventricular pressure), for given preload and after load pressures, ANS control directly the length of this cardiac phase.

- Atrio-Ventricular conduction time-delay

  As the name suggests it is a time not an instantaneous frequency that is controlled.

- repolarisation period and cardiac muscle relaxation

  Once again it is a period that is controlled.

Evidences reported in the literature for RR-interval as a suitable effector mechanism

In our knowledge, the only finding that corroborates RR-interval as the correct baroreflex output signal that we found in literature was given by Smyth et al. in 1969 [147]. Nowadays, all published reports which estimate BRS use RR-interval as output signal and express BRS as ms/mmHg [62, 120, 121, 122, 124, 147].

Concluding, modeling on physiological bases lead to the conclusion that the real effector mechanism by which ANS control blood flow and pressure in the cardiovascular system is the RR-interval rather than HR.

3.4.6 Pharmacological validation of spectral baroreflex sensitivity

Recently, it has been suggested that spectral analysis could provide a technique to non-invasively estimate BRS by a spectral ratio of RR-interval to ABP variability at respiratory frequencies and in a band around 0.1 Hz, where ABP and RR show high coherence values. An experimental demonstration was therefore applied to establish a clear link between spectral analysis and classical drug results. Robbe found a high correlation (r=0.94) between the results of the spectral method, in the LF band, and the results of phenylephrine method [138]. Pagani compared phenylephrine results to spectral results, in both the LF and HF band, to estimate changes in autonomic regulation induced by training in mildly hypertensive subjects [119]. He found a correlation between the two methods (r=0.60) and essentially the same gain was found in the two different frequency bands, concluding that the two methods furnish complementary information.

3.4.7 Sequential Baroreflex sensitivity

Bertinieri et al. studying the spontaneous baroreflex in cats, identified for one quarter of the total cardiac cycles, sequences of three or more consecutive beats during which heart period and arterial pressure underwent simultaneous increases or decreases [9]. These spontaneous sequences appeared to reflect baroreflex mechanisms, as they were drastically reduced by sino-aortic desafferentation, therefore they called them *baroreflex sequences*. Several researchers found, in humans, the so called *non-baroreflex* sequence in which the RR interval and the systolic blood pressure (SBP) changed in opposite direction

[62, 77, 124]. These authors hypothesized that these spontaneous *non-baroreflex* sequences were likely to reflect the *positive feedback* mechanisms normally interacting with the *negative feedback* mechanisms.

Usually, three conditions must be satisfied before accepting any RR-SBP sequence as significant:

- a non interrupted rise or fall in both SBP and RR of 5 or more mmHg and of 3 or more bpm, respectively;
- an absolute rate of change of SBP of at least 0.5 mmHg/s;
- a value of $p < 0.05$ for the linear regression of RR as a function of SBP.

Experimental comparison between the sequence method and the pharmacological gold standard had been made. Parlow concluded that the sequence slope estimate provides a reliable, non-invasive assessment of human vagal cardiac baroreflex sensitivity [124]. In addition, Iellamo showed that the sequence method provides good BRS reproducibility under various stimuli differently affecting the neural control of circulation [64].

3.4.8 Baroreflex sensitivity: Sequential or spectral method?

Several researchers found a close correlation between the two methods and concluded that they share common elements and therefore are not exclusive [62, 111, 120].

The principal difference between them is their underlying assumptions about the physiology of the baroreflex. The sequential method presumes that the activation of the baroreceptor is an adaptative and intermittent mechanism [120]. The spectral method assumes a permanent association between ABP and RR-interval over well defined frequency band, i.e. the LF and HF spectral components [120].

In our view, the baroreflex and non-baroreflex sequences are only the image of a dynamical system characterised by a complex operator (commonly expressed in the form of gain and phase) that is function of frequency. In fact, the origin of baroreflex and non-baroreflex sequences has to be found in the phase function of baroreflex mechanism. If the baroreflex transfer function is a real positive gain, the phase function would be zero in the entire frequency domain and non-baroreflex sequences could not be found. On the other hand, if the baroreflex transfer function is a real negative gain, the phase function would be equal to π in the entire frequency domain and only non-baroreflex sequences could be found. Therefore, a baroreflex gain function which is a function of the frequency would produce baroreflex and non-baroreflex sequences without the need of an intermittent control mechanism. Experimentally spontaneous baroreflex and non-baroreflex sequences accounted for only 30% of all cardiac cycles occurring during study periods [124, 62]. This could be the result of phase function depending on the frequency and of an input signal composed of several frequency components, such as LF and HF components. In addition, the sequence method does not take into account the dynamic of the baroreflex mechanism. Even if a rectilinear variation in the input signal produces a rectilinear variation in the output signal [147], one can expect that the slope of the relative variation depends on the speed of variation itself. It is obvious that a variation of 5% in the input signal in 4s (HF) set a control reaction that could be different from the one set when an equivalent variation is produced in 10s (LF). The sequence method completely neglects dynamics. Panerai found that low-pass filtering produced significantly smaller values of sequence-BRS but these agreed with spectral-BRS from the LF band. Conversely, high-pass filtering did not affect the sequence-BRS estimates but better agreement was obtained with spectral-BRS estimates based on the HF band [120]. Therefore, sequence-BRS resumes in one measure the information on baroreflex characteristics that, on the other hand, spectral-BRS provides by two different measures which intrinsically take into account baroreflex dynamics. In addition, our group demonstrated that breathing frequency affects the sequence-BRS estimate as well as the HF spectral-BRS [93].

Therefore, to assess BRS we applied spectral method and in some case, such as in chronic heart failure study, the two methods were compared.

Concluding, even if it is a very reductive concept, baroreflex sensitivity in the two frequency bands provides very useful markers of the control of the cardiovascular system by ANS in both physiological and pathological studies as we will demonstrate in the following sections.

4 Spectral analysis of Low and High Frequency bands

4.1 Introduction

This section is meant to be a review of the algorithms applied to cardiovascular time-series to estimate the non-invasive spectral markers previously introduced. We will define the frequency bands of interest (HF and LF), the respiratory role in HF band definition and, finally, the respiratory and cardiovascular parameters that will be applied in physiological and pathological studies as reported in the following section.

RR, systolic- (SBP), diastolic- blood pressure (DBP) values and other related parameters are not constant but change quite considerably on a beat-to-beat basis. The development of ABP and RR non invasive continuous recording and of powerful methods for signal analysis, has allowed the study of this spontaneous variability. Short-term spectral analysis provides parameters able to analyze the properties of the autonomic nervous system and gives significant indicators in physiological conditions (i.e. the response to various provocative tests) in normal subjects, as well as in various pathologies (hypertension, heart failure, etc.). It allows the decomposition of a signal into individual frequency components, establishing the relative intensity of each and estimating baroreflex sensitivity in pre-selected frequency bands as we will define in the following.

4.2 Classical Spectral Analysis

4.2.1 Preliminary signal processing

Short-term spectral analysis of cardiovascular signals considers stationary tracings of at least 128-256 consecutive beats (corresponding to 128-256 s). To reduce discarded periods because of noise or abrupt signal variations, usually, a 50% overlapping function was applied on the 256 point-length buffer. The overlapping at 50% and the Hanning window are currently the most commonly used preprocessing methods. Shorter time interval would considerably decrease the resolution of the spectrum, while a longer duration may affect the stationarity of the time series. We extract the systolic and diastolic beat-to-beat values from the pulsatile pressure recorded by Finapres and the beat-to-beat RR interval series are derived from EKG. The respiratory signal is recorded to derive central respiratory frequency which defines the high frequency band as explained below. These beat-to-beat signals are resampled by spline functions at 2 Hz (or 4 Hz) obtaining discrete time series equidistantly spaced.

4.2.2 Single-channel analysis

Time analysis

Let x_n^{raw} be the n-th sample of the 256 cardiovascular time series, resampled at 2 Hz. The cardiovascular time series are pass-band filtered, eliminating all the frequency components outside the frequency band of interest (0.05-0.40 Hz) such as linear trend and high frequency noise. We apply a Finite Impulse Response (FIR) filter that has a constant delay (easily evaluated) in the entire frequency band allowing the time relationship between all the cardiovascular signals to be kept. It is now possible to assess the signal power ($\sigma^2_{x^{raw}} - P_{VLF}$) in the considered frequency band:

$$\sigma^2_{x^{raw}} - P_{VLF} = \sigma_x^2 = \frac{1}{N}\sum_{i=0}^{N-1}(x_i - \tilde{x})^2$$

where $\tilde{x}$ is the mean value of the pre-filtered time series x_n in the analyzed period. This allows us to assess, in the following, the normalized values as suggested by Malliani, see equation (33).

Time-series Spectral analysis

The discrete Fourier Transform (DFT) can be used to estimate the spectra. The Hanning weighting function is applied to reduce side and main lobes of DFT filters without altering the locations of the centers of the filter and reducing the leakage error.

Indicating by w_i the i-th value of 256-Hanning window, the DFT used to obtain a discrete estimate of the *complex spectrum* $X(k\Delta f)$ of a truncated series x_n is:

$$\textit{Complex Spectrum} \quad X(k\Delta f) = \sum_{i=0}^{N-1} x_i \, w_i \, e^{-j2\pi k\Delta f i T_o}$$

Where N=256 points, $T_o = 0.5\,s$ is the time-step of the resampled data series , w_i stands for i-th value of 256-Hanning window and $\Delta f = 1/T = 0.008Hz$ is the discrete frequency step (or spectral frequency resolution).

From the above complex spectrum the two sided *Amplitude Spectral Density Function* (ASDF), in short amplitude spectrum $D_x(k\Delta f)$, is computed according to:

$$\textit{Amplitude Spectral Density Function} \quad D_x(k\Delta f) = |X(k\Delta f)| = \sqrt{X_R^2(k\Delta f) + X_I^2(k\Delta f)}$$

$X_R^2(k\Delta f)$ and $X_I^2(k\Delta f)$ represent the real and imaginary parts of the complex spectrum $X(k\Delta f)$ respectively.

The two-sided *Power Spectral Density Function* (PSDF), or, in short, the power spectrum, or autospectrum, in the discrete form is defined as:

$$\textit{Smoothed Power Spectral Density } D_{xx}(k\Delta f) = D_x(k\Delta f)^2 = X_R^2(k\Delta f) + X_I^2(k\Delta f)$$

The spectra were then averaged to reduce standard deviation. Spectral averaging can be obtained by averaging a set of spectral estimates of disjoint sub-records of the same time length -i.e. Bartlett's procedure. Another approach to minimize the variance of the spectral estimate is to average over a number of discrete spectral components. This method, simply called *smoothing*, is applied to all the spectra calculated in our experimental studies.

$$\textit{Smoothed Power Spectral Density } \bar{D}_{xx}(k\Delta f) = \frac{1}{M+1} \sum_{k=-\frac{M}{2}}^{\frac{M}{2}} D_{xx}(k\Delta f)$$

in which M is odd (we fixed M=5). A smoothed spectral estimate will be denoted by an over-lined capital, passing from D_{xx} (unsmoothed) to $\bar{D}_{xx}$ (smoothed).

4.2.3 Multi-channel analysis

Cross spectral analysis

Consider now an ideal single input single output system, with input x(t), output y(t) and system frequency response function $H_{xy}(f)$, as shown in figure (24). For the two signals x(t) and y(t) the so called *Cross Spectral Density Function* (CSDF) or cross-spectrum $D_{xy}(k\Delta f)$, is defined as follows:

$$\textit{Cross Spectral Density } D_{xy}(k\Delta f) = X^*(k\Delta f)Y(k\Delta f) = C_{xy}(k\Delta f) - jQ_{xy}(k\Delta f)$$

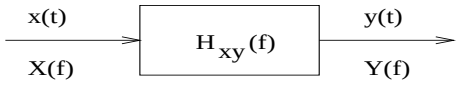

Figure 24: *Ideal single-input single-output system, with transfer function $H_{xy}(f)$.*

where $X^*(k\Delta f)$ is the complex conjugate of the spectrum $X(k\Delta f)$ and where $C_{xy}(k\Delta f)$ and $Q_{xy}(k\Delta f)$ are the Coincident spectral density function and the Quadrature spectral density function. The unit of the cross-spectrum is mmHg per ms if x and y are the ABP and RR-interval respectively.

For the single-input single-output system the following relationship between the transfer function and the input and output power spectra exists:

$$|H_{xy}(k\Delta f)|^2 = \frac{D_{yy}(k\Delta f)}{D_{xx}(k\Delta f)} \tag{39}$$

The ratio of the input and output power spectra reveals only the gain factor of the transfer function $H_{xy}(k\Delta f)$ and no phase estimate can be obtained, equation (39). In the literature, the parameters estimated by eq. (39) are referred to as α index (in both the LF and HF band) as introduced by Pagani et al. [119].
On the other hand, the complex relation between the cross-spectrum $D_{xy}(k\Delta f)$ and the input power spectrum $D_{xx}(k\Delta f)$ can be broken down into a pair of equations for both the gain and phase factors of the system transfer function $H_{xy}(k\Delta f)$:

$$H_{xy}(k\Delta f) = \frac{D_{xy}(k\Delta f)}{D_{xx}(k\Delta f)} \quad \begin{cases} \text{gain:} & |H_{xy}(k\Delta f)| = \dfrac{|D_{xy}(k\Delta f)|}{D_{xx}(k\Delta f)} \\ \text{phase:} & \Phi_{xy}(k\Delta f) = \arctan \dfrac{\mathcal{I}m\,[D_{xy}(k\Delta f)]}{\mathcal{R}e\,[D_{xy}(k\Delta f)]} \end{cases} \tag{40}$$

It should be noted that the estimation of the gain factor with equation (40) is unbiased even if extraneous noise, uncorrelated with the measured input, is present at the output. Whereas the gain estimation by equation (39) will be always biased, except when the coherence function equals the unity. Recently, it has been demonstrated that the α index (in both the LF and HF band) has a lower correlation with phenylephrine estimate BRS than spectral-BRS estimate in LF band (no estimation in the HF band was reported). In addition, the α index showed a greater bias than the spectral-BRS [83].

Defining the *Smoothed Cross Spectral Density* as :

$$\textit{Smoothed Cross Spectral Density } \bar{D}_{xy}(k\Delta f) = \frac{1}{M+1} \sum_{k=-\frac{M}{2}}^{\frac{M}{2}} X^*(k\Delta f) Y(k\Delta f)$$

the *gain factor* $|H_{xy}(k\Delta f)|$ and the *phase factor* $\Phi_{xy}(k\Delta f)$ are obtained by the following two relations:

$$\textit{Gain Factor} \quad |H_{xy}(k\Delta f)| = \frac{|\bar{D}_{xy}(k\Delta f)|}{\bar{D}_{xx}(k\Delta f)} = \frac{\sqrt{\bar{C}^2_{xy}(k\Delta f) + \bar{Q}^2_{xy}(k\Delta f)}}{\bar{D}_{xx}(k\Delta f)}$$

$$\textit{Phase Factor} \quad \Phi_{xy}(k\Delta f) = \arctan\left\{\frac{-\bar{Q}_{xy}(k\Delta f)}{\bar{C}_{xy}(k\Delta f)}\right\}$$

Note that all over-lined terms in these equations are smoothed spectral estimates. In the case of the ABP-RR transfer, systolic ABP series can be considered as the (single) input and the RR series as the output of the reflex system.

Coherence analysis

In analogy to the squared correlation coefficient R^2, which gives the total amount of variance explained by a linear regression model, a squared coherence function $\gamma^2_{xy}(k\Delta f)$ can be defined. This powerful function, which we will briefly denoted as the coherence function, is defined by squared amplitude of the cross-spectrum, normalized by the power spectral of both input and output:

$$\textit{Coherence Function } \gamma^2_{xy}(k\Delta f) = \frac{\left|\bar{D}_{xy}(k\Delta f)\right|^2}{\bar{D}_{xx}(k\Delta f)\bar{D}_{yy}(k\Delta f)}$$

The coherence function can be interpreted as the portion of the output which is linearly related to the input spectrum. The function has values between 0 and 1, being 0 if the input and output signals are fully uncorrelated. In practice a value greater than zero but less than unity can occur due to one or more of the following reasons:

- a non-linear relation between input and output and/or time-varying system parameters;
- the presence of other uncorrelated inputs besides the considered input x(t);
- bias in the cross-spectral and auto-spectral estimates used to compute the cross-spectral function;
- time delay T_d between input and output signals in relation to the recorded length T, causing a relative bias of approximately T_d/T.

In almost all papers on BP-RR transfer function analysis a coherence value of 0.5 is taken as a border value to accept the transfer function estimate as sufficiently reliable.

In this context the coherence of ABP and pulse interval can be taken as a quantitative measure for the range of expected baroreceptor interactions. Baroreflex mechanism studies in the frequency domain rely on the assumption that the cardiac branch of the baroreflex can only modulate RR within a certain frequency range.

In conclusion, in order to study cause-effect relations coherence analysis cannot be neglected because if coherence is not significant no cause-effect relation between the variables can be present. The reverse is not true. Coherence is a measure of correlation in spectra. The presence of significant correlation does not prove a cause-effect relationship between the variables.

4.2.4 Spectral analysis interpretation

The interpretation of a power spectrum is straightforward: it shows the amount of variation in the data for each frequency. If the coherence is low for certain frequency, the gain and phase cannot be reliable estimates. Thus, it is now possible to calculate the energy, gain and coherence in the low and high frequency bands. The power spectral density of the preprocessed signals should be computed and the area under the spectral density curve between two limits should be estimated providing the energy in the low and high frequency bands. One problem remains: the frequency band definition.

4.3 Spectral Analysis Applied to Cardiovascular and Respiratory time series

4.3.1 Spectral band assessment

Respiration role and High Frequency band definition

The use of spectral analysis to describe central nervous system activity requires determining the breathing activity to allow for the comparison of cardiovascular spectral components between different periods. Several studies have shown that respiratory rate and tidal volume exert major influences on RR-interval or HR fluctuations [3, 19], throughout all this report we will be concentrated only on the breathing rate, leaving the tidal volume spontaneously regulated by the subjects. These studies are important because if fluctuations of RR intervals are considered to be valid indexes of autonomic neural traffic, then they should reflect such traffic faithfully and should not be greatly influenced by respiratory-autonomic interactions unrelated to the net cardiac neural outflow. Brown [19] found that respiratory rate and tidal volume strongly influence low and respiratory frequency RR-interval power but not the mean RR value. Thus vagal activity during the respiratory cycles varied considerably, whereas the overall tonic level remained constant. Other studies also document a dependence of RR-interval (or HR) fluctuations such as those by Hirsch and Bishop [59] and also of ABP fluctuations, for instance Novak [108], on respiratory parameters. Only when respiratory variables are statically controlled there is an evidence of a reasonable correspondence between β-blocked heart period and respiratory sinus arrhythmia amplitude [52]. Thus, respiratory parameters need to be controlled when using RSA amplitude as an index of cardiac vagal tone.
That is why throughout our study we applied the following principles which are not usually taken into account in the medical environment:

- analyses are made only on periods with regular breathing activity in order to have a well-defined single spectral peak on respiratory SPSD;
- breathing rate was estimated by peak estimate on respiratory SPSD. This allows us to study, at constant breathing rate, changes in cardiovascular spectral components induced by sleep stages [104], by drug infusion [94] and by chronic heart failure disease [93]. In addition, by varying breathing rate we were able to use respiratory activity as a probe to gain insight into cardiovascular system variability and to test ANS effectiveness in physiological and pathological conditions [93, 92];
- the regularity of the breathing activity was estimated by a spectral dispersion index defined below;
- the HF band was centered on the current breathing rate;
- the HF band was defined with a narrow spectral bandwidth (0.06 Hz bandwidth) and hence the energy in the HF band really represents the energy of cardiovascular spectral component which is synchronous to respiration. Other spectral components are not taken into account in HF energy, which would not be the case if a pre-defined frequency band was considered - as is usually done.

High Frequency band limitations

It is obvious that in reality respiratory activity is not regular. Some important physiological information about ANS control of the cardiovascular system may be lost when we limit the analysis to only regular breathing periods: our group in a sleep study [104], limited REM analysis to only tonic-REM which is known to have more breathing instability than phasic-REM [4]. In addition, imposing an exogenous breathing rate alters the natural regulation of the breathing rate and the interactions between the

respiratory center and the cardiovascular center. In fact, voluntary breathing involves specific cortical regions in the brain, which have been localized in humans [40]. Furthermore, robust connections exist between the cerebral cortex, the brainstem respiratory motoneurons, and the hypothalamic area [33, 70], a cardiovascular and respiratory integrative structure. Taken together, these neural findings reveal that when we impose an exogenous breathing rate, the indexes estimated by cardiovascular signals can not be considered as "spontaneous" indexes, but they depend on the paced breathing condition. On the other hand, this experience provides useful indexes both in normal and pathological conditions, as showned by our group [93].

Low Frequency band definition

Low frequency oscillation is not a steady state phenomenon, in fact without doubt it changes both in amplitude and in frequency with time. In the literature, a frequency band has been provided as a reference [0.04 Hz; 0.12 Hz] [44]. Throughout our studies, we chose a fixed LF window as suggested by the research community.

4.3.2 Spectral parameters assessment

Respiratory parameters

We consider the breathing rate (BR) and the dispersion index (DI) of the respiratory spectrum, given by FFT analysis. BR and DI are computed as follows:

$$\begin{aligned} &\textit{Breathing rate} \quad BR = \left\{ k\Delta f : \bar{D}_{resp,resp}(k\Delta f) = max\left\{ \bar{D}_{resp,resp} \right\} \right\} \\ &\textit{Dispersion index} \quad DI = \frac{\sum_{k\Delta f \in AW} (k\Delta f - BR)^2 \, \bar{D}_{resp,resp}(k\Delta f)}{\sum_{k\Delta f \in AW} (k\Delta f - BR)^2 \, \bar{D}_{resp,resp}(BR)} \end{aligned} \tag{41}$$

The BR corresponds to the frequency of the maximum in the respiratory SPSD, $\bar{D}_{resp,resp}(k\Delta f)$. The DI provides an estimation of the regularity of the breathing activity. DI assessment allows us to select periods with a regular respiratory activity without apneas and abrupt changes in both breathing-rate and -amplitude and to assess this regularity quantitatively. In medical environment, a Poincaré plot, defined as a scatter plot of the current signal sample against the previous one, is usually used to provide a qualitative picture of respiratory behavior. The DI may quantify the Poincaré qualitative estimation of the presumed regularity of the spontaneous respiratory activity. The DI takes value between zero and one and evaluates the dispersion of the respiratory spectrum around BR. The DI is equal to zero if the breathing activity is merely sinusoidal and the respiratory SPSD completely concentrated around the actual BR. The more regular the respiratory activity is, the more respiratory spectrum is concentrated around BR, the more regular the ellipsoidal shape of the Poincaré plot is and the smaller the DI is (an example of this comparison is shown in fig. (25) in a sleep study).

Cardiovascular parameters

Once the frequency bands have been defined (LF: 0.05-0.13Hz and HF: a 0.06Hz bandwidth around the actual BR), we evaluate the signal energy and the mean coherence and baroreflex sensitivity in these bands:

$$
\begin{array}{ll}
\textit{Spectral components} & FB_x = \sum_{k\Delta f \in FB} \bar{D}_{xx}(k\Delta f) \\
\textit{Normalized spectral components} & FBnu_x = \dfrac{\sum\limits_{k\Delta f \in FB} \bar{D}_{xx}(k\Delta f)}{\sigma_x^2} \\
\textit{Coherence values} & cFB_{x,y} = \frac{1}{\mathcal{L}_{FB}} \sum_{k\Delta f \in FB} \gamma_{xy}^2(k\Delta f) \\
\textit{Baroreflex sensitivity} & gFB_{x,y} = \frac{1}{\mathcal{L}_{FB}} \sum_{k\Delta f \in FB} |\bar{H}_{xy}(k\Delta f)|
\end{array}
\tag{42}
$$

where the frequency band FB can be HF or LF, $\mathcal{L}_{*F}$ is the bandwidth expressed in the number of points that allows us to assess the mean coherence and the mean gain values in both the HF and LF bands. The coherence function will be evaluated between: the RR-interval time series and the systolic (SBP) or diastolic (DBP) pressure time series, and between the respiratory time series and the cardiovascular time series. The correct interpretation of the *Baroreflex sensitivity* requires high coherence in these frequency bands; therefore the calculation of $gLF_{x,y}$ and $gHF_{x,y}$ is made after verifying a high value (> 0.5) of coherence in the LF and HF bands.

5 Spectral analysis applied to physiological and pathological conditions

5.1 Introduction

This section shows and discusses the results obtained by our group applying the spectral indexes previously described in both a physiological and a pathological study. We will demonstrate the usefulness of baroreflex sensitivity estimation in both the HF and LF band and the utility of the use of respiratory activity as a probe to gain insight into the functioning of the autonomic nervous system.

We applied the previously described spectral indexes in both physiological and pathological conditions :

- Sleep study

  During the night, sleep follows several cycles of 90 minutes approximately, each comprising, light sleep, slow wave sleep (SWS) and rapid eye movement (REM) sleep. Results of sleep studies are often conflicting, but neither respiratory parameters, although breathing activity considerably influences spectral power [3, 88], nor time evolution all along the night were taken into account. That is why we explored cardiovascular spectral components and baroreflex sensitivity (BRS) in two ways: on the one hand, according to sleep stages influence alone by averaging them over all the night, on the other hand, according to the time course of the sleep, by analysing stage II cycle by cycle.

- Chronic Heart Failure Study

  Autonomic nervous system dysfunction is common in patients with chronic heart failure (CHF) [43]. Indexes of autonomic imbalance and neurohormonal activation add prognostic information to the left ventricular ejection fraction and predict early mortality [133, 139, 26]. Elucidation of the mechanisms underlying the genesis of autonomic dysfunction in CHF is of crucial importance since autonomic dysregulation plays a key role in the progression of the disease. Heart rate modulation via low and high pressure baroreflexes is blunted in heart failure. This is ascribable to a combination of several factors, including abnormalities at the cerebral level [126, 81], a shift in sympathovagal interactions towards sympathetic excitation, and alterations at several input sites in the peripheral system [97]. Various noninvasive methods based on spectral computation of transfer functions [140] have been developed to evaluate baroreflex sensitivity. The cross-spectral ratio or gain between heart rate and blood pressure oscillations determined using a Fourier transform has been found reliable for evaluating baroreflex sensitivity [111, 122, 119]. In addition, instant spectral methods such as time-frequency analyses offer new possibilities for assessing the instantaneous response of cardiovascular oscillations to a varying breathing rate. We conducted the present study to evaluate with time and spectral methods the modulating effects of voluntary breathing on the cardiovascular system controller gain in CHF patients. Part of this work has been reported elsewhere [91].

	W_st.I	REM	St.II	SWS
BR	.24 (.008)	.23 (.005)	.23 (.008)	.24 (.008)
DI	.1840 (.008)	.1848 (.008)	.1594 (.002) ‡**	.1555 (.005)‡ **
$cHF_{resp,RR}$	.61 (.04)	.59 (04)	.66 (03) *	.68 (.03) *
$cHF_{resp,SBP}$	.63 (.04)	.60 (.04) †	.67 (.03) **	.65 (.04) *
$cHF_{resp,DBP}$	.54 (.04)	.51 (.03)	.57 (.03) **	.59 (.03) *

Table 2: *Mean respiratory variable changes between sleep stages. Values are means (SEM). BR -breathing frequency- [Hz], DI -dispersion index- in [0-1], cHF_{resp}, CV -coherence between respiration and CV signals in HF band- in [0-1]. Symbol legend: † : REM vs W_St.1; ‡ : W_St.1 vs St. II or SWS; *: REM vs St. II or SWS. Degree of significance: $p \leq 0.05$, one symbol; $p \leq 0.01$, two symbols. From [104].*

5.2 Spectral Analysis in Physiological Condition: Sleep study

5.2.1 Methods

Data acquisition.

Sleep analysis was visually made according to Rechtschaffen and Kales [136] and scored as stages I (St.I), II (St.II), III, IV and REM sleep. Nocturnal awakenings were defined as awakenings of at least 1 min duration occurring during the sleep period.

Periods selection

We selected only periods with regular breathing activity and a well-defined breathing rate, excluding periods with abrupt changes of breathing rate or other breathing abnormalities. This selection probably limited REM analysis to only tonic-REM which is known to have more breathing stability [4].

Averaged sleep stages analysis.

All periods of a given sleep stage were merged together, independently of sleep cycle, to analyse between sleep-stages differences; concealing time evolution of the different stages during the night.

Specific sleep stage II analysis throughout the night.

St.II evolution over the night was followed to analyse between sleep-cycles differences. First and last cycle were compared to estimate the time course of CV and respiratory parameters throughout the night. St.II alone was analysable in this way, because always present from the first to the last cycle (stages III-IV were at the beginning of the night and last REM was not always present).

Sleep stage classification.

We classified analysis periods as: nocturnal awakening and stage I (W_St.I), St.II, SWS (slow wave sleep, stages III and IV), and REM. NREM refers to St.II and SWS, sleep stages refer to NREM and REM sleep.

5.2.2 Results

Sleep stages comparison

Respiratory parameters (see table 2).

	W_St.I	REM	St. II	SWS
$mean_{RR}$	994 (18)	1005 (33)	1000 (36)	1011 (40)
$mean_{SBP}$	114 (5)	113 (4)	114 (4)	113 (3)
$mean_{DBP}$	68 (3)	70 (3)	69 (3)	69 (2)
Std_{RR}	61 (7)	50 (5)	55 (4)	40 (3) *§‡‡
Std_{SBP}	7.37 (0.90)	5.18 (0.41)††	5.51 (0.33) ‡	4.72 (0.28) §‡‡
Std_{DBP}	4.95 (0.84)	3.19 (0.25)††	3.51 (0.31) ‡	2.69 (0.19) §‡‡

Table 3: *Mean and standard deviation of RR, SBP and DBP. Mean and (SEM): $mean_{RR}$ [ms]; $mean_{BP}$ [mmHg]. Standard deviation and (SEM): Std_{RR} [ms]; Std_{BP} [mmHg]. Symbol legend: † : REM versus W_St.1; ‡ : W_St.1 versus St. II or SWS; *: REM versus St. II or SWS; § : St.II versus SWS. Degree of significance: $p \leq 0.05$, one symbol; $p \leq 0.01$, two symbols. From [104].*

In selected periods $mean_{BR}$ was constant across all sleep stages with a very small intra-individual Std, around 0.016Hz (not shown). In fig. (25), the Poincaré plot (scatter plot of the respiratory signal against

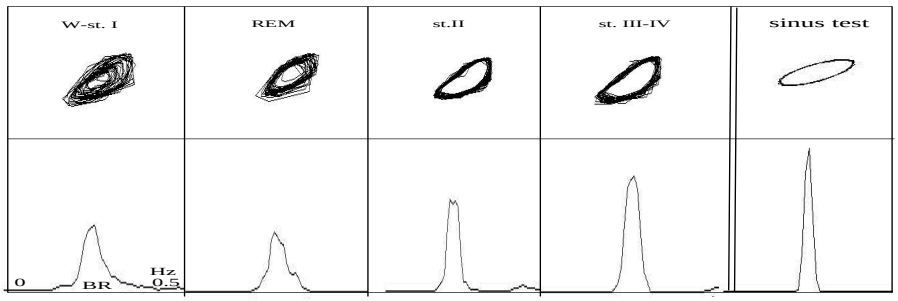

Figure 25: *Poincaré plot (top part) and FFT spectrum of 2min recordings of breathing (2Hz resampled signal in arbitrary units) in one subject during the 4 selected sleep periods: W_St.I (wakefulness and stage I), REM sleep, stage II and stages III-IV. Comparison with a sinusoidal signal is shown on the right hand side to underscore the qualitative feature of Poincaré plot and quantitative feature of dispersion index in assessing regularity of breathing activity. Mean breathing rate is constant around 0.23-0.24 Hz, while breathing dispersion index increases in W_St.I and REM sleep (DI=.1840 and DI=.1848 respectively) compared to NREM sleep (DI=.1594 for St.II and DI=.1555 for St.III-IV) which is underscored by a progressive increase in regularity of Poincaré plot and by a progressive narrowing of respiratory power spectra around actual breathing rate. From [104].*

the previous one) and the spectrum of a typical respiratory signal and a sinusoidal signal are compared. The more regular is respiratory activity, the more the respiratory spectrum is concentrated around BR and the more regular is the ellipsoidal shape of the Poincaré plot. DI (lower in NREM) quantitatively confirmed that breathing is more regular in NREM than in REM and W_St.I. Coherence values between breathing and CV signals (greater in NREM) revealed a greater linear influence of the respiration on HF components in NREM than in REM sleep.

Mean values and spectral components (see tables 3, 4 and 5).

	W_St.I	REM	St. II	SWS
HF_{RR}	2.57 (1.11)	2.98 (1.22)	2.89 (1.09)	2.65 (1.06)
$HFnu_{RR}$	.231(.04)	.222(.04)	.298(.04) **‡‡	.320(.06) *
HF_{SBP}	.0035 (.001)	.0026 (.0008)	.0046 (.0003)	.0030 (.0011)
HF_{DBP}	.00094 (.00028)	.00089 (.00003)	.00078 (.00026)	.00056 (.00018)
$gHF_{SBP,RR}$	20.8 (3.92)	25.9 (3.92) †	24.3 (3.85)	25.5 (4.16) ‡
$gHF_{DBP,RR}$	39.8 (8.05)	47.0 (8.16)	46.46 (5.28)	51.80 (7.70)‡

Table 4: *High frequency (HF) spectral components and gain for RR, SBP, DBP. Values are means (SEM). HF_{RR} [ms^2/Hz], $HFnu_{RR}$ in normalized unit [0-1], HF_{BP} [$mmHg^2/Hz$], $gHF_{BP,RR}$ -gain between BP and RR in HF band- [ms/mmHg]. Symbol legend: † : REM versus W_St.1; ‡ : W_St.1 versus St. II or SWS; *: REM versus St. II or SWS. Degree of significance: $p \leq 0.05$, one symbol; $p \leq 0.01$, two symbols. From [104].*

	W_St.I	REM	St. II	SWS
LF_{RR}	9.22 (4.08)	8.71 (2.48)	7.00 (2.43)	4.64 (1.45) *
$LFnu_{RR}$	.76 (.04)	.77 (.04)	.70 (.04) **‡‡	.67 (.06) **
LF_{SBP}	.037 (.011)	.023 (.005) †	.019 (.004)	.022 (.004)
LF_{DBP}	.0180 (.0057)	.0092 (.0020) †	.0074 (.0015)‡	.0075 (.0014)
$gLF_{SBP,RR}$	14.7 (2.42)	17.7 (2.45) ††	15.64 (2.47)	12.83 (1.40) **
$gLF_{DBP,RR}$	21.8 (3.37)	26.1 (3.55) ††	23.95 (3.84)	22.16 (2.93) *

Table 5: *Low frequency (LF) spectral components and gain for RR, SBP, DBP. Values are mean (SEM). LF_{RR} [ms^2/Hz], $LFnu_{RR}$ in normalized unit [0-1], LF_{BP} [$mmHg^2/Hz$]; $gLF_{BP,RR}$ -gain between BP and RR in LF band- [ms/mmHg]. Symbol legend: † : REM versus W_St.1; ‡ : W_St.1 versus St. II or SWS; *: REM versus St. II or SWS. Degree of significance: $p \leq 0.05$, one symbol; $p \leq 0.01$, two symbols. From [104].*

There were no significant differences between sleep stages for mean values. HF showed a dissociation between results expressed in absolute and normalised units: HF_{RR} had no change whatever the sleep stage was, whereas $HFnu_{RR}$ were lower in REM than in NREM. For LF, results agreed: LF_{BP} was higher in REM than in SWS, revealing a between sleep-stage difference. LF_{BP} were lower in REM than in W_St.I, LF_{DBP} was lower in St.II than in W_St.I, showing a between wake-sleep difference.

Arterial baroreflex sensitivity (see tables 3 and 4).

$gHF_{BP,RR}$ were higher in REM and SWS than in W_St.I, revealing a between wake-sleep difference; whereas $gLF_{BP,RR}$ were higher in REM than in SWS, showing a between sleep-stage difference.

Sleep stage II analysis during succeeding sleep cycles

Time course of CV and respiratory parameters in a typical subject is shown in fig. (26).

$mean_{RR}$ and HF components increased whereas BR decreased progressively all along the night. Changes in BRS varied between subjects, without a general pattern as shown in fig. (27).

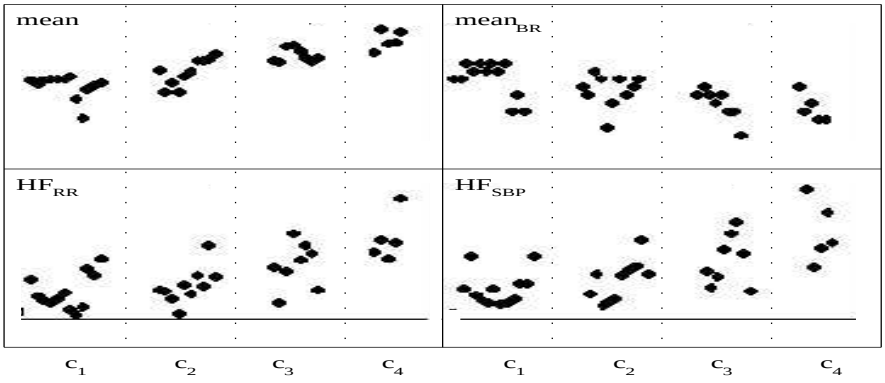

Figure 26: *Cycle-by-cycle evolution (from c1 to c4) of $mean_{RR}$ [ms], $mean_{BR}$ [Hz], HF_{RR} [ms^2/Hz] and HF_{SBP} [$mmHg^2/Hz$], in one typical subject during sleep stage II. Each data point represents an average value over 2 min. $Mean_{RR}$ progressively increases and simultaneously HF_{RR} and HF_{SBP} rise while $mean_{BR}$ slightly decreases. From [104].*

	First cycle	Last cycle	Significance P value
$mean_{RR}$	979 (47)	1068 (44)	**
$mean_{BR}$	.23 (.008)	.21 (.008)	*
$mean_{SBP}$	128.2 (5.37)	116.3 (5.86)	.10
HF_{RR}	1.82 (.76)	3.92 (1.54)	**
$HFnu_{RR}$	.300 (.260)	0.405 (.239)	.09
HF_{SBP}	.0027 (.001)	.0060 (.002)	*
HF_{DBP}	.00047 (.00043)	.001 (.001)	*
$LFnu_{RR}$	.700 (.269)	.595 (.239)	.09
LF_{SBP}	.021 (.012)	.012 (.002)	*
LF_{DBP}	.006 (.005)	.004 (.003)	**

Table 6: *Mean variables during first and last cycles, in St. II, for 7 subjects. Values are mean (SEM). $mean_{RR}$ [ms], $mean_{BR}$ [Hz], $mean_{SBP}$ [mmHg], HF_{RR} [ms^2/Hz], $HFnu_{RR}$ and $LFnu_{RR}$ in [0-1] HF_{BP} and LF_{BP} [$mmHg^2/Hz$]. Degree of significance: $p \leq 0.05$, one symbol; $p \leq 0.01$, two symbols; numerical values are reported for $p \leq 0.10$. From [104].*

First and last sleep cycle comparison.

CV parameter changes between first and last sleep cycles are reported in table (6) for 7 subjects. $mean_{RR}$ and $mean_{BR}$ decreased significantly (note that $mean_{BR}$ decrease was very slight), $mean_{SBP}$ nearly significantly. Whatever the spectral component unit is, HF increased, (in particular, HF_{RR} and HF_{BP} approximately doubled) showing a large between sleep-cycle difference. In the LF band, only LF_{BP} decreased significantly. Contrary to the others CV parameters, gHF_{BP},RR and $gLF_{BP,RR}$ had no changes (see fig. 27).

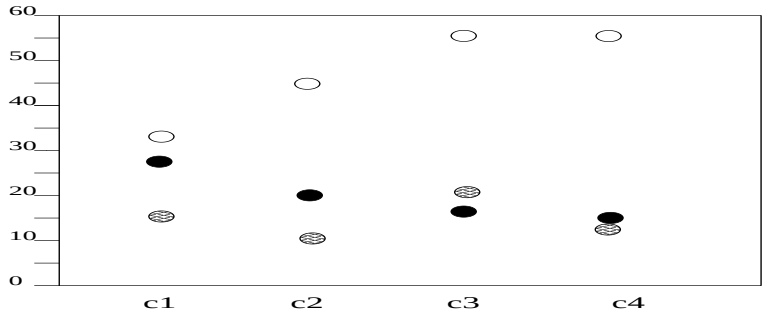

Figure 27: *Cycle-by-cycle evolution (from c1 to c4) of $gHF_{BP,RR}$ [ms/mmHg] for 3 subjects during sleep stage II, evidencing the lack of a common pattern. Each data point represents an average value over one cycle. From [104].*

5.2.3 Discussion

Cardiovascular (CV) variability and baroreflex sensitivity (BRS) depend on both stages and cycles organisation. CV variability is largely affected by sleep stage organisation: the greatest vagal activity combined to the lowest vascular sympathetic activity is found in NREM; and also by the sleep cycle organisation, the vagal activity increased and the vascular sympathetic activity decreased from the first to the last cycle. We show that changes of CV spectral components are independent of mean BR changes. In addition, we confirm the greater respiratory stability and linear influence between breathing and CV system during NREM than REM. BRS estimation in both LF and HF bands allows to unify previous results obtained by drug and non invasive methods: BRS is greater in sleep than in nocturnal wake and further increased in NREM. In sleep stages organisation, BRS has a band dependent behaviour: in NREM, the high $gHF_{SBP,RR}$ value combined to the low $gLF_{SBP,RR}$ value favour the short term control, whereas in REM, the two BRS components are high, contributing together to the strongest control in this state. Sleep cycle organisation does not clearly affect BRS, BRS varies without significant pattern over the night, suggesting that other CV control mechanisms are predominant. Our results suggest that both sleep-cycle organisation and BRS estimation in both LF and HF band should be taken into account in sleep study analysis.

Respiration

The comparison of CV spectral components between different periods requires the determination of BR. This way alone is able to dissociate CV spectral variations partially due to BR variations from variations independent of it. $mean_{BR}$ is the same across sleep stages, as in another analysis not concerned by breathing selection [39]. In St.II analysis over the night, $mean_{BR}$ has a very small decrease of 0.02Hz (1.2 cycles/min), and, therefore, enable to explain the great HF differences between the first and last cycles. In fact, the transfer function features from respiratory activity and RR and BP show that small changes of BR around 0.23Hz could provide only small changes in CV spectral components [108, 141]. These two results show that CV spectral components changes are independent of BR changes.

The greater respiratory stability and linear influences between breathing and CV system in NREM than in REM, found in [18, 90, 36] is confirmed by the analysis of the breathing dispersion and the coherence between signals: DI is greater, HF coherence is smaller in REM than in NREM.

Sympathetic and parasympathetic activity

Cardiac autonomic activity.

Sleep studies results are conflicting: $mean_{RR}$ is higher and the RR-variability lower [106, 36, 172] in NREM than in REM, but not always [5, 61, 148, 161]. Estimated vagal activity is found higher in NREM than in REM [5, 8, 106, 36, 161] but not always [162, 163, 172]. Estimated cardiac sympathetic activity is higher [5, 106, 36, 161, 162], smaller [8, 125] or equal [172] in REM than in NREM. These differences could be due in part to the use of different variables to estimate the cardiac autonomic activity. Indeed the use of $mean_{RR}$ and absolute spectral values (HF_{RR} and LF_{RR}) [8, 162, 163, 172] or the use of relative values ($HFnu_{RR}$, $LFnu_{RR}$) [5, 106, 36] and the power ratio LF_{RR}/HF_{RR} [161] do not lead to the same results as shown in the table 3. In our point of view, meanRR could better reflect changes in cardiac autonomic tone as it is the result of the net opposite effects of the sympathetic and parasympathetic tonic activity on the sinus node [49]. Conversely relative spectral power $LFnu_{RR}$ and $HFnu_{RR}$, could better represent autonomic modulation of meanRR around a given autonomic tone [134, 94]. Together they could provide different information on sympathovagal interactions [32]. The dissociation between meanRR and RR variability in the sleep stage analysis is in agreement with the hypothesis of two independent control mechanisms [134, 94]. The absence of change in meanRR could reflect an absence of change in autonomic tone, whereas the higher value of $HFnu_{RR}$ (lower for $LFnu_{RR}$) in NREM than in nW-St.I and REM suggests a shift of the autonomic modulation towards a vagal predominance in this state. On the contrary, a parallel evolution in $mean_{RR}$ and RR variability is found in the cycle-by-cycle St.II analysis. The increase in $mean_{RR}$ and $HFnu_{RR}$ and the decrease in $LFnu_{RR}$ suggest that the autonomic tone and modulation of RR are modified together towards a progressive relative greater cardiac vagal activity along the night. Autonomic tone is more sleep-cycle than sleep-stage organisation dependent, whereas autonomic modulation is influenced by both patterns.

Vascular sympathetic activity.

LF_{BP} is similar between NREM and REM, contrary to sympathetic output to skeletal muscles blood vessels which is markedly increased during REM at a level similar or even higher than during wakefulness [148, 110, 61], as previously found [36]. This may be a consequence of the opposite sympathetic drives found in animal studies: a decrease in the splanchnic and in renal circulation and an increase in the skeletal muscle vessels occurring during REM [90, 125]. Cycle by cycle St.II analysis shows an overall decrease of sympathetic vascular activity. Therefore, vascular sympathetic activity is both wake-sleep transition and sleep-cycle organisation dependent.

Baroreflex sensitivity

Smyth assessing drug-BRS concluded that BRS is higher in sleep (REM and NREM) than in nocturnal wake (nW) [147] but, in later studies, this was only partially confirmed [18, 28]. More recently, Van De Borne assessing spectral-BRS only in the low frequency band ($gLF_{SBP,RR}$) concluded that BRS is higher in REM than in NREM and nW, but found no difference between nW and NREM sleep is not found [36].

Note that drug-BRS still represents the gold standard although it is an invasive method [83]. The simultaneous assessment of $gLF_{SBP,RR}$ and $gHF_{SBP,RR}$ could explain that Smyth and Van De Borne results are not conflicting and that the non invasive spectral analysis gives the same results as obtained by drug application. BRS evolution in low frequency, $gLF_{SBP,RR}$, is the same as assessed by Van De Borne whereas BRS evolution in high frequency, $gHF_{SBP,RR}$, is the same as assessed by Smyth. This could be due to the fact that the sequence-BRS enlight especially short RR-SBP sequences reflecting the short term control, as found in [62, 93, 120]. Thus, the simultaneous assessment of $gLF_{SBP,RR}$ and $gHF_{SBP,RR}$ allows us to distinguish the relative part of the long and short term control in the baroreflex loop.

Sleep stage organisation differently affects short ($gHF_{SBP,RR}$) and long term ($gLF_{SBP,RR}$) control. BRS increase from wake to sleep is principally due to short term control whereas the further BRS increase from NREM to REM is principally due to long term control. REM has the greatest values for $gLF_{SBP,RR}$, as found in [18, 121, 147, 36], and for $gHF_{SBP,RR}$: this increased neural feedback could more effectively buffer CV perturbations secondary to bursts of brainstem stimulation during phasic REM and also could maintain a strong CV control during longer tonic REM periods. REM and nW-St.I represent opposite situations: in REM, $gHF_{SBP,RR}$ and $gLF_{SBP,RR}$ are greater whereas BP global variance and LF_{BP} variability are lower than in nW-St.I, showing that in nW-St.I, the CV control is less involved in buffering CV perturbations. In SWS, a great $gHF_{SBP,RR}$ and a low $gLF_{SBP,RR}$ seem to favour the short-term control which is in agreement with the fact that CV control in SWS is mainly linked to respiratory influence. BRS efficiency is a band dependent phenomenon, as, in every sleep stage, $gHF_{SBP,RR}$ is greater than $gLF_{SBP,RR}$ ($P \leq 0.01$, not shown); this is in agreement with Parati who observed that sequence-BRS decreased as the time over which baroreceptor modulated the sinus node increased and concluded that BRS is the most effective when engaged briefly [121]. No BRS pattern evolution throughout the night was evidenced in gHFSBP,RR or in gLFSBP,RR, consistent with Parati's results [121]. This suggests that the BRS is not clearly influenced by sleep-cycle organisation and that other mechanisms are predominant on the CV autonomic control throughout the night. Therefore, the HF_{CV} increase and the LF_{CV} decrease during the night might be related to a reduced low-pass characteristic of vascular system due to a decrease in total peripheral resistance, one of the mechanisms responsible for the blood pressure fall in sleep [18]. The different time evolution of BRS between subjects might be due to different resetting mechanisms of the cardiac baroreflex, previously illustrated [147, 18].

5.3 Spectral Analysis in Pathological Condition: Chronic heart failure study

5.3.1 Methods

For five minutes, the subjects were trained to pace their breathing with a periodic auditory stimulus. After a 15-minute rest, the recordings were performed during two, five-minute, random-order periods of breathing paced at 0.25 Hz (15 breaths/min, which is close to the spontaneous breathing rate) and 0.15 Hz (9 breaths/min), respectively. During the paced-breathing periods, the subjects were allowed to control the depth and shape of each breath so as to mantain normal alveolar ventilation.

5.3.2 Results

Controls

The mean RR interval , systolic pressure and the standard deviation (StD) of the SBP signal were the same at the two breathing rates, see table (7). RR and SBP oscillations in the HF and LF domains were increased at the slower breathing rate, $P < 0.05$ table (7). Coherence function values between the RR interval and blood pressure oscillations were around 0.8-0.9, indicating a strong correlation between the two parameters (data not shown). This allowed the spectral gain to be calculated.

At the slower breathing rate, the baroreflex gain increased in the HF domain, denoting a frequency-dependent response, table (9), whereas the baroreflex gain remained unchanged in the LF domain.

The mean regression slope was higher at the slower breathing rate: 10 ± 2.8 ms/mmHg at 0.25 Hz vs. 12 ± 2.4 ms/mmHg at 0.15 Hz; a typical example is shown in fig. (28).

CHF patients

	Control (n=6)			Heart Failure (n=7)		
	SB	CB		SB	CB	
BR (Hz)	.28	.25	.15	.25	0.25	0.15
RR (ms)	779 ± 94	768 ± 100	795 ± 100	804 ± 80	793 ± 73	790 ± 68
StD RR (ms)	27 ± 20	21 ± 9	40 ± 20 *	17 ± 12	15 ± 8	18 ± 12 ‡
SBP (mmHg)	114 ± 20	108 ± 14	110 ± 14	118 ± 13	119 ± 11	114 ± 14
StD SBP (mmHg)	3 ± 1	4 ± 1	4 ± 1	4 ± 1	3 ± 2	4 ± 2
DBP (mmHg)	63 ± 12	60 ± 10	60 ± 10	66 ± 12	65 ± 12	64 ± 13
StD DBP (mmHg)	2 ± 0.5	2 ± 0.5	2 ± 0.5	2 ± 1	2 ± 1	2 ± 1

Table 7: *Data are expressed as mean $\pm$ StD. SB: spontaneous breathing. CB: controlled breathing. StD: standard deviation. BR: breathing rate. Symbol key: $*$: $p \leq 0.05$ 0.15 Hz vs. 0.25 Hz; ‡: $p \leq 0.05$ Heart Failure patients vs. control group during controlled breathing periods. From [93].*

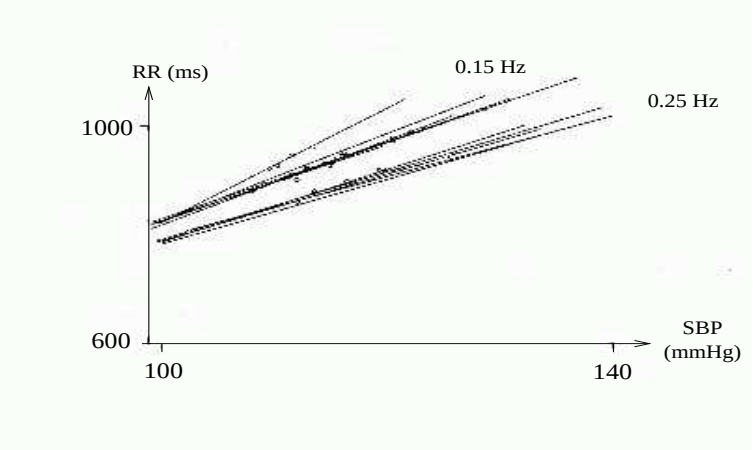

Figure 28: *Spontaneous cardiac baroreflex in the time domain in a control subject. At the slower breathing rate, the baroreflex gain increased . From [93].*

Frequency Domain	Control (n=6)			Heart Failure (n=7)		
	SB	CB		SB	CB	
HF_{RR}	0.7 ± 0.8	0.8 ± 0.8	8 ± 9 *	0.5 ± 0.5	0.7 ± 0.7 †	1.1 ± 1.7 *‡
LF_{RR}	0.9 ± 0.9	0.4 ± 0.2 †	3 ± 2.4 *	0.6 ± 0.6	0.4 ± 0.5	0.7 ± 0.6 ‡
HF_{SBP}	10 ± 9	6 ± 3	20 ± 10 *	3 ± 2	4 ± 4	10 ± 10 *‡
LF_{SBP}	3 ± 4	10 ± 4 †	20 ± 7 *	9 ± 7	5 ± 5 ‡	9 ± 7
HF_{DBP}	1 ± 1	0.9 ± 0.9	5 ± 1 *	0.5 ± 0.4	1 ± 3 †	4 ± 5 *
LF_{DBP}	6 ± 4	4 ± 2 †	5 ± 1 *	7 ± 9	1 ± 1	2 ± 0.8

Table 8: *Data are expressed as mean$\pm$StD. SB: spontaneous breathing. CB: controlled breathing. Symbol legend: $*$: $p \leq 0.05$ 0.15 Hz vs. 0.25 Hz; ‡: $p \leq 0.05$ Heart Failure patients vs. control during controlled breathing periods; †: $p \leq 0.05$ 0.25 Hz controlled breathing vs. spontaneous breathing. From [93].*

Gain (ms/mmHg)	Control (n=6) SB	Control (n=6) CB		Heart Failure (n=7) SB	Heart Failure (n=7) CB	
$gHF_{SBP,RR}$	10 ± 5	12 ± 7	15 ± 7 *	6 ± 3	6 ± 5	4 ± 3 *‡‡
$gLF_{SBP,RR}$	7 ± 6	6 ± 3	7 ± 3	5 ± 2	4 ± 1	4 ± 2 ‡
$gHF_{DBP,RR}$	26 ± 19	24 ± 13	32 ± 19 *	22 ± 15	21 ± 13	12 ± 7 *‡
$gLF_{DBP,RR}$	10 ± 6	12 ± 9	14 ± 7	8 ± 2	7 ± 3	7 ± 3 ‡

Table 9: *Data are expressed as mean$\pm$StD. SB: spontaneous breathing. CB: controlled breathing. Symbol key: $*$: $p \leq 0.05$ 0.15 Hz vs. 0.25 Hz; ‡ $p \leq 0.05$, ‡‡ $p \leq 0.01$ Heart Failure patients vs. control during controlled breathing periods. From [93].*

The mean RR interval, systolic pressure and the SD of the SBP signal were similar at the two breathing rates, see table (7). HF oscillations of the RR interval and SBP were increased at the slower breathing rate.

As compared to the control subjects, HF and LF oscillations of the RR interval and SBP oscillations were attenuated but showed greater depression at the slower breathing rate. The marked increase in the HF amplitude of SBP oscillations was accompanied by a slight increase in the HF peak of RR oscillations at the slower breathing rate. Coherence function values between the RR interval and blood pressure oscillations in the HF and LF domains were high, indicating that the baroreflex in the patients, although blunted, was present. Consequently, we were able to calculate the BR gain. In the CHF patients, the

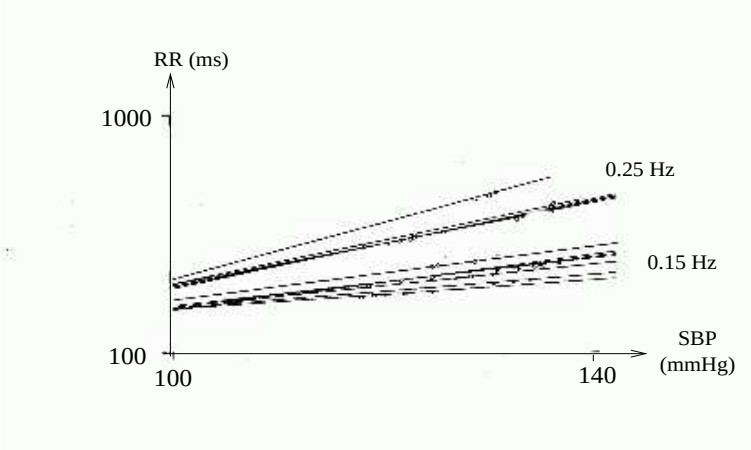

Figure 29: *Spontaneous cardiac baroreflex in the time domain in a CHF subject. At the slower breathing rate, the baroreflex gain decreased . From [93].*

slower breathing rate was associated with a decrease in the gain between the RR interval and SBP in the HF domain, table (9), whereas the opposite was seen in the control subjects. In the LF domain, the BR gain was unchanged. The mean regression slope was less steep and decreased at the slower breathing rate, a typical example is shown in fig. (29).

5.3.3 Discussion

The main finding of this study is that voluntary breathing in CHF patients was associated with alterations in the baroreflex gain of the cardiovascular system: slower paced-breathing decreased the BR gain in CHF whereas the opposite was apparent in the control group. The reversal of the normal pattern of breathing rate-driven BR gain change in the CHF patients suggests major dysfunction of the central neural regulation of autonomic outflow.

Central mechanisms regulating cardiovascular and respiratory rhythms

Cardiovascular rhythms are modulated by central mechanisms and afferent inputs from arterial baroreceptors, chemoreceptors, cardiac receptors, and stretch receptors in the thorax, including the lungs. During spontaneous respiration in healthy subjects, the baroreflex and cardiopulmonary reflexes are involved in the genesis of both HF and LF oscillations of heart rate and blood pressure [129]. In addition, the central nervous system (CNS) has been shown to play a role in the genesis of oscillatory components in cardiovascular rhythms [99, 117, 75, 31, 35]. Montano et al. demonstrated LF and HF components in the discharge variability of brainstem neurons recorded in anesthetized and artificially ventilated cats with sinoaortic deafferentation: an HF component synchronous with the artificial ventilation rate was observed in the spectrum of neuronal discharge variability [99]. Pagani et al. showed that both LF and HF of the RR interval can result from an autochthonous central rhythm, which influences autonomic output [117]. Simultaneous changes in rhythmic organization have been detected in brainstem neurons, respiration, the cardiovascular system, and the EEG [75]. Voluntary breathing involves specific cortical regions in the brain, which have been localized in humans [40]. The forebrain can transmit signals to the respiratory system along an independent pathway, bypassing the automatic metabolic control center (spontaneous breathing) in the brainstem [107]. Furthermore, robust connections exist between the cerebral cortex, the brainstem respiratory motoneurons, and the hypothalamic area [33, 70], a cardiovascular and respiratory integrative structure. In healthy subjects, high frequency BR gain is enhanced when the breathing rate is slowed-down, i.e. there is an inverse relation between the baroreflex sensitivity and the respiratory rate [130]. Greater tidal volume causes higher cardiac output and SBP oscillations, therefore justifying the increase in the BR gain to buffer such oscillations. During voluntary breathing, the CNS also contributes to the regulation of the peripheral BR controller gain [70].

Altered central nervous system processing in CHF patients

Autonomic modulation of cardiovascular variabilities in CHF is characterized by alterations at the cerebral level [126, 81], sympathetic excitation and vagal withdrawal [43], and profound neurohormonal derangements [26]. Arterial and cardiopulmonary baroreflex are also blunted and CNS abnormalities play a major role in the impaired regulation of autonomic outflow in CHF patients [126, 81, 31, 35]. However, the origin of these CNS alterations remains complex. Major changes in specific cerebral areas including alterations in neuron activation occur, probably as a result of exaggerated sympathetic outflow [126]. Excessive circulating levels of catecholamines, angiotensin, or vasopressin may alter autonomic regulatory function at the central level as well [126, 81]. It should be borne in mind that the patients studied were not severe, as indicated by the clinical data and the preservation of LF RR interval oscillations [35]. Consistent with this fact, respiratory modulation of the baroreflex sensitivity was preserved. In CHF, voluntary breathing has major effects on the controller gain of the cardiovascular system. This novel finding reinforces the notion of a central impairment regulating autonomic outflow: using an instant non linear time-domain method, i.e. the complex demodulation technique, we previously observed major phase fluctuations between cardiovascular oscillations and respiration during volitional paced-breathing, indicating a transient lack of synchronization between these physiological signals [92]. Various methods for baroreflex assessment such as the phenylephrine method, the cross-spectral gain in the LF and HF

domains, and sequential methods have been used to measure baroreflex sensitivity in CHF patients. Although neither the phenylephrine method nor spectral analysis is ideal, the spectral gain and the sequential methods have the enormous advantage of being safe for the patients [34, 27].

6 Time-varying analysis

6.1 Introduction

This section is meant be a review of the principals chatacteristics of the Complex Demodulation (CDM) and the Smoothed Pseudo Wigner-Ville distribution (SPWVD) and their application to cardiovascular signal processing. We will demonstrated the complementary advantages that the two methods offer: in one hand, the CDM algorithm gives a measure of the phase relationship between the respiratory activity and the high frequency oscillation in the cardiovascular time series, a relationship not estimable by the SPWVD technique. On the other hand, the SPWVD gives useful indexes, developped below, directly related to the noise present in the signal and to the interaction between the different spectral components present in the cardiovascular time-series, indexes not estimable by the CDM method. Therefore, together they provide a reliable technique to assess the instantaneous spectral parameters in non-stationary cardiovascular time-series.

Most physiological or pathological events occur in a narrow time span, and the ANS reacts very quickly to regulate CV functions. The transient changes produced in the CV variability series remove the assumption of stationarity even for short data.

Conventional PSD estimation is therefore unsuitable for these situations. If we look more carefully at the frequency representation $X(\nu)$ of a signal x(t), obtained by the *Fourier transform* ($\mathcal{F}$):

$$X(\nu) = \mathcal{F}[x(t)] = \int_{-\infty}^{+\infty} x(t)\ e^{-j2\pi\nu t}\ dt$$

we will note that $X(\nu)$ can be seen as the coefficient function obtained by expanding the signal x(t) into the family of infinity waves, $exp\{j2\pi\nu t\}$, which are completely unlocalized in time. Thus, the spectrum tells us which frequencies are present, together with their amplitude and phase, but not at which times these frequencies occur.

Time-frequency joint distributions and harmonic analysis methods have recently appeared to have most of the suitable characteristics to describe a non stationary time series.

6.2 Instantaneous frequency

6.2.1 Instantaneous frequency definition

The Instantaneous Frequency (IF) of a signal has been already widely investigate [12, 13], but we want to point out here some aspects of the IF definition that will be very important in the suite.

Let us analyse the expression of a real signal:

$$s(t) = a(t)\ cos(2\pi\ f_o\, t + \phi(t)) \tag{43}$$

where a(t) is amplitude and $\theta(t) = 2\pi\ f_o\, t + \phi(t)$ is the phase of the signal, both of which vary as a function of time t. Gabor proposed a method to generate a unique complex signal from a real one and define the instantaneous frequency of a non stationary signal [48] as:

$$\begin{aligned} z(t) &= s(t) + j\mathcal{H}[s(t)] \\ &= a(t)\ e^{j\,\phi(t)} \end{aligned} \tag{44}$$

where z(t) is Gabor's complex signal, s(t) is the real signal and $\mathcal{H}$ is the Hilbert transform, defined as

$$\mathcal{H}[s(t)] = p.v. \int_{-\infty}^{+\infty} \frac{s(t-\tau)}{\pi\ \tau} d\tau \tag{45}$$

where p.v. denotes the Cauchy principal value of the integral. The signals, s(t) and $\mathcal{H}[s(t)]$, are often said to be inquadrature, because in theory they are out of phase by $\pi/2$.

Note that the following equation defined for a real signal:

$$a(t)\ \cos\theta(t) + j\mathcal{H}[a(t)\ \cos\theta(t)] = a(t)\ e^{j\,\theta(t)}$$

can be verified if and only if the spectrum $A(f) = \mathcal{F}\{a(t)\}$ lies entirely in the region $|f| < f_o$ and the spectrum $\mathcal{F}\{\cos\theta(t)\}$ exists outside this region (Bedrosian's theorem for real signals, [24]). In the next sections, we will note that amplitude and phase functions will be assumed to vary slowly over time. This hypothesis allows the original signal to verify the condition of Bedrosian's theorem, and therefore there will be only one analytic signal and only one instantaneous frequency associated to a real signal.

6.2.2 Limitation of the instantaneous frequency concept

The analytic signal definition by equation (44) is not able to solve the intrinsic limitation of the concept of instantaneous frequency, for example let us consider one simple real signal $s(t)$ and the analytical signal associated to it:

$$z(t) = z_1(t) + z_2(t) = a_1\, e^{j(\omega_o - \Delta\omega/2)t} + a_2\, e^{j(\omega_o + \Delta\omega/2)t} \tag{46}$$

where $\omega_o = 2\pi\, f_o$ and $\Delta\omega = \Delta\, f/(2\pi)$. If we express z(t) in terms of envelope a(t) and phase $e^{j\Phi(t)}$, we have

$$\Phi(t) = \arctan \frac{(-a_1 + a_2)\sin(\Delta\omega/2)t}{(a_1 + a_2)\cos(\Delta\omega/2)t}$$

and now the instantaneous frequency is

$$IF(t) = \frac{1}{2\pi}\ \frac{d}{dt}\,[arg\ \ z(t)] = f_o + \frac{\Delta\, f}{2}\,\frac{-{a_1}^2 + {a_2}^2}{{a_1}^2 + {a_2}^2 + 2a_1a_2\cos\ \Delta\omega t} \tag{47}$$

The IF given by (47) varies with time, but excursion of f(t) about f_o are not symmetrical; the "instantaneous frequency" is entirely upwards if $a_2 > a_1$, entirely downwards if $a_2 < a_1$ and $IF(t) \equiv f_o$ if $a_2 = a_1$.

However, in this example, we may argue that the analytic signal in (46) corresponds to the bicomponent real signal $s(t) = s_1(t) + s_2(t)$ and we would like to obtain the instantaneous frequency of the two components. Hence, the IF is not meaningful for s(t) but only for the single component signals $s_1(t)$ and $s_2(t)$ taken separately.

Concluding, the notion of instantaneous frequency implicitly assumes that, at each time instant, there exists only one frequency component. So, IF is not sufficient to represent all the non-stationarity multicomponent signals. But, if further a priori information are available, either an harmonic analysis or a time-frequency representation may be useful to characterise the signal's evolution in both amplitude and frequency in time.

6.3 Harmonic analysis: Complex DeModulation

6.3.1 Principle of Complex DeModulation (CDM)

The CDM method has been widely investigated [11, 56, 57, 146, 145], but we point out some aspects related to its application to cardiovascular time-series.

CDM provides a flexible approach to data with transient changes when the distribution of the frequency components is a priori known, such as in cardiovascular time-series.

CDM may be seen as a *local* version of harmonic analysis: analogous to harmonic analysis in describing amplitude and phase of an oscillation, and local in that the amplitude and phase are determined only by the data in the neighborhood of t, rather than by the whole series. Let the real signal x(t) be a narrow band with the center frequency (λ_o) larger than the bandwidth (BW) of its spectra X(f). Note that this constraint has been shown to be necessary and sufficient to properly extract the envelope and phase functions of x(t) with the use of complex demodulation [74]. Therefore, the time series x_t includes a component with an actual frequency $\lambda(t)$ which changes slowly around a frequency of λ_o within the range $\lambda_o \pm \lambda_w$, then x_t can be written as:

$$x_t = a_t \cos(2\pi\lambda_o + \Phi_t) + z_t \tag{48}$$

with:

$$\lambda(t) \in [\lambda_o - \lambda_w; \lambda_o + \lambda_w] \quad \forall t \tag{49}$$

where a_t and Φ_t are the slowly changing instantaneous amplitude and phase of the component of interest, and z_t is the residual time series including all other components and noises such as continuous component and trends. The difference between the actual frequency λ and λ_o is expressed as the slope of Φ_t versus time:

$$\lambda(t) = \lambda_o + \frac{1}{2\pi}\frac{d\Phi_t}{dt} \tag{50}$$

The aim of the analysis is to extract approximation of a_t and Φ_t as functions of time.

Using the Hilbert transform ($\mathcal{H}$), Gabor's complex analogue of x_t is:

$$X_t = x(t) + j\mathcal{H}[x(t)] = a_t \; e^{j(2\pi\lambda_o + \Phi_t)} + Z_t \tag{51}$$

where Z_t is Gabor's complex signal of z_t. Note that, by definition, the time series x_t satisfies Bedrosian's theorem. Then let y_t be the signal obtained by shifting all the frequencies in X_t by $-\lambda_o$.

$$Y_t = X_t \, e^{j(-2\pi\lambda_o t)} = a_t \; e^{j\Phi_t} + Z_t \; e^{j(-2\pi\lambda_o t)} \tag{52}$$

From the frequency-domain point of view, the power spectrum of X_t has a peak around a frequency of λ_o (within the range between $\lambda_o \pm \lambda_w$), which represents the component of interest. As the result of a leftward shift of all frequencies, this peak is moved to around zero frequency (within the frequency range between $\pm\lambda_w$) in the power spectrum of Y_t. Although the peaks of all other components in X_t are also moved leftward, those at an original frequency above $\lambda_o + \lambda_w$ do not reach zero frequency (remain above λ_w), and those below $\lambda_o - \lambda_w$, including direct current trends component, move into the negative part of the frequency axis (below $-\lambda_w$). Thus, a low-pass filter with a corner frequency of λ_w excludes all components except the component of interest and then the amplitude can be obtained as the signal intensity of Y_t. Therefore, if W_t is the signal obtained by passing Y_t through a low pass filter with a λ_w cut-off frequency, we will have:

$$W_t = a_t \, e^{j\,\Phi_t} \tag{53}$$

and then we can can obtain amplitude and frequency function as:

$$\begin{aligned} CDM\_IAmp &= a_t = |W_t| \\ CDM\_IPh &= \Phi_t = \arctan \frac{imag(W_t)}{real(W_t)} \end{aligned} \tag{54}$$

Finally, because the slope of the phase versus time indicates the deviation of instantaneous operative frequency from the reference frequency (50), the instantaneous frequency (IF_t) of the component can be obtained from λ_o and the first order differentiation of Φ_t from the Eq. (54):

$$CDM\_IF = IF_t = \lambda_o + \frac{1}{2\pi} \frac{d\Phi_t}{dt} \tag{55}$$

6.3.2 Application of the complex demodulation to cardiovascular signals

As we are only interested in the LF and HF peaks in CV signals, we filtered out the VLF component to obtain a signal with few, well separated spectral components (if the breathing rate is greater than 0.15Hz), as shown in fig. (30). The IF interpretation is meaningless since the signal is intrinsically bicomponent

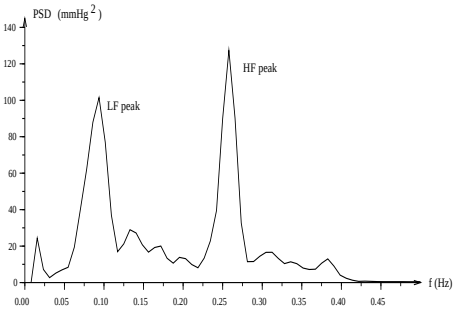

Figure 30: *Example of spectral analysis (by FFT) of systolic blood pressure (SBP) signal. The spectrum has two major well separated peaks, the LF and HF peak. Here, an instantaneous frequency interpretation is meaningless, but on the other hand we can still define an instantaneous central frequency.*

as in example (46).

By changing the central frequency , λ_o, in eq. (50) and the cut-off frequency, λ_w, in eq. (49) of CDM method, it is possible to repeat this procedure, analyzing all spectral components actually present. This is the classical CDM procedure applied by Shin and Hayano [146, 145, 56, 57] who fixed $\lambda_o = 0.09Hz$, $\lambda_w = 0.05Hz$ and $\lambda_o = 0.31Hz$, $\lambda_w = 0.15Hz$ for the LF and HF components respectively. Unfortunately, their method does not exploit the real actual breathing frequency that at least approximates the HF peak position in the signal spectra, and they need "a priori" knowledge of the mean value of the breathing rate. Therefore, the low-pass filter must have greater cut-off frequencie than is really needed.

Recently, Vermeiren used the actual breathing rate to improve the CDM method; this technique was called modified CDM (mCDM) [165]. Therefore, the HF component of CV signals (HF_{CV}) was demodulated fixing $\lambda_o = BR(t)$ lowering the cut-off frequency of the low-pass filter to $\lambda_w = 0.04Hz$. This method greatly reduces noise effects and gives a better time resolution of amplitude variations in a noisy environment. In addition, by mCDM, the phase Φ_t, assessed by equation (54), has a clear meaning: it represents the real phase relation between respiratory and CV activity and not, as in the classical CDM method, a phase relation between an "a priori" complex oscillator and HF_{CV} oscillations. The

mCDM allows us to pass from a single channel analysis (output point of view), to a multichannel analysis (input-output point of view), providing frequency and amplitude relationships between two signals.

The phase function, and its evolution over time, depends on both breathing rate and breathing-cardiovascular interactions. To gain insight into CV and respiratory interactions we may impose a paced breathing activity. Let us give a very simplified example to explain our conclusions. Let $\alpha(t)$ be the input signal of a linear system with a transfer function H(f) and $\beta(t)$ the corresponding output signal, as shown in fig. (31).

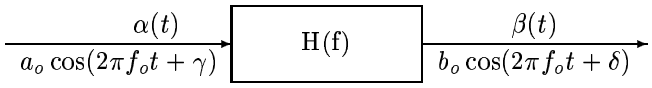

Figure 31: *Assuming a complex gain H(f) between an input signal $\alpha(t)$ and an output signal $\beta(t)$, their phase difference depends on both the characteristics of the gain function H(f) and on the frequency f_o of the input signal.*

The phase difference between $\alpha(t)$ and $\beta(t)$ depends on the characteristics of the complex gain H(f) (amplitude $|H(f)|_{f=f_o}$ and phase $\angle H(f)_{f=f_o}$) and also on the frequency f_o of the input signal. In fact $\delta - \gamma = \angle H(f)_{f=f_o}$ where $\angle H(f)_{f=f_o}$ is the argument of the gain assessed at $f = f_o$. Assuming that $\alpha(t)$ is the respiratory signal and that $\beta(t)$ is the HF_{CV} signals, then H(f) will represent the overall complex interactions between respiratory and CV activity and f_o will correspond to the breathing rate. By pacing respiratory activity, phase variations will be attributed directly to the $\angle H(f)_{f=f_o}$ time variations independently of f_o variations. So, in the HF band, the most important information on CV-respiratory system organization and co-ordination will not be the frequency, but, obviously, the phase between the respiratory signal, used as the reference signal, and the HF_{CV}. The phase could be seen as the difference between the frequency of the respiratory signal (BR) and the frequency of the HF_{CV} components; from equation (50) we can write:

$$\Phi_t = 2\pi \int_0^t [\lambda(\tau) - \lambda_o]\, d\tau = 2\pi \int_0^t [\lambda(\tau) - BR(\tau)]\, d\tau \tag{56}$$

where $BR(\tau)$ is the instantaneous breathing rate. Therefore, a constant phase value in time would mean complete co-ordination between respiratory activity and high frequency CV activity.

The only constraint to apply the CDM method is that x(t) has to be a narrow band type signal in the sense that the bandwidth BW is small compared to λ_o. But any signal has energy outside the frequency of interest $\lambda_o \pm \lambda_w$. Thus, a reliable bandpass filter must be applied before the extraction of the envelope and phase within the narrow frequency band of interest. We introduced two filters: the first one for LF component analysis (from 0.04 up to 0.12Hz); the second one for HF component analysis (the HF band has a narrow bandwidth centered around a fixed breathing rate). The whole signal processing schema is shown in fig. (32).

6.3.3 Limitations of complex demodulation technique

The CDM technique is based on the assumption that only the component of interest is present within the defined frequency band ($f_o \pm f_w$) otherwise the algorithm would yield unpredictable and noised related CDM_IF and CDM_IPh values. Therefore, to avoid this limitation, the CDM_IF and CDM_IPh values were considered reliable only when the associated $IAmp$ is greater than an *a priori* fixed threshold value [57]. In one hand, this definition does not really take into account the noise present in the signal:

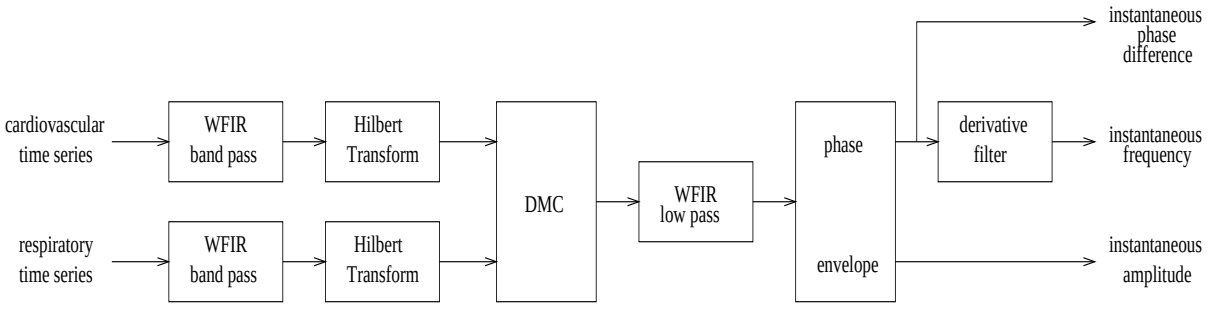

Figure 32: *Signal processing algorithm to apply the CDM technique to CV signals, implemented in LARY_CR in the SCILAB-SCICOS environment ([95]). This flow chart shows the HF component processing; for the LF component an a priori complex oscillator is used instead of the respiratory signal.*

the CDM_IF and CDM_IPh estimate could be biased by a low signal-to-noise ratio and not only by a low CDM_IAmp value. This is the case in some clinical deseases, such as chronic heart failure (CHF) [92] and in some pharmacological studies, such as complete autonomic blockade [94], where CV variability in the high- and low-frequency band is largely decreased. On the other hand, this definition does not take into account that the HF and the LF oscillatory components may interact together, such as when the breathing rate is slowed down to around 0.15 Hz. As CDM is not able to evaluate the influence of noise on instantaneous parameter estimation and the interaction between the two frequency components, we jointly use a time-frequency method, the smoothed pseudo Wigner-Ville distribution (SPWVD). The SPWVD provides an approximation of the beat-to-beat relative contribution of the noise to the instantaneous power of the signal and an approximation of the beat-to-beat spreading of the instantaneous power distribution of the signal, respectively SPW_N_{est} and $SPWVD\_IDisp$ as defined below. This allows us to discard periods during which CDM_IF and CDM_IPh estimate are not reliable due to a low signal-to-noise ratio and to a large interaction between the two frequency components.

6.4 Time-frequency analysis: Smoothed Pseudo Wigner-Ville distribution

6.4.1 Definition of Smoothed Pseudo Wigner-Ville Distribution

A time-frequency energy distribution recently used in physiological signal analysis is the *Smoothed Pseudo Wigner-Ville distribution* defined as:

$$SPW_x^{N,M}(n,\omega) = \sum_{m=-\infty}^{+\infty} g_M(m) \sum_{k=-\infty}^{+\infty} h_N^2(k)\, x(n+k+m)\, x^*(n-k+m)\, e^{-j2\omega k} \qquad (57)$$

where N and M stand for the window sizes of h_N and g_M respectively. The window $g_M(m)$ determines the number of spectra involved in the average and hence the effectiveness for cross term suppression. The window $h_N(k)$ determines frequency smoothing of the SPWVD. Therefore, the two windows $g_M(m)$ and $h_N(k)$ perform smoothing in the time and frequency directions, respectively.

Several studies have shown that averaging the spectra in the time direction is effective for reducing cross terms and negative regions which usually characterize Wigner-Ville distribution. Unfortunately, the marginal properties are no longer valid and, in particular, the time resolution is reduced [131]. In

spite of this, in the case of signals with few, well separated components, such as CV variability series, see fig. (30), the smoothing procedure is suitable for solving or at least reducing the interferences problem. In the SPWVD a trade-off is required between the time-frequency resolution and the suppression of the cross-term: the more you smooth in time and/or in frequency, the poorer the resolution in time and/or frequency [131].

In computing the SPWVD, the discrete fourier tranform (DFT) is employed. For the DFT, the width of the frequency bin is inversely proportional to the window size N, if no padding of zeros is employed, i.e. the bin-width is given by

$$f_b = 0.5/N * f_s$$

where f_s is the frequency sampling. To assess the peak position with an error of 0.002 Hz we apply a zero padding, as in the previous similations, using a frequency smoothing window $\tilde{h}^2_{T,N}(j)$ of T=1024 points defined as:

$$\tilde{h}^2_{N,T}(j) = \begin{cases} 0 & j = 1 \;..\; (T-N)/2 \\ h^2_N(k) & j = (T-N)/2+1 \;..\; (T-N)/2+N \\ 0 & j = (T-N)/2+N+1 \;..\; T \end{cases}$$

thus, with a frequency sampling of $f_s = 4Hz$, the frequency resolution is

$$f_b = 0.5/T * f_s = 0.002\ Hz$$

and eq. (57) becomes:

$$SPW_x^{N,T,M}(n,\omega) = \sum_{m=-\infty}^{+\infty} g_M(m) \sum_{k=-\infty}^{+\infty} \tilde{h}^2_{N,T}(k)\, x(n+k+m)\, x^*(n-k+m)\, e^{-j2\omega k} \tag{58}$$

6.4.2 Application of Smoothed Pseudo Wigner Ville to cardiovascular like time series

Significant improvement in the IF and IAmp estimate can be achieved if some *a priori* information about the IF frequency domain or about the rate of variation in the IF and IAmp are available. This information usually involves some assumption about the IF and IAmp being slowly varying, which can be used to "smooth" (or postfilter) the sequence of IF and IAmp estimates, and also some assumption of the frequency interval inside which IF can change, which can be used to prefilter the signal.

In the CV context we known *a priori* the frequency band of both the HF and LF components, and we can exploit this knowledge to improve the IAmp and IF estimate by prefiltering the signal, as previously described for the CDM algorithm.

Instantaneous frequency estimate

Instantaneous frequency ($SPW\_IF_{x_f}$) could be estimated by first order moment of the SPWVD:

$$SPW\_IF_{x_f}(n) = \frac{\sum_{\omega=-\infty}^{+\infty} \omega SPW_{x_f}^{N,T,M}(n,\omega)}{\sum_{\omega=-\infty}^{+\infty} SPW_{x_f}^{N,T,M}(n,\omega)} \tag{59}$$

Instantaneous amplitude estimate

Even if in SPWVD marginal properties are no longer valid, we can use it to obtain useful approximations of HF and LF power ($IPow_{x_f}$) in cardiorespiratory signals.

$$SPW\_IPow_{x_f}(n) = \sum_{\omega=-\infty}^{+\infty} SPW_{x_f}^{N,T,M}(n,\omega) \tag{60}$$

Because CDM provides the magnitude of individual spectral components as amplitude values in time, the power obtained by time-frequency analysis for each component was converted to the instantaneous amplitude (IAmp) as follows:

$$IAmp_{x_f}(n) = \sqrt{IPow_{x_f}(n)}\,\alpha \tag{61}$$

where α is a constant assessed by simulations.

Signal to noise ratio assessment

Given an ideal *t-f* distribution (TFD) which describes the energy density of a signal simultaneously in time and in frequency, we could define an index to estimate the noise in a signal. If the oscillation of interest lies within an *a priori* known frequency band (FB), and that the noise lies outside ($\bar{FB}$), we could prefiltering the signal and then estimate the relative contribution of the noise to the instantaneous power of the signal as

$$NSR = 1 - \frac{\int_{\nu\in FB} TFD_x(t,\nu)\,d\nu}{\int TFD_x(t,\nu)\,d\nu} = \frac{\int_{\nu\in\bar{FB}} TFD_x(t,\nu)\,d\nu}{|x(t)|^2} \tag{62}$$

where $TFD_x(t,\nu)$ stands for the TFD transform of the signal x(t). The Noise to Signal power Ratio (NSR) takes value in [0,1], 0 when all the energy of the signal is inside the FB region and 1 in the opposite situation. Therefore, we can estimate the noise power present in the signal by an ideal *t-f* energy distribution and this is exactly what CDM fails to tell us. Unfortunately, such an ideal *t-f* energy distribution does not exist [25] and hence NSR estimate is not possible. SPWVD cannot be interpreted exactly as an energy distribution as it may assume negative values and a negative energy value is meaningless. Therefore, applying eq. (62) to the SPWVD of an analytical signal x(t), the NSR parameter can take negative values. Neverthless, an estimation of the noise present in the signal could be obtanied as follow

$$SPW\_N_{est} = \left| 1 - \frac{\sum_{\omega\in FB} SPW_{x_f}^{N,T,M}(n,\omega)}{\sum SPW_{x_f}^{N,T,M}(n,\omega)} \right| \tag{63}$$

A very small frequency smoothing is needed so that the signal time-frequency representation really lies within the predefined frequency band. Therefore, to estimate IAmp et Nest by SPWV algorithm, we chose a frequency smoothing window of size N=T/2 in eq. (58). The SPWVD of a monocomponent signal, linearly modulated in frequency is concentrated in one point [14, 25] and SPW_N_{est} is equal to 0 if this point belongs to the FB region, 1 otherwise. Oscillating cross-terms and negative regions imply that SPW_N_{est} approximates the NSR index; an effective signal prefiltering and WVD smoothing become very important for the SPW_N_{est} estimation. We will demonstrate that the smaller SPW_N_{est} is, the more reliable IF and IPh are.

Instantaneous dispersion

To estimate the spread in frequency of the SPWVD we could use a classical definition of variance which, interestingly, corresponds to the third moment of a distribution:

$$SPW\_Ivar(n) = \frac{\sum_{\omega=-\infty}^{+\infty} \omega^2 \; SPW_{x_f}^{N,T,M}(n,\omega)}{\sum_{\omega=-\infty}^{+\infty} SPW_{x_f}^{N,T,M}(n,\omega)} - SPW\_IF(n) \tag{64}$$

Unfortunately, this "pseudo variance" has no reason to be positive everywhere since SPWVD also takes negative values. Therefore $SPW\_Ivar_{x_f}(n)$ assessed by eq. (64) could not be interpreted as a dispersion around $SPW\_IF_{x_f}(n)$. To estimate the dispersion of the distribution of the signal energy, we defined an index as follows:

$$SPW\_IDisp_{x_f}(n) = \frac{\sum_{\omega=-\infty}^{+\infty} \left[\omega - IF_{x_f}^{mom}(n)\right]^2 \left|SPW_{x_f}^{N,T,M}(n,\omega)\right|}{\sum_{\omega=-\infty}^{+\infty} SPW_{x_f}^{N,T,M}(n,\omega)} \tag{65}$$

The SPW_IDisp is always positive and equal to the SPW_Ivar if and only if SPWVD is positive. The SPWVD of a monocomponent signal, linearly modulated in frequency is concentrated in one point [14, 25] and, hence, the SPW_IDisp is equal to 0. For large SPW_IDisp values, IF estimates are meaningless as the signal is not monocomponent. We will demonstrate that the smaller SPW_IDisp is, the more reliable IF and IPh are.

Complementarity of the two indexes

SPW_N_{est} estimates the ratio between the energy of the signal in an *a priori* defined frequency band and the total energy of the signal. SPW_IDisp estimates the spreading of the SPWVD in the frequency direction, without a frequency band definition. Low SPW_N_{est} and high SPW_IDisp values could reveal that a large FB contains all the energy of the widely spreaded spectrum of the signal (case of LF band). Conversely, high SPW_N_{est} and low SPW_IDisp values could reveal that the spectral peak is outside the frequency band. Hence, SPW_N_{est} and SPW_IDisp, jointly, are effective tools to validate IF and IPh estimate.

SPW_N_{est} estimates the ratio between the energy of the signal in an *a priori* defined frequency band and the total energy of the signal, whereas SPW_IDisp estimates the spreading of the SPWVD in the frequency direction, without a frequency band definition. Therefore, given a very large FB definition, such as in the LF band, SPW_N_{est} could be very low when the signal energy is really concentrated in FB, whereas the SPW_IDisp could be very large making the IF of the signal meaningless. On the other hand, the SPW_N_{est} could be very large and the SPW_IDisp could be very small when the spectral peak is outside the frequency band of interest, also in this case the IF of the signal is meaningless as it does not correspond to the component of interest. Concluding, the SPW_N_{est} and SPW_IDisp jointly provide a quantitative method to validate the IF and the IPh estimate of a signal.

Smoothed Pseudo Wigner-Ville processing schema

The whole signal processing schema using the SPWV technique is shown in fig 33. The WFIR band pass filter could be set either to the LF band or to the HF band, estimating $SPW\_IF_{x_f}$, $SPW\_IAmp_{x_f}$, $SPW\_IDisp_{x_f}$ and SPW_N_{est} in both frequency bands.

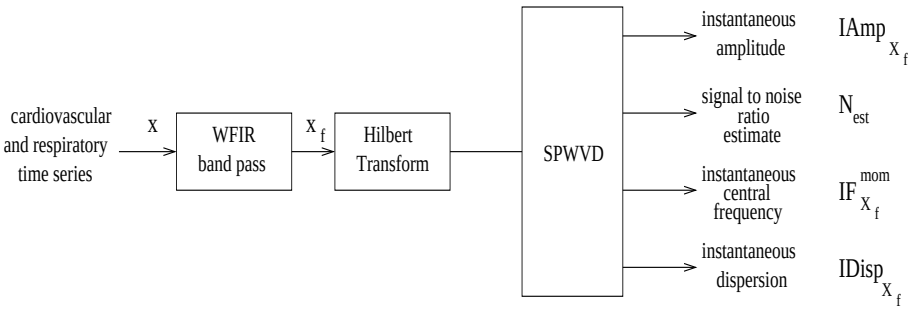

Figure 33: *Signal processing algorithm to apply the SPWVD technique to cardiovascular signals as performed by LARY_CR in the SCILAB-SCICOS environment ([95]).*

6.4.3 Smoothed Pseudo Wigner-Ville algorithm limitations

In the application of SPWVD to actual cardiovascular data, phase estimation presents a problem. The IPh between two monocomponent signals, x_t and y_t, could be calculate as follows

$$\Phi_t = 2\pi \int_0^t [IF_x - IF_y]\, d\tau \; + \; \Phi_0 \tag{66}$$

where IF_x and IF_y are the instantaneous frequency of the two oscillations x_t and y_t, respectively. When IF_x and IF_y are equals, the time-integral in eq. (66) is constant, revealing a constant phase relationship between the two signals. SPWVD allows IF_x and IF_y estimate but it is not suited for estimating Φ_0. In fact, having $IAmp_{x_f(n)}$ and $IF_{x_f}(n)$, one could estimate the phase ϕ_o minimizing the error

$$\sum_{n=-\infty}^{+\infty} \left(x_f(n) - IAmp_{x_f}(n)\, e^{j(2\,\pi\, IF_{x_f}(n) + \phi_o)} \right)^2$$

This approach has not been developed in this report. Thus, by SPWVD it is possible to estimate phase variations in time between two signals, for example between RR_{HF} and the respiratory activity, but not the absolute phase difference between the two signals. So, the SPWVD technique provides only phase-shift over time between the two signals but not the absolute phase between them. Therefore the SPWVD technique is useful to estimate time-varying amplitude, and frequency but it is suited to estimate the phase relationship between two signals, such as the HF_{CV} and the respiratory activity.

7 Time varying analysis applied to physiological and pathological conditions

7.1 Introduction

This section shows and discuss the results obtained by our group applying the instantaneous spectral indexes previously described in both RR-like time series, physiological and pathological study. We will show the complementary caracteristics of SPWVD and CDM method and their usefulness for instantaneous spectral estimate in different conditions.

- Validation of the joint SPWVD-CDM method

  The SPWVD and CDM methods have been already used separately to estimate time-dependent changes in the instantaneous amplitude ($IAmp$) and frequency (IF) of the oscillatory components present in the CV time series [56, 57, 67, 92, 94, 131, 146, 145]. However, each of these methods has limitations that a joint utilisation could largely reduce, due to their having interesting complementary features. CDM is suitable to assess the instantaneous phase (IPh) relationship between two oscillations; SPWVD is suitable to assess the reliability of IF and IPh estimate. The aim of this section is to validate the joint SPWVD-CDM method on simulations and physiological experiments. We propose two indexes related to the noise present in the signal and to the dispersion of the power spectrum in order to detect and quantify the time-changes in the CV variability, even when this variability is greatly reduced, such as in autonomic blockade and ANS deficiency.

- Use of the joint SPWVD-CDM method in Pathological conditions

  Autonomic nervous system dysfunction is common in patients with chronic heart failure (CHF) [43]. Elucidation of the mechanisms underlying dysautonomia in heart failure is of crucial importance for risk stratification since impaired indexes of autonomic activity, such as heart rate variability and baroreflex sensitivity, have been shown to predict mortality in CHF patients. Autonomic dysregulation plays a key role in progression of the disease. Various noninvasive signal processing techniques have been developed for analyzing cardiovascular oscillations. In the frequency domain, power spectral analysis using Fast Fourier transform is the method most widely used in clinical studies. However, it averages frequency and amplitude throughout the observation period and is therefore reliable with an assumption of relative stationarity. Many situations of physiological interest require instant analysis of cardiovascular autonomic control. Continuous and instantaneous assessments of cardiovascular and respiratory oscillations [67, 91] provide interesting data on cardiorespiratory dynamics. Complex demodulation measures changes over time in amplitude, frequency, and phase of oscillations in a frequency band of interest. Thus, it is well-suited to the investigation of unstable oscillations [56]. The objective of the present study was to gain insight into cardiorespiratory system dynamics in chronic heart failure patients by assessing continuously the instant amplitude, phase, and frequency of cardiovascular oscillations during application of a forcing stimulus, i.e. respiration.

7.2 Evaluation of the methods

7.2.1 Evaluation of the instant parameter estimators based on synthetic signals

We compared the estimated parameters to the theoretical ones on several RR-like series testing the ability of SPW_N_{est} and SPW_IDisp to detect unreliable IF and IPh estimates. The most representative time-series are the following:

- $x_1(k) = 1000 + VLF_1 + Amp_{LF}\sin(2f_{LF}(t)\,\pi\,k/4) + Amp_{HF}\sin(2f_{HF}(t)\,\pi\,k/4) + WGN_1$
  - $Amp_{LF}(t)$ and $Amp_{HF}(t)$ are the time varying amplitudes in the LF and HF bands;
  - $f_{LF}(t)$ and $f_{HF}(t)$ are sinusoidally modulated LF and HF components, around 0.09 Hz with amplitude 0.01 Hz and period 150 s for LF, around 0.25 Hz with amplitude 0.01 Hz and period 80 s for HF.
  - VLF_1 is a bicomponent signal at frequency 0.03 Hz and 0.005 Hz of amplitude 0.6 s and 0.5 s respectively;
  - WGN_1 is a white Gaussian noise with mean 0 s and standard deviation of 0.5 s.
- $x_2(k) = 1000 + VLF_2 + Amp_{LF}\sin(2f_{LF}(t)\,\pi\,k/4) + Amp_{HF}\sin(2f_{HF}(t)\,\pi\,k/4) + WGN_2$
  - VLF_2 is a bicomponent signal at frequency 0.03 Hz and 0.005 Hz of amplitude 0.8 s and 0.9 s respectively;
  - WGN_2 is a white Gaussian noise with mean 0 s and standard deviation of 2 s.

In the $x_2(k)$ time-series, a greater VLF amplitude and WGN standard deviation produced a larger noise contribution to signal variability. These time series concentrate their energy in the well-defined HF

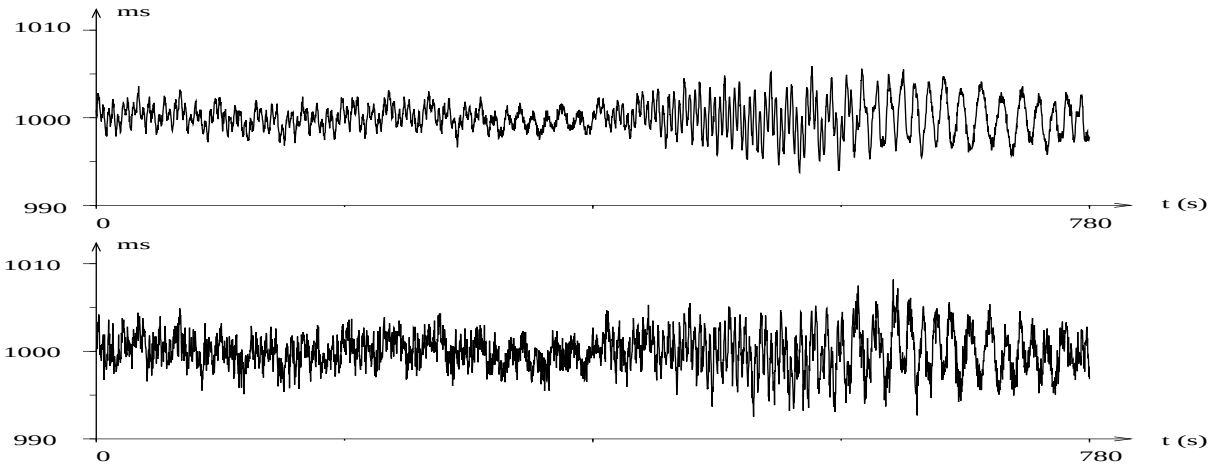

Figure 34: *The two synthetic RR-like series, $x_1(k)$ on the top, $x_2(k)$ on the bottom.*

and LF regions of the *t-f* plane. They simulate time-dependent changes in the frequency location and amplitude of the respiratory sinus arrhythmia of an RR series during a 0.25 Hz paced breathing test (Fig. 34). They simulate typical real CV time series in normal but also in reduced variability conditions usually evidenced in autonomic deficiency.

7.2.2 Evaluation of the instant parameter estimators based on real CV data

ECG, blood pressure (Finapres) and respiratory (Respitrace Systems) signals were recorded at 500Hz by a specific computer software (Acknowledge III, BIOPAC systems, USA). Signal processing was performed with LARY_CR, a physiological signal analysis software developed at INRIA, in the scientific environment SCICOS-SCILAB. Rhythm detection was applied to raw CV signals: for RR, an adaptative

threshold was applied to the derivative ECG; systolic (SBP) and diastolic (DBP) blood pressure were determined with a variant of Pan's algorithm, as described in [92, 94].

The joint SPWVD-CDM method was applied on several testing conditions to evaluate the influence of different parameters (HF band definition, BR, CV variability) on the estimation of the instantaneous spectral parameters:

1. *During spontaneous breathing in normal subjects*

   Spontaneous breathing requires a wide HF band because of large changes in BR. The subjects were recorded over a period of five minutes in quiet conditions.

2. *During paced breathing in normal and CHF subjects*

   Paced breathing allows a narrow HF band definition centered around the actual breathing rate. BR was fixed to 0.25 Hz and 0.15 Hz. The CHF subjects present a reduced variability. Subjects were recorded during two periods of five minutes, corresponding to 0.25 Hz and 0.15 Hz BR.

3. *During head-up tilt in normal subjects*

   The time-evolution of the CV variability during the transition from supine to standing is well known [67, 131] and can be compared to SPWVD-CDM results. The subjects were recorded during two periods of five minutes, first supine, then standing at 0.25 Hz paced breathing.

4. *During autonomic blockade in normal subjects*

   The CV variability is largely reduced by a total autonomic blockade [94]. The subjects, under atropine and bisopropol administration, were recorded during thirty minutes at 0.25 Hz paced breathing.

7.2.3 Signal processing

The two methods were applied with the following parameters:

- Preliminary band-pass filters: the LF band was centered on 0.09 Hz (0.09 ± 0.04 Hz, Task Force definition [44]) and the HF band on 0.25 Hz (0.25 ± 0.03 Hz) for RR-like series or the 0.25 Hz paced breathing, on 0.15 Hz (0.15 ± 0.03 Hz) for the 0.15 Hz paced breathing or on 0.25 (0.25 ± 0.15 Hz, Task Force definition [44]) for the spontaneous breathing.

- CDM: reference frequencies f_o were 0.09 Hz for the LF band and the instantaneous BR for the HF band. IF was assessed with the actual modulating BR.

- SPWVD: frequency and time smoothing Hamming windows h_N and g_M, of 512 points and a 21 points, respectively.

7.3 Results

The joint SPWVD-CDM method provides an excellent performance for each test: outside the periods of unreliable spectral estimate, corresponding to high SPW_N_{est} and SPW_IDisp values, they give identical results in $IAmp$ and IF estimates, very close to real values in RR-like series, as shown in Fig. (35).

7.4 Evaluation of the instantaneous spectral parameters on synthetic signals

The $IAmp$ falls in Fig. (35) are accompanied by an increase in SPW_N_{est} and SPW_IDisp, corresponding to an unreliable IF estimate. The noisier time series corresponds to higher SPW_N_{est} and SPW_IDisp estimates, Fig. (35b), and this increase is more visible when the $IAmp$ is lower (by comparing the first and the second part of Fig. (35b)).

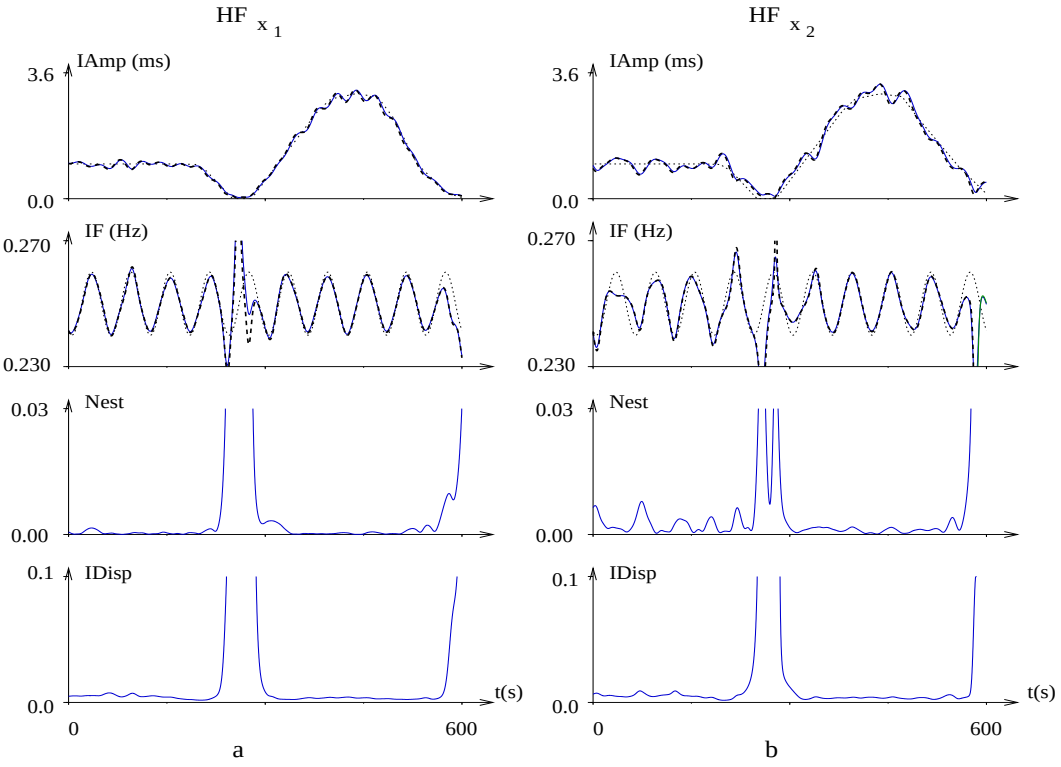

Figure 35: *Estimation of the HF instantaneous parameters with CDM and SPWVD on the $x_1(k)$, on the left, and $x_2(k)$ time series, on the right. Dotted lines stand for real $IAmp$ and IF values. Dashed lines stand for $IAmp$ and IF estimated by CDM method. Continuous lines stand for $IAmp$ and IF estimated by SPWVD method. CDM and SPWVD results are equivalent.*

7.5 Evaluation of the instantaneous spectral parameters on real CV time series

7.5.1 During spontaneous breathing in normal subjects

The figure (36) displays general characteristics, found in all other tests (Fig. (38), (40), (41), (42)): high SPW_N_{est} and SPW_IDisp estimates correspond to a dissociation between SPW_IF and CDM_IF values. Therefore, IF estimate becomes unreliable. The IF estimate is generally more biased in the LF band than in the HF band.

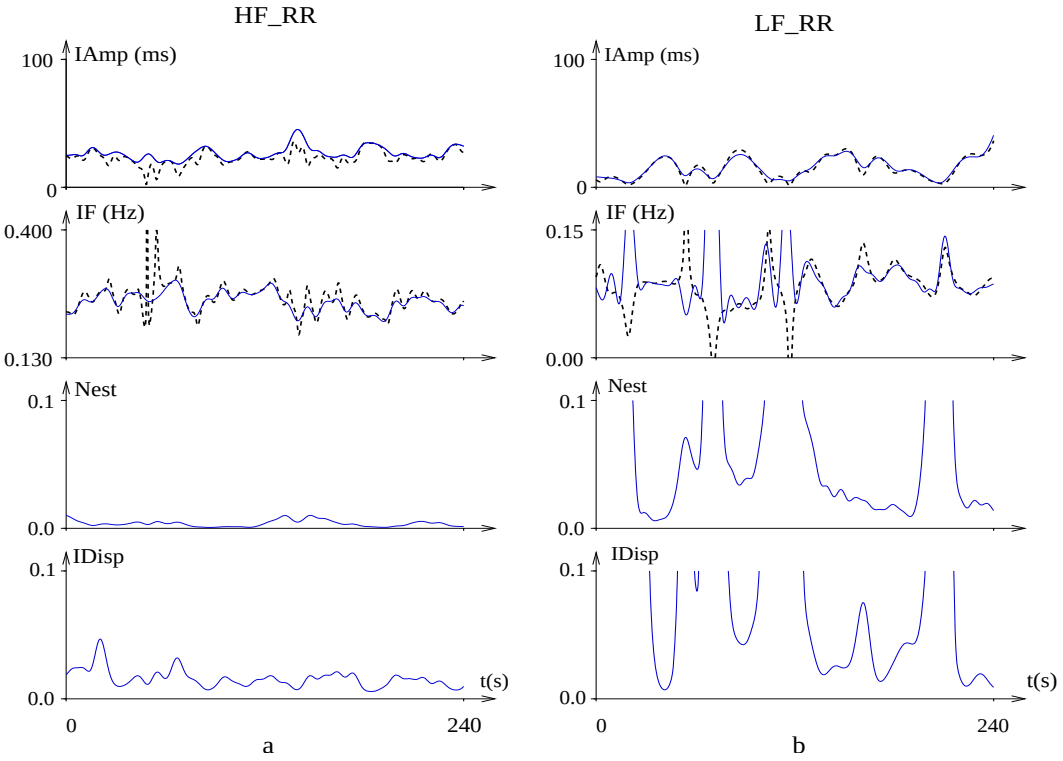

Figure 36: *Estimation of the instantaneous parameters, IAmp and IF, with CDM and SPWVD on an RR series in a normal subject during spontaneous breathing. Continuous lines stand for SPWVD and dashed lines for CDM results.*

7.5.2 During paced breathing in normal subjects

In the HF band, paced breathing activity is reflected by regular $IAmp$ and IF estimates; the IF corresponds exactly to the imposed respiratory rhythm (Fig. (38a) and (40a)). The very low SPW_N_{est} and

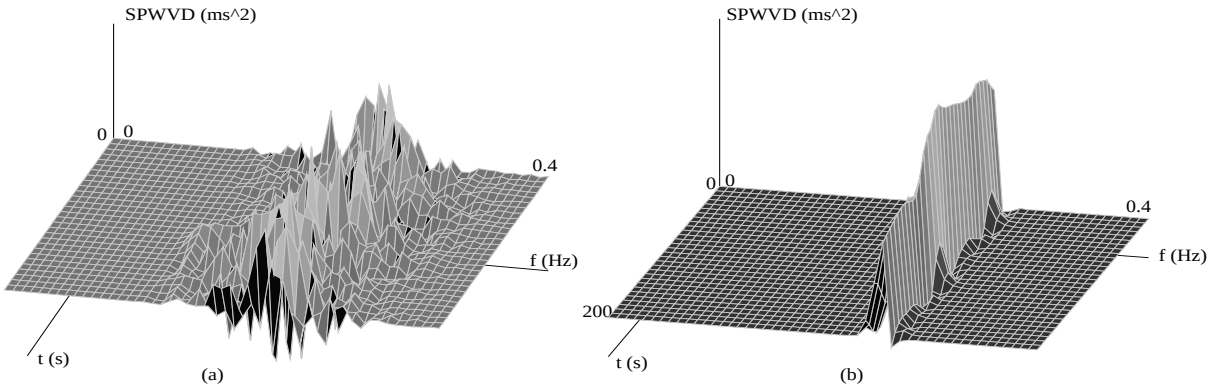

Figure 37: *Three-dimensional time dependent spectrum in the HF band of an RR series in a normal subject during spontaneous breathing (a) and 0.25Hz paced breathing (b).*

SPW_IDisp values reflect the perfect concentration of the SPWVD around the BR, shown at 0.25Hz BR on Fig. (37b). The $IAmp$ values are higher at 0.15Hz than at 0.25Hz BR, as already evidenced [3, 92]. The three-dimensional representation of the SPWVD shows the differences between spontaneous (Fig. (37a)) and paced breathing (Fig. (37b)): the higher spectral dispersion during spontaneous rather than paced breathing explains the reduced reliability of IF estimate, as shown by figures (36a) and (38a). In the LF band, the three-dimensional representation of the SPWVD does not show a clear difference between spontaneous (Fig. (39a)) and paced breathing (Fig. (39b)). Nevertheless, for the same subject under paced breathing, SPW_N_{est} and SPW_IDisp estimates evidence differences between the 0.25Hz and 0.15Hz BR: the IF estimate is less accurate at 0.15Hz because of the proximity of the HF and LF components, as shown by figures (38b) and (40b). 0.15Hz BR represents a limit condition for a reliable IF estimate in the LF band.

7.5.3 During head-up tilt and autonomic blockade in normal subjects

With the head-up tilt test, the HF $IAmp$ is high when the suject is supine then strongly reduced when the subject is standing as already described [67, 131]; in parallel, the SPW_N_{est} and SPW_IDisp estimates are higher for standing than for supine (Fig. (41a)). The two conditions, head-up tilt in the standing position (Fig. (41a)) and autonomic blockade (Fig. (42a)), show that even with a low variability, SPW_N_{est} and SPW_IDisp are very small, allowing an IF estimate in the HF band.

7.5.4 During paced breathing in normal and Chronic Heart Failure subjects

A qualitative analysis of the regularity of the respiratory and of the HF component of SBP (HF_{SBP}) time series is provided by Poincaré plot, a scattered plot of the current sample against the previous one, see Fig. (43). Normal subjects have a 1:1 coupling between their breathing rate and the imposed rhythm, hence the limit cycle of their respiratory time series is very clear, see Fig. (43a) on the top. In addition,

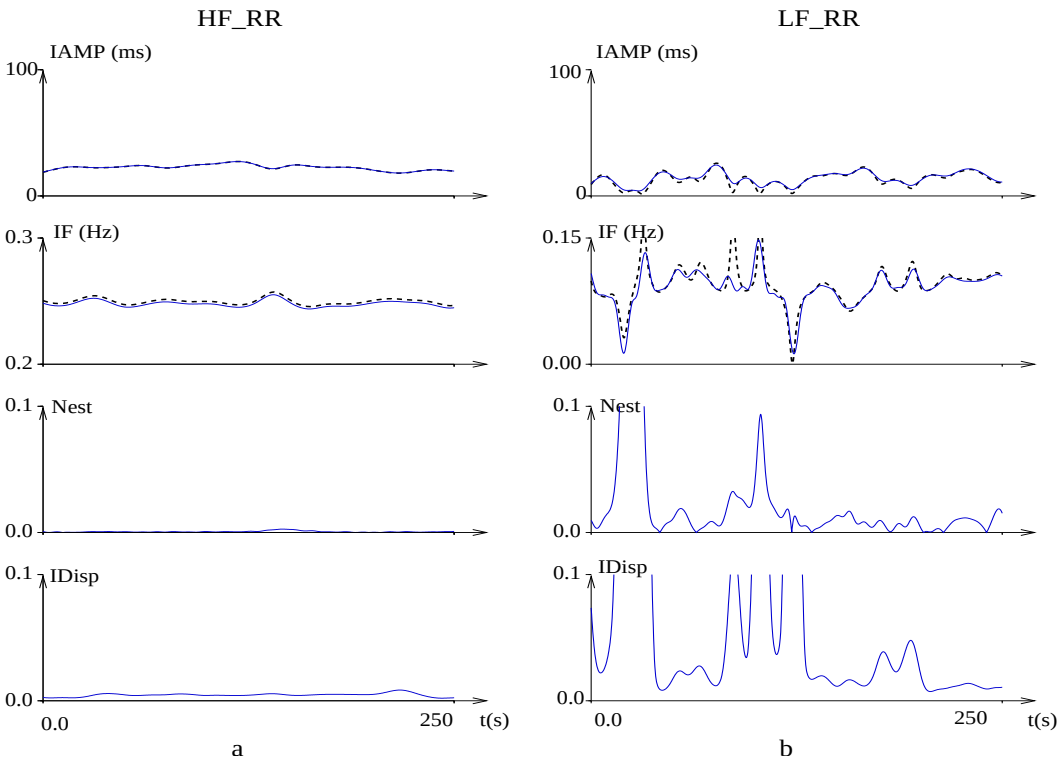

Figure 38: *Estimation of the instantaneous spectral parameters, IAmp and IF, with CDM and SPWVD on an RR series in a normal subject during 0.25Hz paced breathing. Continuous lines stand for SPWVD and dashed lines for CDM results.*

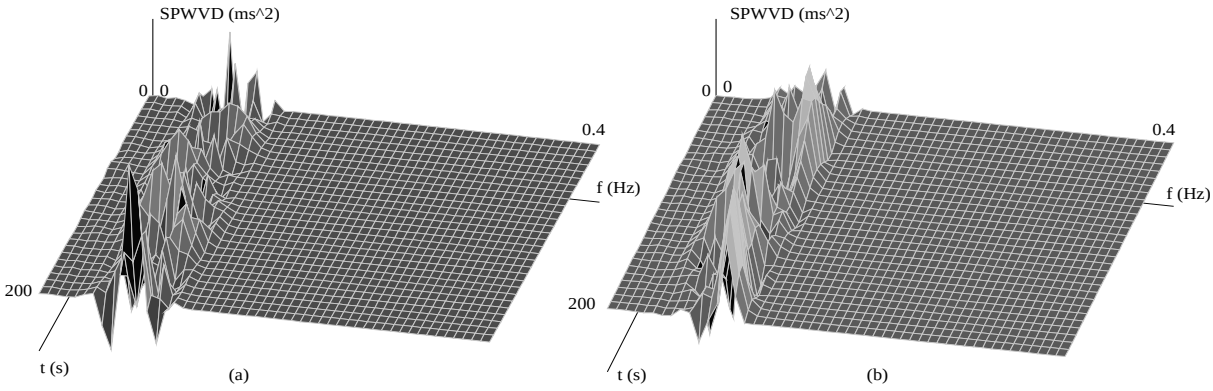

Figure 39: *Three-dimensional time dependent spectrum in the LF band of an RR series in a normal subject during spontaneous breathing (a) and 0.25Hz paced breathing (b).*

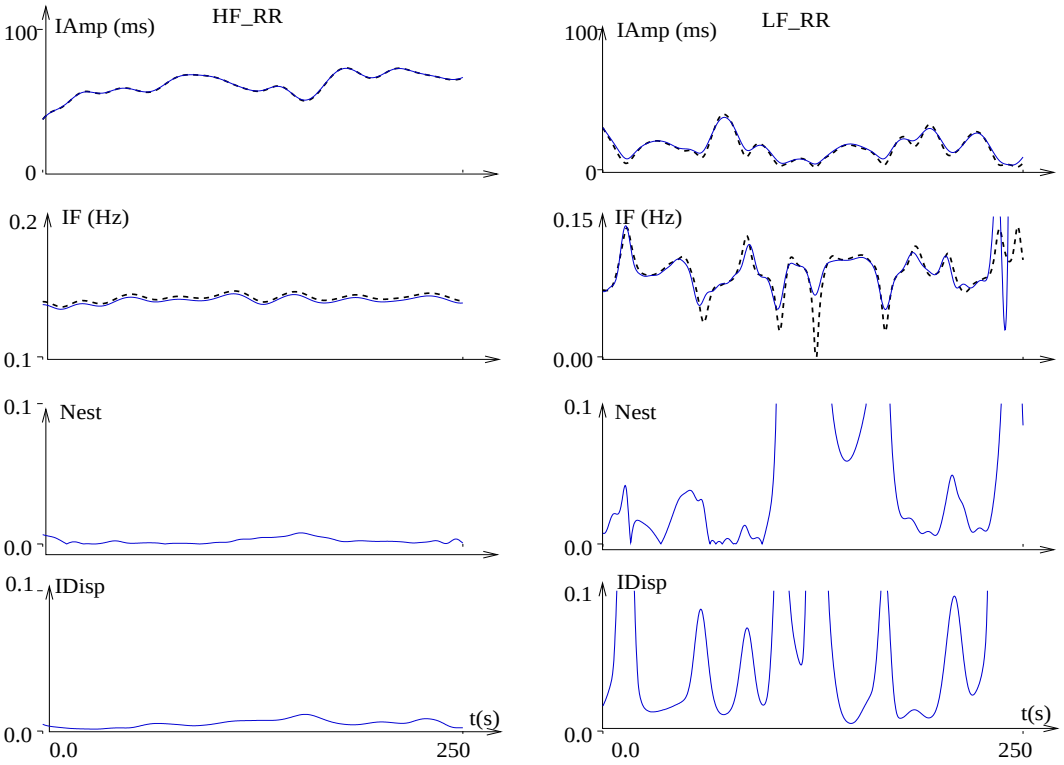

Figure 40: *Estimation of the instantaneous spectral parameters, $IAmp$ and IF, with CDM and SPWVD on an RR series in a normal subject during 0.15Hz paced breathing. Continuous lines stand for SPWVD and dashed lines for CDM results.*

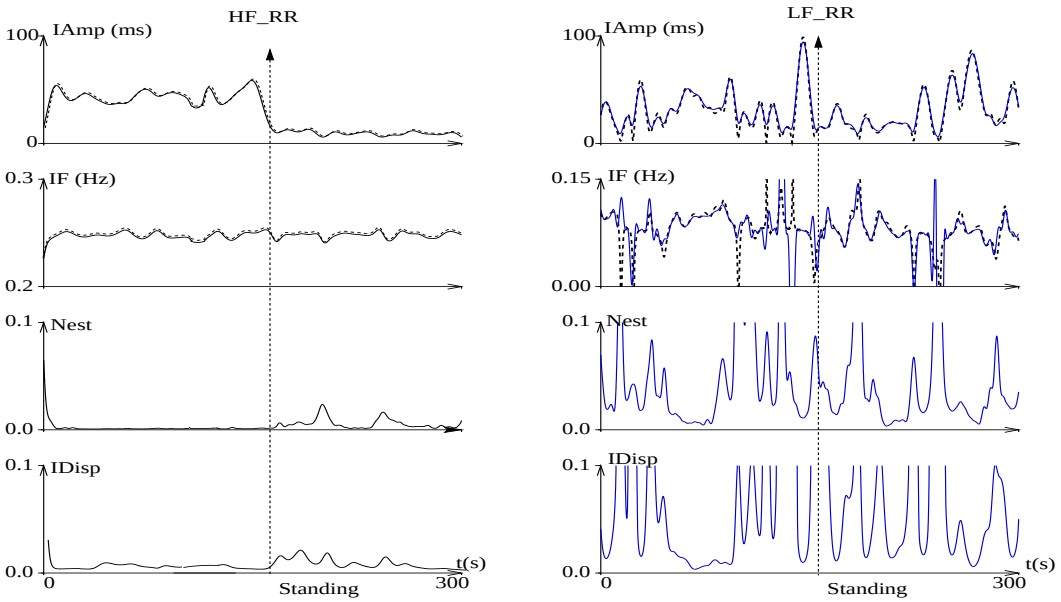

Figure 41: *Estimation of the instantaneous spectral parameters, $IAmp$ and IF, with CDM and SPWVD on an RR series in a normal subject during head-up tilt test and 0.25Hz paced breathing. Continuous lines stand for SPWVD and dashed lines for CDM results.*

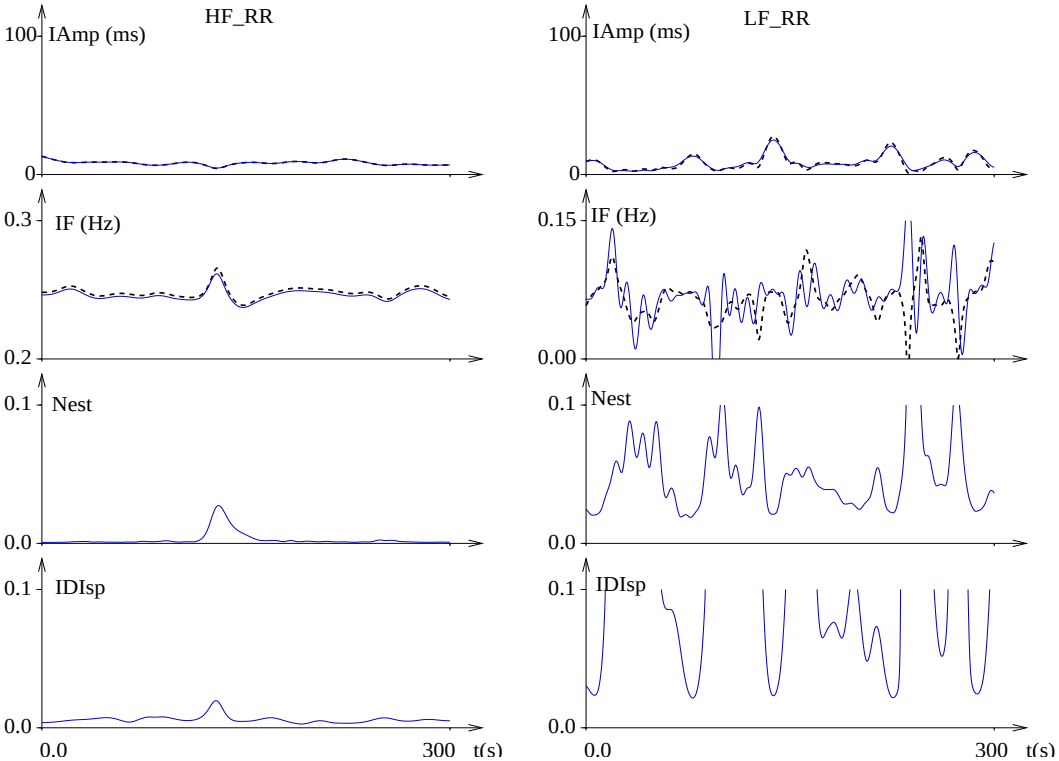

Figure 42: *Estimation of the instantaneous spectral parameters, $IAmp$ and IF, with CDM and SPWVD on an RR series in a normal subject under autonomic blockade and during 0.25Hz paced breathing. Continuous lines stand for SPWVD and dashed lines for CDM results.*

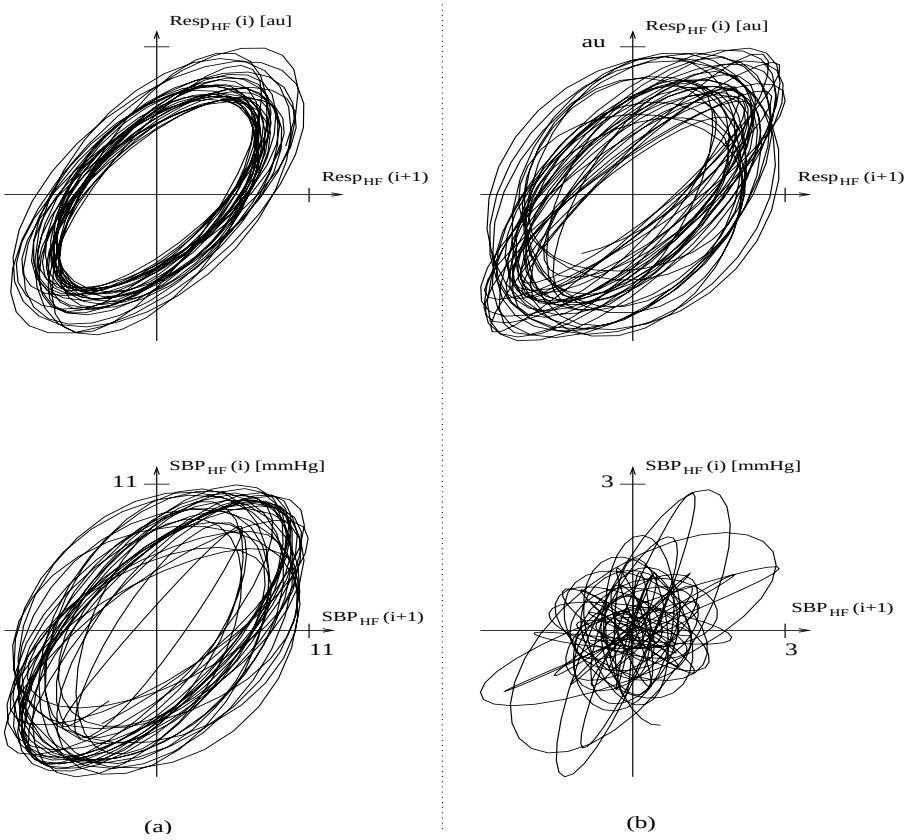

Figure 43: Poincare plot of respiratory signal (on the top) and of the High Frequency component in the systolic blood pressure signal (on the bottom) for a control subject (a) for a Chronic Heart Failure subject (b) during the 0.15Hz imposed breathing rate period. Normal subject has a stable respiratory and HF_{SBP} trajectory, whereas patient has an irregular respiratory and HF_{SBP} trajectory revealing some difficulty to follow the imposed external rhythm.

the limit cycle of the HF_{SBP} time series is similar to the respiratory time series one, see Fig. (43a) on the bottom. In control subjects, the stability in the IPh reflects a good synchronisation between breathing and the HF component of the CV series, Fig. (44a). On the other hand, CHF subjects are not able to follow imposed breathing rhythm as reflected by a reduced regularity of the respiratory limit cycle, see fig. (43b) on the top. Moreover, in CHF-subjects, HF_{SBP} time series is very irregular, with largely reduced amplitude values and without an observable limit cycle, see fig. (43b) on the bottom. This evidencies a lack of synchronisation between HF_{SBP} and respiratory time series in CHF subjects. In CHF subjects, the $IAmp$ is greatly reduced and presents sudden falls, Fig. (44b), corresponding to shifts in IPh and great SPW_N_{est} and SPW_IDisp values. In these periods, the meaningless IPh

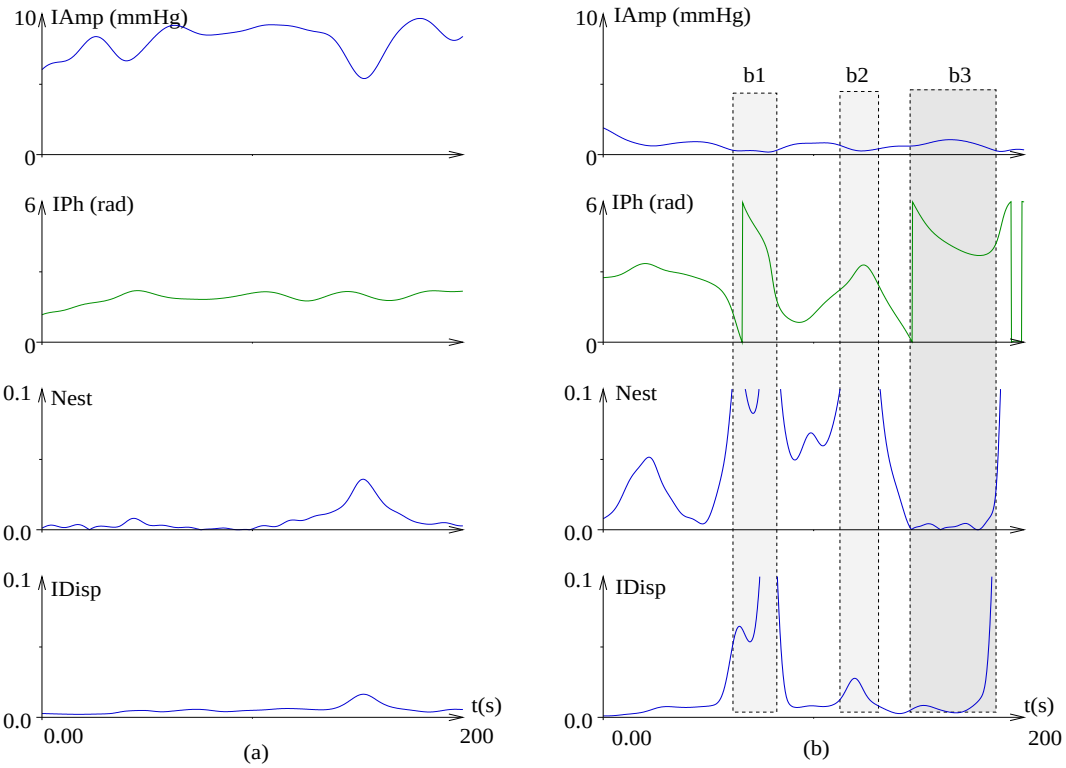

Figure 44: *Estimation of the instantaneous spectral parameters, IAmp and IPh, on a SBP time series in a normal subject (a) and a Chronic Heart Failure subject (b) during 0.15Hz paced breathing. b1 and b2 correspond to periods with IPh shifts and IAmp falls while b3 corresponds to a period with IPh shifts without IAmp falls.*

shifts are explained by the total disappearance of the HF component in CV time series (periods b1, b2 in Fig. (44b)). In other periods large IPh shifts occur without $IAmp$ falls or high SPW_N_{est} and SPW_IDisp values (period b3 in Fig. (44b)). IPh estimate is then reliable and can be interpreted: the HF component still exists but respiratory and high frequency CV activity are desynchronised. This test particularly shows the usefulness of the SPW_N_{est} and SPW_IDisp estimates to bring to light dysfunctions in the autonomic nervous system, such as in CHF subjects.

7.6 Discussion

7.6.1 Validation of the joint SPWVD-CDM method to assess instantaneous cardiovascular parameters

The ability of the joint SPWVD-CDM method to detect abrupt changes in the instantaneous $IAmp$, IF and IPh in CV time series was validated in all tested conditions. We showed that the $IAmp$ level is not sensitive enough to assess the reliability of IF and IPh as usually proposed [57], but that this reliability is greatly improved by the joint use of the SPW_N_{est} and SPW_IDisp indexes.

Whenever $IAmp$ falls, the SPW_N_{est} and SPW_IDisp indexes are high, IF and IPh cannot be interpreted because the HF component has completely disappeared from the CV time series (periods b1, b2 in Fig. (44b)). But sometimes, reduced $IAmp$ values are combined with low SPW_N_{est} and SPW_IDisp values, allowing the IF and IPh interpretation; typical examples are the standing position of head-up tilt (Fig. (41a)) or autonomic blockade (Fig. (42a)) in the HF band. In the LF band, non negligible $IAmp$ values are often combined with high SPW_N_{est} and SPW_IDisp values and the SPWVD is scattered over the frequency axis. In these cases, IF and IPh interpretation is meaningless. Neverthless, in the LF band, IF and IPh are more often reliable when breathing at 0.25 than 0.15 Hz, (Figs. (38b) and (40b)). At 0.15 Hz breathing, HF and LF components interact with each other as revealed by SPW_N_{est} and SPW_IDisp indexes but not by $IAmp$. In this case, the reliability of instantaneous spectral estimators is reduced.

The performances are then generally better in the HF than LF band and furtherly improved by paced breathing, as shown in Fig. (36a) and Fig. (38a).

In the LF band, the joint use of SPW_N_{est} and SPW_IDisp shows that the interpretation of the IF and IPh estimates should be discarded in many real-life situations. Conversely, in the HF band, even in conditions of reduced variability induced by head-up tilt, pharmacological autonomic blockade or autonomic desease, the joint use of SPW_N_{est} and SPW_IDisp shows the reliability of the IF and IPh estimates.

7.6.2 Estimation of the Instantaneous Spectral Parameters

There is no single "best" method to assess the instantaneous spectral parameters in real CV time-series as this choice depends on the parameters that one wants estimate, as shown in table (10).

Table 10: Schematic listing of best method to assess spectral instantaneous parameters.

Method	Estimable Spectral parameters	Pro	Contra
CDM	$IAmp, IF, IPh$	computationally efficient	not reliable IF and IPh estimate
SPWVD	$IAmp, IF, IDisp, Nest$	reliable IF estimate	great computational load
SPWVD-CDM	$IAmp, IDisp, Nest, IF, IPh$	reliable IF and IPh estimate	great computational load

In fact, to estimate the $IAmp$ parameter, both methods are very reliable in every condition and in both the HF and LF bands, see Fig. (36)-(42). The CDM is preferable as the computational load required by the SPWVD is much greater. The detection of reliable IF and IPh estimate periods requires the use of the SPWVD method by the means of an "*a priori*" defined threshold value for SPW_Nest and

SPW_IDisp parameters. The definition of this threshold value requires a trade-off between the whished reliability and the necessity to keep time-significant periods for statistical purposes. A threshold equal to 0.03 over a period of at least 30 seconds seemed well-suited, according to our simulations and real CV data.

7.6.3 Time-varying analysis in Chronic Heart Failure subjects

A novel finding from our study is that during voluntary breathing in CHF patients, major phase fluctuations occurred between cardiovascular oscillations and respiration, indicating transient lack of synchronization between these physiological signals, see fig. (44). Also, the amplitude of high-frequency cardiovascular oscillations in CHF patients showed larger changes when the breathing rate was slowed down, as compared to controls, see fig. (43), for statistical results see [92]. This altered pattern of cardiovascular oscillations during voluntary breathing suggests an impairment in the central regulation of autonomic outflow in CHF patients. In humans, specific regions of the brain cortex have been shown to be active during volitional breathing [40]. Furthermore robust connections exist between the cerebral cortex, the brainstem respiratory motoneurons, and the hypothalamic area [33, 75], a cardiovascular and respiratory integrative structure. Simultaneous changes in rhythmic organization have been demonstrated in brainstem neurons, respiration, the cardiovascular system, and the EEG [75]. In our study, voluntary breathing which involves cortical center in the brain, creates periodic forced stimulation of autonomic outflow regulating cardiovascular oscillations. The role of the central nervous system in generating oscillatory components in cardiovascular rhythms has been emphasized recently [75, 99, 117]. Montano et al. demonstrated LF and HF components in the discharge variability of brainstem neurons recorded in anaesthetized and artificially ventilated cats with sinoaortic deafferentation [99]: an HF component synchronous with the artificial ventilation rate was evidenced in the spectrum of neuronal discharge variability. Both LF and HF oscillations of the RR interval result in part from an autochthonous central rhythm, which influences autonomic output [117]. The disturbances in cardiovascular oscillation patterns observed in CHF patients during voluntary breathing suggest major dysfunction of the central mechanisms regulating the autonomic outflow. Autonomic modulation of cardiovascular variabilities in CHF is characterized by alterations at the cerebral level [126] , sympathovagal imbalance [43], and profound neurohormonal derangements. Excessive circulating levels of catecholamines, angiotensin, or vasopressin may alter autonomic regulatory function at the central level [126]. It should be noted that the patients in our study did not have severe CHF, as indicated by the clinical data and the preservation of LF oscillations of cardiovascular variabilities. Consistent with this fact, respiratory modulation of autonomic outflow was preserved. The importance in CHF of a primary impairment of a central mechanism regulating autonomic function has been emphasized [31]. However, the origin of this impairment is complex. The effects in our study of voluntary breathing, which has a major influence on autonomic regulation of cardiovascular oscillations, supports the hypothesis of a central autonomic regulatory impairment in CHF patients. Furthermore, under strictly controlled breathing conditions, the standard deviation of the mean breathing rate was higher in the CHF patients than in the controls: this breathing pattern variability on a breath-by-breath basis is in favor of a central alteration in respiratory drive as well.

8 Conclusions and Perspectives

Throughout this report we were interested on frequency and time-frequency analysis of cardiovascular and respiratory variability to study the control of the autonomic nervous system of the cardiovascular system. Moreover, we concentrate our analysis on only one of the fourth principal reflexes carried out by the nervous system, i.e. the arterial blood pressure - heart period reflex (ABP-RR reflex). Very significant results have been obtained in different physiological and pathological conditions, but further analyses are needed. A model-based signal processing could allow the study of the other effector reflexes: arterial blood pressure-stroke volume, -peripheral resistance and -compliance, which can provide further and complementary information on the ANS. In fact, sometimes the classical ABP-RR reflex may become only a secondary reflex, as we suggested in the discussion about the evolution of cardiovascular signal throughout the night, and other controlling mechanisms may take over. Therefore, an explicitely model-based estimation of the other cardiovascular parameters is needed to have a better insight on the ANS control of cardiovascular system in many real-life conditions.

References

[1] S. Akselrod, D. Gordon, J.B. Madwed, N.C. Snidman, D.C. Shannon, and R.J. Cohen. Hemodynamic regulation: investigation by spectral analysis. *Am J Physiol.*, 249 (4 Pt 2):H867–H875, 1985.

[2] S. Akselrod, D. Gordon, F.A. Ubel, D.C. Shannon, A.C. Berger, and R.J. Cohen. power spectrum analysis of heart rate fluctuation: a quatitative probe of beat-to-beat cardiovascular control. *Science*, 213 (4504), 1981.

[3] A. Angelone and Coulter N.A. Respiratory sinus arrhythmia: a frequency dependent phenomenon. *J. Appl. Physiol.*, 19 (3), 1964.

[4] E. Aserinsky. Periodic respiratory pattern occuring in conjunction with eye movements during sleep. *Science*, 150:763–766, 1965.

[5] A. Baharav, S. Kotagal, V. Gibbons, B.K. Rubin, G. Pratt, J. Karin, and S. Akselrod. Fluctuations in autonomic nervous activity during sleep displayed by power spectrum analysis of heart rate variability. *Neurology*, 45:1183–1187, 1995.

[6] G. Baselli, S. Cerutti, S. Civardi, D. Liberati, F. Lombardi, A. Malliani, and M. Pagani. Spectral and cross-spectral analysis of heart rate and arterial blood pressure variability signals. *Comput Biomed Res.*, 19 (6):520–534, 1986.

[7] G. Baselli, S. Cerutti, S. Civardi, A. Malliani, and M. Pagani. Cardiovascular variability signals: Towards the identification of closed-loop model of the neural control mechanism. *IEEE Trans. on Biomed. Engin.*, 35:1033–1045, 1988.

[8] I. Berlad, S. Shlitner, B. Ben-Haim, and P. Lavie. Power spectrum analysis and heart rate variability in stage 4 and rem sleep: evidence for state specific changes in autonomic dominance. *J. Sleep Res.*, 2:88–90, 1993.

[9] G. Bertinieri, M. Di Rienzo, A. Cavallazzi, A.U. Ferrari, and G. Mancia A. Pedotti. Evaluation of baroreceptor reflex by blood pressure monitoring in unanesthetized cats. *Am. J. Physiol.*, 254:H377–H383, 1988.

[10] J. Bestel. *Modèle différentiel de la contraction musculaire controlée. Applicaton au système cardiovasculaire.* PhD thesis, Université Paris-IX Dauphine. U.F.R. Mathématique de la décision., 2000.

[11] P. Bloomfield. *Complex demodulation.*, pages 118–150. P. Bloomfield. New York: Wiley, 1976.

[12] B. Boashash. Estimating and interpreting the instantaneous frequency of a signal - part 1: Fundamentals. IEEE, 1992. 80, no. 4: 520-538.

[13] B. Boashash. Estimating and interpreting the instantaneous frequency of a signal - part 2: Algorithms and applications. IEEE, 1992. vol. 80, no. 4: 539-568.

[14] B. Boashash and P. Black. An efficient real-time implementation of the wigner-ville distribution. *IEEE Trans Acoust. Speech, Signal Processing*, 35 (11):1611–1618, 1987.

[15] R.W. De Boer, J.M. Karemaker, and J. Strackee. Hemodynamic fluctuations and baroreflex sensitivity in humans: a beat-to-beat model. *Am. J. Physiol. 253 (Heart Circ. Physiol. 22)*, pages 680–689, 1987.

[16] C. Borst and J.M. Karemaker. Time delays in the human barorecepto reflex. *Journal of the Autonomic Nervous System*, 9:399–409, 1983.

[17] WJ. Bos, J. van Goudoever, GA. van Montfrans, AH. van den Meiracker, and KH. Wesseling. Reconstruction of brachial artery pressure from noninvasive finger pressure measurements. *Circulation*, 94(8):1870–5, 1996.

[18] J.D. Bristow, A.J. Honour, T.G. Pickering, and P. Sleight. Cardiovascular and respiratory changes during sleep in normal and hypertensive subjects. *Cardiovasc. Res.*, 3:476–485, 1969.

[19] T.E. Brown, L.A. Beightol, J. Koh, and D.L. Eckberg. Important influence of respiration on human rr interval power spectra is largely ignored. *J. Appl. Physiol.*, 75, no 5:2310–2317, 1993.

[20] A.C. Burton. *Physiology and biophysics of the circulation.*, chapter 18, page 164. year book medical publishers.

[21] A. Capello, G. Gnudi, and C. Lamberti. Identification of the three-element windkessel model incorporating a pressure-dependent compliance. *Annals of Biomedical Engineering*, 23:164–177, 1995.

[22] S. Cerutti, M. Alberti, G. Baselli, O. Rimoldi, and M. Pagani A. Malliani, M. Merri. Automatic assessment of the interaction between respiration and heart rate variability signal. *Med Prog Technol.*, 14 (1):7–19, 1988.

[23] S. Chandra, VK. Bahl, SC. Bose Reddy, B. Bhargava, A. Malhotra, and H.S. Wasir. Comparison of echocardiographic acoustic quantification system and radionuclide ventriculography for estimating left ventricular ejection fraction: Validation in patients without regional wall motion abnormalities. *Am heart J.*, 133:359–363, 1997.

[24] M. Chiollaz, B. Escudie, and A. Hellion. Une condition necessaire et suffisante pour l'ecriture du modele exponentiel des signaux d'energie fini. *Ann. Telecommunic*, 33, nos. 1-2:69–70, 1978.

[25] L. Cohen. Time-frequency distribution-a review. *Proc. IEEE*, 77 (7), 1989.

[26] N.J. Cohn, T.B. Levine, and M.T. Olivari et al. Plasma norepinephrine as a guide to prognosis in patients with chronic congestive heart failure. *N Engl J Med*, 311(13):819–823, 1984.

[27] R. Colombo, G. Mazzuero, G. Spinatonda, P. Lanfranchi, P. Giannuzzi, P. Ponikowski, A. Coats, and G. Minuco. Comparison between spectral analysis and the phenylephrine method for the assessment of baroreflex sensitivity in chronic heart failure. *Clin Sci*, pages 503–513, 1999.

[28] J. Conway, N. Boon, J.V. Jones, and P. Sleight. Involvement of the baroreceptor reflexes in the changes in blood pressure with sleep and mental arousal. *Hypertension Dallas*, 5:746–748, 1983.

[29] J. Conway and P. Lund-Johansen. Thermodilution method for measuring cardiac output. *Eur HeartJ*, 11 (Suppl 1):17–20, 1990.

[30] W.H. Cooke, J.B. Hoag, A.A. Crossman, T.A. Kuusela, K.U. Tahvanainen, and D.L. Eckberg. Human responses to upright tilt: a window on central autonomic integration. *J Physiol.*, 5127 (Pt 2):617–628, 1999.

[31] R.L. Cooley, N. Montano, C. Cogliati, P. Van De Borne, W. Richenbacher, R. Oren, and V.K. Somers. Evidence for a central origin of the low-frequency oscillation in rr-interval variability. *Circulation*, 98:556–561, 1998.

[32] P. Coumel, P. Maison-Blanche, and D. Catuli. Heart rate and heart rate variability in normal young adults. *J. Cardiovasc. Electrophysiol.*, 5:899–911, 1994.

[33] P.W. Davenport and R.L. Reep. Cerebral cortex and respiration. In *Regulation of Breathing*, chapter 8, pages 365–388. Dempsey JA, Pack AI (Eds) New York, 1994.

[34] L.C. Davies, D.P. Francis, P. Jurak, T. Kara, M. Piepoli M, and A. Coats. Reproducibility of methods for assessing baroreflex sensitivity in normal controls and in patients with chronic heart failure. *Clin Sci*, 97:515–522, 1999.

[35] P. Van de Borne, N. Montano, N. Pagani, R. Oren, and V.K. Somers. Absence of low frequency variability of sympathetic nerve activity in severe heart failure. *Circulation*, 95:1449–1454, 1997.

[36] Ph. Van de Borne, H. Nguyen, P. Biston, P. Linlowski, and J.P. Degaute. Effects of wake and sleep stages on the 24-h autonomic control of blood pressure and heart rate in recumbent men. *Am. J. Physiol.*, 266:H548–H554, 1994.

[37] D. de Zuttere, T. Touche, G. Saumon, A. Nitenberg, and R. Prasquier. Doppler echocardiographic measurement of mitral flow volume: validation of a new method in adult patients. *J Am Coll Cardio*, 11:343–350, 1988.

[38] K. Denning, HJ. Nesser, HU. Haase, and A. Schömig. Assessment of ventricular filling volumes with an automated color doppler method: validation in a pulsatile flow model. *J Am soc Echocardiogr*, 14:343–352, 2001.

[39] N.J. Douglas, D.P. White, C.K. Pickett, J.V. Weil, and C.W. Zwillich. Respiration during sleep in normal man. *Thorax*, 37:840–844, 1982.

[40] K.C. Evans, S.A. Shea, and A.J. Saykin. Functional mri localisation of central nervous system regions associated with volitional inspiration in humans. *J Physiol*, 520:383–392, 1999.

[41] T.J.C. Faes, P. Lanting, B.J. TenVoorde, and O. Rompelman. The origin of respiratory sinus arrhythmia: towards a closed-loop identification of autonomic regulation in the cardiovascular system using respiratory induced fluctuations in heart rate and blood pressure. *Automedica*, 13:33–44, 1990.

[42] R. Fagard and J. Conway. Measuremt of cardiac output: fick principle using catheterization. *Eur Heart J*, 11 (Suppl 1):1–5, 1990.

[43] J.S. Floras. Clinical aspects of sympathetic activation and parasympathetic withdrawal in heart failure. *J Am Coll Cardiol*, 22:72–84, 1993.

[44] Task force of the European Society of Cardiology, the North American Society of pacing, and electrophysiology. Heart rate variability: standards of measurement, physiological interpretation, and clinical use. *Circulation*, 93:1043–1065, 1996.

[45] YC. Fung. *Biomechanics. Mechanical properties of living tissues.* Springer, second edition, 1993.

[46] R. Furlan, S. Dell'Orto, Crivellaro W., P. Pizzinelli, S. Cerutti, Lombardi F., Pagani M., and Malliani A. Effects of tilt and treadmill exercise on short-term variability in systolic arterial pressure in hypertensive men. *J. Hypertension*, 5 (suppl. 5):S423–S425, 1987.

[47] R. Furlan, Guzzetti S., Crivellaro W., Dassi S., Tinelli M., Baselli G., Lombardi F., Pagani M., and Malliani A. Continous 24-h assessment of the neural regulation of systemic arterial pressure and rr variabilities in ambulant subjects. *Circulation*, 81:537–547, 1990.

[48] D. Gabor. Theory of communications. *Proc. IEEE*, 93 (III):429–457, 1946.

[49] J.J. Goldberger. Sympathovagal balance: how should we measure it? *Am. J. Physiol. 276 (Heart Circ. Physiol. 45)*, pages H1273–H1280, 1999.

[50] J.J. Goldberger, Y.H. Kim, M.W. Ahmed, and A.H. Kadish. Effect of graded increases in parasympathetic tone on heart rate variability. *J Cardiovasc Electrophysiol.*, 7 (7):594–602, 1996.

[51] I. Gratz, J. Kraidin, AG. Jacoi, NG. deCastro, P. Spagna, and GE. Larijani. Continuous noninvasive cardiac output as estimated from the pulse contour curve. *J Clin Monit*, 8:20–27, 1992.

[52] P. Grossman, J. Karemaker, and W. Wieling. Prediction of tonic parasympathetic cardiac control using respiratory sinus arrhythmia: the need for respiratory control. *Psychophysiology*, 28(2):201–216, 1991.

[53] AC. Guyton, JM. Ross, O. Carrier, and JR. Walker. Evidence for tissue oxygen demand as the major factor causing autoregulation. *Circulation research.*, Vols XIV and XV (Supp I):I60–I69, 1964.

[54] H. Hainsworth. The control and physiological importance of heart rate. *??*, ??:??, ??

[55] MP. Harms, KH. Wesseling, F. Pott, M. Jenstrup, J. Van Goudoever, and NH. Secher. Continuous stroke volume monitoring by modelling flow from non-invasive measurement of arterial pressure in humans under orthostatic stress. *Clin Sci (Lond).*, 97(3):291–301, 1999.

[56] J. Hayano. Continuous assessment of hemodynamic control by complex demodulation of cardiovascular variability. *Am. J. Physiol. 264 (Heart Circ. Physiol. 33)*, pages H1229–H1238, 1993.

[57] J. Hayano. Assessment of frequency shifts in rr interval variability and respiration with complex demodulation. *J. Appl. Physiol.*, 77(6):2879–2888, 1994.

[58] H.H. Heicht. Comparative physiological and morphological aspects of pacemaker tissue. *Ann. N.Y. Acad. Sci.*, 127:49–83, 1965.

[59] J.A. Hirsch and B. Bishop. Respiratory sinus arryhtmia in humans: how breathing pattern modulates heart rate. *Am. J. Physiol. 241 (Heart Circ. Physiol. 10)*, pages H620–H629, 1981.

[60] F.C. Hoppensteadt and C.S. Peskin., editors. *The heart and Circulation*, chapter 5, pages 105–138. Springer-Verlag in Applied Mathematics, 1992.

[61] M. Hornyak, M. Cejnar, M.Elam, M. Matousek, and G. Wallin. Sympathetic nerve activity during sleep in man. *Brain*, 114:1281–1295, 1991.

[62] R.L. Hughson, L. Quintin, G. Annat, Y. Yamamoto, and C. Gharib. Spontaneous baroreflex by sequence and power spectral methods in humans. *Clinical physiology*, 13:663–676, 1993.

[63] B.W. Hyndman and R.K. Mohn. A pulse modulator model of pacemaker activity. In *Digest of the 10th Int. Conf. Med. & Biol. Eng.*, page 223, Dresden, 1973.

[64] F. Iellamo, J.M. Legramante, R. Gianfranco, F. Castrucci, M. Massaro, and G. Peruzzi. Evaluation of reproducibility of spontaneous baroreflex sensitivity at rest during laboratory tests. *J. of Hypertension*, 4:1099–1104, 1996.

[65] Bp. Imholz, W. Wieling, GA. van Montfrans, and KH. Wesseling. Fifteen years experience with finger arterial pressure monitoring: assessment of the technology. *Cardiovasc Res*, 38 (3):605–16, 1998.

[66] JRC. Jansen, JJ. Schreuder, JJ. Settels, L. Kornet, OCKM. Penn, PGH. Mulder, A. Versprille, and KH. Wesseling. Single injection thermodilution. *Anesthesiology*, 85:481–490, 1996.

[67] S. Jasson, C. Médigue, P. Maison-Blanche, N. Montano, L. Meyer, P. Mansier C. Vermeiren, P. Coumel, A. Malliani, and B. Swynghedauw. Instant power spectrum analysis of heart rate variability during orthostatic tilt using a time-/frequency-domain method. *Circulation.*, 96 (10):3521–3526, 1997.

[68] M. Karamanoglu. On line synthesis of the human ascending aortic pressure pulse from the finger pulse. *Hypertension*, 30:1416–1424, 1997.

[69] P.G. Katona and Jih F. Respiratory sinus arrhytmia: noninvasive measure of parasympathetic cardiac control. *J. Appl. Physiol.*, 39, no 5:801–805, 1975.

[70] K.M. Spyer KM. Central nervous mechanisms contributing to cardiovascular control. *J Physiol*, 474:1–19, 1994.

[71] H.P. Koepchen. History of studies and concepts of blood pressures waves. In *Mechanism of blood pressure waves*, pages 3–23. Japan science society press, berlin germany springer verlag edition, 1984.

[72] E. Koushanpour. Baroreceptor process in the carotid sinus. In *Regulation and control in physilogical systems*, pages 350–354. Instrument society of america pittsburg edition, 1973.

[73] E. Koushanpour. Baroreceptor discharge behaviour and resetting. In *Baroreceptor Reflexes. Integrative Functions and Clinical Aspects*, pages 9–44. Springer-verlag edition, 1991.

[74] P.Y. Ktonas and N. Papp. Instantaneous envelope and phase extraction from real signal: theory, implementation and an application to eeg analysis. *Signal Processing*, 2:373–385, 1980.

[75] M. Lambertz and P. Langhorst. Simultaneous changes of rhythmic organization in brainstem neurons, respiration, cardiovascular system and eeg between 0.05 hz and 0.5 hz. *J Auton Nerv Syst*, 68:58–77, 1998.

[76] GJ. Langewouters, KH. Wesseling, and WJA. Goedhard. The static elastic properties of 45 human thoracic and 20 abdominal aortas in vitro and the parameters of a new model. *J. Biomechanics*, 17 (6):425–435, 1984.

[77] J.M. Legramante, G. Raimondi, M. Massaro, S. Cassarino, G. Peruzzi, and F. Iellamo. Investigating feedforward neural regulation of circulation from analysis of spontaneous arterial pressure and heart rate fluctuation. *Circulation*, pages 1760–1766, 1999.

[78] M.N. Levy and P.J. Martin. Neural control of the heart. In *Handbook of physiology: the cardiovascular system I*, pages 581–620. 1976.

[79] M.N. Levy and H. Zieske. Autonomic control of cardiac pacemaker activity and atrioventricular trasmission. *J. Appl. Physiol.*, 27:465–470, 1969.

[80] L.A. Lipsitz, J. Mietus, G.B. Moody, and A.L. Goldberger. Spectral characteristics of the heart rate variability before and during postural tilt. *Circulation*, 81:1803–1810, 1990.

[81] J.L. Liu, H. Murakami, and M. Sanderford et al. Ang ii and baroreflex function in rabbits with chf and lesions of the area postrema. *Am J Physiol*, 277:H342–H350, 1999.

[82] F. Lombardi, G. Sandrone, S. Pernpruner, R. Sala, M. Garimoldi, S. Cerutti, G. Baselli, M. Pagani, and A. Malliani. Heart rate variability as an index of sympathovagal interaction after acute myocardial infarction. *Am J Cardiol.*, 60 (16):1239–1245, 1987.

[83] R. Maestri, G.D. Pinna, A. Mortara, M.T. La Rovere, and L. Tavazzi. Assessing baroreflex sensitivity in post-myocardial infarction patientes: comparison of spectral and phenylephrine techniques. *J. Am. Coll. Cardiol.*, 31:344–351, 1998.

[84] A. Malliani. Cardiovascular sympathetic afferent fibers. *Rev Physiol. Biochem. Pharmacol.*, 94:11–74, 1982.

[85] A. Malliani. Association of heart rate variability components with physiological regulatory mechanisms. *From: Malik and Camm (eds.): Heart Rate Variability. Armonk, NY. Futura Publishing Company*, pages 173–188, 1995.

[86] A. Malliani. Individual recognition by heart rate variability of two different autonomic profiles related to posture. *Circulation*, 96:4143–4145, 1997.

[87] A. Malliani. *Principles of cardiovascular Neural Regulation in Health and Disease.* Kluwer Academic Publishers, Netherlands, first edition, 2000.

[88] A. Malliani, M. Pagani, F. Lombardi, and S. Cerutti. Cardiovascular neural regulation explored in the frequency domain. *Circulation*, 84:482–492, 1991.

[89] A. Malliani, M. Pagani, N. Montano, and G. S. Mela. Sympathovagal balance: a reappraisal. *Circulation*, 98:2640–2643, 1998.

[90] G. Mancia. Autonomic modulation of the cardiovascular system during sleep. *N. Engl. J. Med.*, 328:347–349, 1993.

[91] L. Mangin, A. Monti, and C. Médigue. Baroreflex during cardiac failure: abnormal gain during paced-breathing. *Eur J Heart Failure*, 1:236 (Abstract), 1999.

[92] L. Mangin, A. Monti, and C. Médigue. Cardiorespiratory system dynamics in chronic heart failure. *European Journal of Heart Failure*, 2001.

[93] L. Mangin, A. Monti, C. Médigue, I. Macquin-Mavier, M.E. Lopes, P. Gueret, A. Castaigne, B. Swynghedauw, and P. Mansier. Altered baroreflex gain during voluntary breathing in chronic heart failure. *European Journal of Heart Failure*, 3:189–195, 2001.

[94] C. Médigue, A. Girard, D. Laude, A. Monti, M. Wargon, and J.L. Elghozi. Relation between vagal tone and respiratory sinus arrhythmia: a time- and frequency-domain analysis of the effects of atropine. *Plügers Archive European Journal of Physiology*, 441:650–655, 2001.

[95] C. Médigue, A. Monti, and A. Wambergue. Lary_cr: Software package for the analysis of cardio vascular and respiratory rhythms, in the scilab_scicos environment. *Rapport Technique INRIA, projet SOSSO, n°*259:http://www.inria.fr/rrrt/rt–0259.html, 2002.

[96] I. Misrky and W.W. Parmley. *Cardiac mechanics: Physiological, Clinical, and Mathematical considerations*, chapter 4. J. Wiley, 1974.

[97] P.K. Mohanty, J.A. Arrowood, K.A. Ellenbogen, and M.D. Thames. Neurohumoral and hemodynamic effects of lower body negative pressure in patients with congestive heart failure. *Am Heart J*, 118:78–85, 1989.

[98] N. Montano, C. Cogliati, A. Porta, M. Pagani, A. Malliani, K. Narkiewicz, F.M. Abboud, C. Birkett, and V.K. Somers. Central vagotonic effects of atropine modulate spectral oscillations of sympathetic nerve activity. *Circulation*, 98(14):1394–9, 1998.

[99] N. Montano, T. Gnecchi-Ruscone, A. Porta, F. Lombardi, A. Malliani, and S.M. Barman. Presence of vasomotor and respiratory rhythms in the discharge of single medullary neurons involved in the regulation of cardiovascular system. *J Auton Nerv Syst.*, 57:116–122, 1996.

[100] N. Montano, F. Lombardi, T. Gnecchi Ruscone, M. Contini, M.L. Finocchiaro, G. Baselli, A. Porta, S. Cerutti, and A. Malliani. Spectral analysis of sympathetic discharge, r-r interval and systolic arterial pressure in decerebrate cats. *J Auton Nerv Syst.*, 40 (1):21–31, 1992.

[101] N. Montano, T. Gnecchi Ruscone, A. Porta, F. Lombardi, and A. Malliani. Power spectral analysis of heart rate variability to assess the changes in sympathovagal balance during greaded orthosatic tilt. *Circulation*, 90:1826–1831, 1994.

[102] A. Monti. Modélisation du système cardiovasculaire. Rapport of training period at the Polytechnic School, France, June 1997.

[103] A. Monti. Modelling the cardiovascular system. Master's thesis, Milan Polytechnic, Italy, July 1998.

[104] A. Monti, C. Médigue, H. Nedelcoux, and P. Escourrou. Cardiovascular autonomic control during sleep in normal subjects. *accepted by the European Journal of Applied Physiology*, 2002.

[105] RL. Morrissey, SC. Siu, JL. Guerrero, JB. Newell, AE. Weyman, and M.H. Picard. Automated assessment of ventricular volume and function by echocardiography: Validation of automated border detection. *J Am Soc Echocardiogr*, 7:107–115, 1994.

[106] R.M. Negoescu and I. E. Csiki. Autonomic control of the heart in some vagal maneuvers and normal sleep. *Physiologie*, 26 (1):39–49, 1989.

[107] J. Newsom-Davis and F. Plum. Separation of descending spinal pathways to respiratory motoneurons. *Exp Neurol*, 34:78–94, 1972.

[108] V. Novak, P. Novak, J. De Champlain, A.R. Le Blanc, R. Martin, and R. Nadeau. Influence of respiration on heart rate and blood pressure fluctuations. *J. Appl. Physiol.*, 74, no 2:617–626, 1993.

[109] V. Novak, P. Novak, and R. Schondorf. Accurancy of beat-to-beat noninvasive measurement of finger arterial pressure using the finapres: a spectral analysis approach. *J. Clin. Monit.*, 10:118–126, 1994.

[110] H. Okada, S. Iwase, T. Mano, Y. Sugiyama, and T. Watanabee. Changes in muscle sympathetic activity during sleep in humans. *Neurology*, 41:1961–1966, 1991.

[111] S. Omboni, G. Parati, A. Frattola, E. Mutti, M. Di Rienzo, P. Castiglioni, and G. Mancia. Spectral and sequence analysis of figner blood pressure variability, comparison with analysis of intra-arterial recordings. *Hypertension*, 22:26–33, 1993.

[112] JT. Ottesen. Nonlinearity of baroreceptor nerves. In Springer-Verlag, editor, *Surveys on Mathematics for Industry*, volume 7 (3), pages 187–201. 1997.

[113] M. Pagani, R. Furlan, P. Pizzinelli, W. Crivellaro, S. Cerutti, and A. Malliani. Spectral analysis of r-r and arterial pressure variabilities to assess sympatho-vagal interaction during mental stress in humans. *J Hypertens Suppl.*, 7 (6):S14–S15, 1989.

[114] M. Pagani, F. Lombardi, and S. Guzzetti. Power spectral analysis of heart rate and arterial pressure variabilities as a marker of sympathovagal interaction in man and conscious dog. *Circ. Res.*, 59:178–193, 1986.

[115] M. Pagani, F. Lombardi, S. Guzzetti, G. Sandrone, O. Rimoldi, G. Malfatto, S. Cerutti, and A. Malliani. Power spectral density of heart rate variability as an index of sympatho-vagal interaction in normal and hypertensive subjects. *J. Hypertension Suppl.*, 2 (3):S383–S385, 1984.

[116] M. Pagani, D. Lucini, O. Rimoldi, R. Furlan, S. Piazza, A. Porta, and A. Malliani. Low and high frequency components of blood pressure variability. *Ann NY Acad Sci*, 783:10–23, 1996.

[117] M. Pagani, N. Montano, A. Porta, A. Malliani, F.M. Abboud, C. Birkett, and V.K. Somers. Relationships between spectral components of cardiovascular variabilities and direct measures of muscle sympathetic nerve activity in humans. *Circulation*, 95:1441–1448, 1997.

[118] M. Pagani, P. Pizzinelli, M. Bergamaschi, and A. Malliani. A positive feedback sympathetic pressor reflex during stretch of the thoracic aorta in conscious dogs. *Circ. Res.*, 50:125–132, 1982.

[119] M. Pagani, V.K. Somers, R. Furlan, S. Dell'Orto, J. Conway, G. Baselli, S. Guzzetti, S. Cerutti F. Lombardi, and A. Malliani. Changes in autonomic regulation induced by physical trianing in mild hypertension. *Hypertension*, 12:600–610, 1988.

[120] R.B. Panerai, M.A. James, J.F. Potter, L. Fan, and D.H. Evans. Baroreceptor sensitivity in human subjects: sequence or spectral analysis? *Computers in Cardiology*, pages 305–308, 1995.

[121] G. Parati, M. Di Rienzo, G. Bertinieri, G. Pomidossi, R. Casadei, A. Groppelli, A. Pedotti, A. Zanchetti, and G. Mancia. Evaluation of the baroreceptor-heart rate reflex by 24-hour intra-arterial blood pressure monitoring in humans. *Hypertension*, 254:H377–H383, 1988.

[122] G. Parati, J.P. Saul, M. Di Rienzo, and G. Mancia. Spectral analysis of blood pressure and heart rate variability in evaluating cardiovascular regulation. *Hypertension*, 25:1276–1286, 1995.

[123] P. Parker, B.G. Celler, E.K. Potter, and D.I. McCloskey. Vagal stimulation and cardiac slowing. *Journal of the Autonomic Nervous System*, 11:226–231, 1984.

[124] J. Parlow, J.P. Viale, G. Annat, R. Hughson, and L. Quintin. Spontaneous cardiac baroreflex in humans. comparison with drug-induced responses. *Hypertension*, 25:1058–1068, 1995.

[125] P. Parmegiani. The autonomic nervous system in sleep. In Saunders Philadelphia, PA, editor, *Principles and Practice of Sleep Medicine (2nd ed.)*, pages 194–203. M.H. Kryger, T. Roth and W.C. Dement., 1994.

[126] K.P. Patel. Role of paraventricular nucleus in mediating sympathetic outflow in heart failure. *Heart Fail Reviews*, 5:73–86, 2000.

[127] A.R. Patwardhan, J.M. Evans, E.N. Bruce, D.L. Eckberg, and C.F. Knapp. Voluntary control of breathing does not alter vagal modulation of heart rate. *J Appl Physiol.*, 78 (6):2087–2094, 1995.

[128] J. Penaz. Photoelectric measurement of blood pressure, volume and flow in the finger (abstract). In *Proc. 10th Int Conf Medical and Biological Engineering*, volume 7-2, page 104, 1973.

[129] M. Piepoli, P. Sleight, S. Leuzzi, F. Valle, G. Spadacini, C. Passino C, J. Johnston J, and L. Bernardi. Origin of respiratory sinus arrhythmia in conscious humans. an important role for arterial carotid baroreceptors. *Circulation*, 95 (7):371–381, 2000.

[130] M.V. Pitzalis, F. Mastropasqua, and F. Massari et al. Effect of respiratory rate on the relationships between rr interval and systolic blood pressure fluctuations: a frequency-dependent phenomenon. cardiovasc. *Research*, 38:332–339, 1998.

[131] S. Pola, A. Macerata, M. Emdin, and C. Marchesi. Estimation of the power spectral density in non-stationary cardiovascular time series: assessing the role of the time-frequency representations (tfr). *IEEE trans. on Biomed. Eng.*, 43 no. 1:46–57, 1996.

[132] B. Pomeranz and al. Assessment of autonomic function in humans by heart rate spectral analysis. *Am. J. Physiol. 248 (Heart Circ. Physiol. 17)*, pages H151–H153, 1985.

[133] P. Ponikowski, S.D. Anker, and T.P. Chua et al. Depressed heart rate variability as an independent predictor of death in chronic congestive heart failure secondary to ischemic or idiopathic dilated cardiomyopathy. *Am J Cardiol*, 79:1645–1650, 1997.

[134] S.W. Porges. Orienting in a defensive world: mammalian modifications of our evolutionary heritage. a polyvagal theory. *Psychophysiol*, 32:301–18, 1995.

[135] JK. Raines, MY Jaffrin, and AH. Shapiro. A computer simulation of arterial dynamics in the human leg. *J. Biomechanics*, 7:77–91, 1974.

[136] A. Rechtschaffen and A. Kales. *Washington, DC: US Govt. Printing Office*, NIH Pub. No 204, 1968.

[137] O. Rimoldi, S. Pierini, A. Ferrari, S. Cerutti, M. Pagani, and A. Malliani. Analysis of short-term oscillations of r-r and arterial pressure in conscious dogs. *Am J Physiol.*, 258(4 Pt 2):H967–76, 1990.

[138] H.W. Robbe, L.J. Mulder, H. Ruddel, W.A. Langewitz, J.B. Veldman, and G. Mulder. Assessment of baroreceptor reflex sensitivity by means of spectral analysis. *Hypertension*, 10:538–543, 1987.

[139] A. Mortara M.T. La Rovere and G.D. Pinna et al. Arterial baroreflex modulation of heart rate in chronic heart failure. clinical and hemodynamic correlates and prognostic implications. *Circulation*, 96:3450–3458, 1997.

[140] J.P. Saul, R.D. Berger, P. Albrecht, S.P. Stein, M.H. Chen, and R.J. Cohen. Transfer function analysis of the circulation: unique insights into cardiovascular regulation. *Am. J. Physiol.*, 261:H1231–H1245, 1991.

[141] J.P. Saul, R.D. Berger, M.H. Chen, and R.J. Cohen. Transfer function analysis of autonomic regulation. ii respiratory sinus arrythmia. *Am. J. Physiol. 256 (Heart Circ. Physiol. 25)*, pages H153–H161, 1989.

[142] J.P. Saul and Cohen R.J. Respiratory sinus arrhythmia. In NY Futura Publishing Co. Inc., Armonk, editor, *Vagal control of heart: experimental basis and clinical implications*, pages 511–536. Levy M.N and Swartz P.J., 1994.

[143] A.M. Scher, D.S. O'Leary, and D.D. Sheriff. Arterial baroreceptor regulation of peripheral resistance and of cardiac performance. pages 75–125. P.B. Persson and H.R. Kirchheim, 1991.

[144] P.J. Schwartz, M. Pagani, F. Lombardi, A. Malliani, and A.M. Brown. A cardiocardiac sympathovagal reflex in cat. *Circ. Res.*, 32:215–220, 1973.

[145] S.J. Shin, W. N. Tapp, S.S. Reisman, and B. Natelson. Baroreflex sensitivity assessed by complex demodulation of cardiovascular variability. *Hypertension*, 29:1119–1125, 1997.

[146] S.J. Shin, W.N. Tapp, S.S. Reisman, and B. Natelson. Assessment of autonomic regulation of heart rate variability by the method of complex demodulation. *IEEE trans. on biomed. engin.*, 36, no 2:274–283, 1989.

[147] H.S. Smyth, P. Sleight, and G.W. Pickering. Reflex regulation of arterial pressure during sleep in man. *Circulation Research*, 24, no 1:109–121, 1969.

[148] V.K. Somers, D. Phil., M.E. Dyken, A.L. Mark, and F.M. Abboud. Sympathetic nerve activity during sleep in normal subjects. *N. Engl. J. Med.*, 328:303–7, 1993.

[149] B. Sramek. Non-invasive continuous cardiac output monitor. US patent, May 1984. num. 4,450,527.

[150] N. Stergiopulos, JJ. Meister, and N. Westerhof. Evaluation of methods for estimation oftotal arterial compliance. *Am J Physiol.*, 268 (37):H1540–H1548, 1995.

[151] N. Stergiopulos, BE. Westerhof, and N. Westerhof. Total arterial inertance as the fourth element of the windkessel model. *Am J Physiol.*, 276 (45):H81–H88, 1999.

[152] N. Stergiopulos, DF. Young, and TR. Rogge. Computer simulation of the arterial flow with applications to arterial and aortic stenoses. *j. Biomechanics.*, 25 (12):1477–1488, 1992.

[153] WJ. Stok, F. Baisch, A. Hillebrecht, H. Schulz, M. Meyer, and JM. Karemaker. Noninvasive cardiac output measurement by arterial pulse analysis compared with inert gas rebreathing. *J Appl Physiol.*, 74(6):2687–93, 1993.

[154] WJ. Stok, RCO. Stringer, and JM. Karemaker. Noninvasive cardiac output measurement in orthostasis: pulse contour analysis compared with acetylene rebreathing. *J Appl Physiol.*, 87(6):2266–2273, 1999.

[155] MF. Taher, ABP. Cecchini, MA. Allen, SR. Gobran, RC. Gorman, BL. Guthrie, KA. Lingenfelter, SY. Rabbany, PM. Rolchigo, J. Melbin, and A. Noordergraaf. baroreceptor responses derived from a fundamental concept. *Annal of Biomedical Engineering*, 16:429–443, 1988.

[156] J.A. Taylor and D.L. Eckberg. Fundamental relations between short-term rr-interval and arterial pressure oscillations in humans. *Circulation*, 93:1527–1532, 1996.

[157] B.J. TenVoorde. *Modeling the baroreflex: a systems analysis approach.* PhD thesis, Vrije Universiteit, Enschede, 1992.

[158] GP. Toorop, N. Westerhof, and G. Elzinga. beat-to-beat estimation of peripheral resistance and arterial complianceduring pressure transients. *Am J Physiol*, 252 (heart Circ Physiol 21):H1275–H1283, 1987.

[159] SM. Toy, J. Melbin, and A. Noordergraaf. Reduced models of arterial systems. *IEE Trans on Biomed Eng*, BME-32 (2):174–176, 1985.

[160] M. Ursino and E. Magosso. Acute cardiovascular response to isocapnic hypoxia. i. a mathematical model. *Am. J. Physiol. Heart Circ. Physiol.*, 279:H149–H165, 2000.

[161] E. Vanoli, P.B. Adamson, Ba Lin, G.D.Pinna, R. Lazzara, and W.C. Orr. Heart rate variability during specific sleep stages: a comparison of healthy subjects with patients after myocardial infarction. *Circulation*, 91:1918–1922, 1995.

[162] B.V. Vaughn, SR. Quint, J.A. Messenheimer, and K.R. Robertson. Heart period variability in sleep. *Electroencephalogr. Clin. Neurophysiol.*, 94:155–162, 1995.

[163] W. Veenhof, M. Hopkins, H. Chevalier, P. Pailing, R.D. Ogilvie, and S.J. Segalowitz. Vagal tone: changes across sleep stage and time of night. *Sleep Research*, 26:88, 1997.

[164] C. Vermeiren. *Analyse et modélisation du système cardiovasculaire et sa régulation à court terme par le système nerveaux autonome.* Génie biologique et médical, Université de Paris Val de Marne, U.F.R. de Sciences et de Technologie, 1996.

[165] C. Vermeiren, P. Escourrou, Y. Papelier, G. Le Vey, and A.W. Przybyszewski. Assessment of the phase relationship between breathing, heart rate and blood pressure by modified complex demodulation. In *Proc. IEEE-EMBS Conference*, pages 943–944, Montreal, 1995. IEEE-EMBS.

[166] A. Gelb Wallace. *Multiple-input Describing Function and Non-linear System Design.* McGraw-Hill Book Company, 1968.

[167] X. Wang, HH. Sun, and JM. Van de Water. An advanced signal processing technique for impedance cardiography. *IEEE Trans. on Biomed. Engineering*, 42 (2):224–230, 1995.

[168] KH. Wesseling. Finger arterial pressure measurement with finapres. *Z Kardiol.*, 85 Suppl 3:38–44, 1996.

[169] KH. Wesseling, B. de Wit, JAP. Weber, and N. Ty Smith. A simple device for the continous measurement of cardiac output. *Adv Cardiovasc Phys*, 5 (Part II):16–52, 1983.

[170] KH. Wesseling, JR. Jansen, JJ. Settels, and JJ. Schreuder. Computation of aortic flow from pressure in humans using a nonlinear, three-element model. *J Appl Physiol.*, 74 (5):2566–73, 1993.

[171] MH. Winter, P. Escourrou, M. Goldman, M. Slama, L. Drieu, and M. Jaffrin. Comparison of invasive and non-invasive blood pressure measurements for determining cardiac output in man. In *Proc. 14th Annual Int Conf IEEE-EMBS*, volume 14, pages 744–745, 1992.

[172] D. Zemaityte, G. Varoneckas, and E. Sokolov. Heart rhythm control during sleep. *Psychophysiology*, 21:279–289, 1984.

Unité de recherche INRIA Rocquencourt
Domaine de Voluceau - Rocquencourt - BP 105 - 78153 Le Chesnay Cedex (France)

Unité de recherche INRIA Lorraine : LORIA, Technopôle de Nancy-Brabois - Campus scientifique
615, rue du Jardin Botanique - BP 101 - 54602 Villers-lès-Nancy Cedex (France)
Unité de recherche INRIA Rennes : IRISA, Campus universitaire de Beaulieu - 35042 Rennes Cedex (France)
Unité de recherche INRIA Rhône-Alpes : 655, avenue de l'Europe - 38330 Montbonnot-St-Martin (France)
Unité de recherche INRIA Sophia Antipolis : 2004, route des Lucioles - BP 93 - 06902 Sophia Antipolis Cedex (France)

Éditeur
INRIA - Domaine de Voluceau - Rocquencourt, BP 105 - 78153 Le Chesnay Cedex (France)
http://www.inria.fr
ISSN 0249-6399